

2016

Chemical Tools for Exploring IFITM3 S-Palmitoylation and Mechanism

Xiaoqiu Yuan

Follow this and additional works at: http://digitalcommons.rockefeller.edu/student_theses_and_dissertations

 Part of the [Life Sciences Commons](#)

Recommended Citation

Yuan, Xiaoqiu, "Chemical Tools for Exploring IFITM3 S-Palmitoylation and Mechanism" (2016). *Student Theses and Dissertations*. Paper 307.



CHEMICAL TOOLS FOR EXPLORING IFITM3
S-PALMITOYLATION AND MECHANISM

A Thesis Presented to the Faculty of

The Rockefeller University

in Partial Fulfillment of the Requirement For

the degree of Doctor of Philosophy

by

Xiaoqiu Yuan

June 2016

CHEMICAL TOOLS FOR EXPLORING IFITM3

S-PALMITOYLATION AND MECHANISM

Xiaoqiu Yuan, Ph.D.

The Rockefeller University 2016

Protein S-palmitoylation is a reversible post-translational lipid modification that regulates the trafficking, stability, and activity of proteins in eukaryotes. The detection of fatty-acylated proteins has been challenging but recent advances in chemical labeling methods have enabled more sensitive detection and proteomic analyses, which I summarize in Chapter 1. The proteomic analysis of S-palmitoylated proteins in dendritic cells and macrophages by our laboratory revealed that the interferon-induced transmembrane proteins (IFITMs) are S-fatty-acylated at conserved cysteine (Cys) residues. IFITMs are unique interferon-induced proteins that restrict the infection of multiple pathogenic viruses. Initial studies by our laboratory showed that S-fatty-acylation on three conserved Cys residues were crucial for IFITM3 anti-influenza virus activity. However, endogenous levels and site-specific functions of S-palmitoylation on the individual IFITM3 Cys residues were unknown and are addressed in Chapter 2. In collaboration with other members of the Hang laboratory, we discovered that endogenous IFITM3 is fully S-fatty-acylated in IFN-stimulated mammalian cells and that Cys72 in particular plays an important role in IFITM3 antiviral activity. My additional biochemical studies suggest S-palmitoylation may regulate IFITM3 protein turnover in mammalian cells.

IFITMs appear to inhibit virus entry into mammalian cells, but the precise mechanisms have been unclear due to limited methods for live-cell imaging and IFITM3 protein-protein interaction studies. To address these limitations, I explored amber codon suppression technology for site-specific IFITM3 labeling with unnatural amino acids for bioorthogonal imaging and covalent protein crosslinking in mammalian cells in Chapter 3. Using the pyrrolysyl-tRNA synthetase (PylRS)/Pyl tRNA_{CUA} system, I showed that unnatural amino acid can be site-specifically incorporated throughout IFITM3 in mammalian cells. The site-specific labeling of IFITM3 with unnatural amino acids has provided new opportunities for live-cell imaging and photocrosslinking studies with specific interacting proteins in Chapter 4. My thesis studies have revealed additional insight into IFITM3 regulation by S-palmitoylation and established new tools to explore the antiviral mechanism of IFITMs.

To my wife

Acknowledgements

Being a Ph.D. student at the Rockefeller University has been both a rewarding and challenging experience that I will cherish and remember. During this journey, many people have helped and provided me invaluable supports and advice. I would like to thank my advisor, Dr. Howard Hang, for bringing me into an exciting world of chemical biology and supporting my research in the lab with great patience and scholarship. I would also like to thank all the members of Hang lab, the past or current. It's been an awesome experience to be around with you both personally and professionally. My special gratitude goes to Dr. Mingzi Zhang, Dr. Kavita Rangan, and Dr. Kelvin Tsou for their guidance when I first started in the lab. They not only served as role models of good scientists but also provided me advises when I felt anxious to figure out what to do starting out in the lab. I want to thank Elizabeth Fitzgerald for being an amazingly efficient and helpful lab manager. I'd like to acknowledge Dr. Jacob Yount, Dr. Ruina He, Dr. Rayshonda Hardy, Dr. Emmanuelle Thinon, Dr. Tao Peng, Avital Percher for lots of constructive discussion and collaboration. I also would like to thank my committees Prof. Thomas Sakmar, Prof. Charles Rice, Prof. Morgan Huse for providing feedback and support during every FAC meeting.

I acknowledge the Rockefeller University resource centers for training and help with the core instruments and facilities. I thank the Dean's Office of the Rockefeller University and the Tri-institutional Program in Chemical Biology for funding and supporting.

Last but not least, I'd like to thank my friends and family for sharing with me all the happiness and tears. Especially, I'd like to thank my wife. We met and fell in love

before I came to the Rockefeller University. Despite all the difficulties and hardships, we managed to work through all of them. Being the light of my life, she gave me supports and comforts during the darkest days, and it wouldn't be possible to complete this journey without her by my side.

TABLE OF CONTENTS

LIST OF FIGURES	x
LIST OF TABLES	xii
LIST OF ABBREVIATIONS	xiii
CHAPTER ONE: BIOCHEMICAL METHODS FOR ANALYZING PROTEIN FATTY-ACYLATION	1
1.1 Introduction to protein fatty-acylation	1
1.1.1 S-fatty-acylation.....	4
1.1.2 N-myristoylation	7
1.1.3 O-acylation.....	9
1.1.4 ϵ -N-Lys acylation.....	10
1.2 Methods for analyzing fatty-acylated proteins.....	11
1.2.1 Detection of fatty-acylation by radiolabeling	13
1.2.2. Bioorthogonal detection of fatty-acylation using chemical reporters.....	13
1.2.3 Acyl-biotin exchange method for S-fatty-acylation detection and enrichment 17	
1.2.4 Acyl-RAC method for S-fatty-acylation detection and enrichment	19
1.2.5 Acyl-PEG exchange method for S-fatty-acylation detection and enrichment 21	
1.2.6 Comparison of different methods for protein S-fatty-acylation detection and enrichment.....	22
1.3 Discovery of new fatty-acylated proteins from chemical proteomics	23
1.3.1 Summary of proteomics studying using chemical reporter and ABE method 23	
1.3.2 Discovery of IFITMs S-fatty-acylation	28

CHAPTER TWO: CHARACTERIZATION OF IFITM3 S-PALMITOYLATION 30

2.1	Summary	30
2.2	Introduction	32
2.2.1	Early findings on IFN-induced effectors	32
2.2.2	Discovery of antiviral activity of IFITMs towards different viruses	33
2.2.3	IFITM3 posttranslational modifications, localization and membrane topology	34
2.3	Results	38
2.3.1	S-fatty-acylation of human IFITMs	38
2.3.2	Characterization of endogenous and site-specific S-fatty-acylation levels of IFITM3 in mammalian cells	42
2.3.3	Anti-influenza virus activity of IFITM3 S-palmitoylation mutants	48
2.3.4	Immunofluorescence analysis of IFITM3 Cys mutants in mammalian cells.	50
2.3.5	Protein turnover of human IFITM3 and Cys mutants.....	52
2.3.6	Effects of protein degradation pathway inhibitors.....	57
2.4	Discussion	60
2.4.1	Key sites of human IFITM3 S-fatty-acylation.....	60
2.4.2	Lipid composition of IFITM3 S-fatty-acylation.....	62
2.4.3	Protein stability regulated by S-fatty-acylation	63
2.4.4	Differences between murine and human IFITM3.....	65
2.4.5	Effect of S-fatty-acylation on protein localization.....	66
2.5	Materials and methods	67
2.5.1	Materials	67
2.5.2	Metabolic incorporation of chemical reporters of protein fatty acylation in living cells	67
2.5.3	Copper(I)-catalyzed alkyne-azide cycloaddition labeling of cell lysates ...	68
2.5.4	Immuno-precipitation using antibody-conjugated resin for click chemistry reaction	69
2.5.5	Site mutagenesis using QuikChange methods for Cysteine mutants.....	69
2.5.6	Transfection of mammalian cell lines.....	71
2.5.7	S-fatty-acylation detection using acyl-PEG exchange.....	71

2.5.8	Microscopy	73
2.5.9	Infections, fluorescence microscopy, and flow cytometry	74
CHAPTER THREE: SITE-SPECIFIC INCORPORATION OF UNNATURAL AMINO ACID INTO IFITM3 IN MAMMALIAN CELLS		75
3.1	Summary.....	75
3.2	Introduction.....	76
3.2.1	Overview of site-specific protein labeling	76
3.2.2	Application of unnatural amino acids for imaging	78
3.2.3	Application of unnatural amino acids for photocrosslinking.....	84
3.3	Results.....	85
3.3.1	Unnatural amino acids incorporation in IFITM3	85
3.3.2	Site-specific bioorthogonal labeling of IFITM3	91
3.3.3	Photo-crosslinking of DiZPK to study IFITM3 interaction partners.....	93
3.3.4	Application of UAA in other membrane proteins.....	95
3.4	Discussion.....	96
3.4.1	Optimization of Amber codon suppression in IFITM3	96
3.4.2	Bioorthogonal labeling of IFITM3 amber codon mutants with UAAs.....	97
3.4.3	Application of amber codon suppression in other membrane proteins.....	97
3.5	Materials and methods	98
3.5.1	Materials	98
3.5.2	Site mutagenesis for amber mutants	98
3.5.3	Unnatural amino acids incorporation in mammalian cell culture.....	101
3.5.4	In-gel fluorescence detection of ligated products	101
3.5.5	UV-induced photo-crosslinking by DiZPK	102
CHAPTER FOUR: CONCLUSION AND PERSPECTIVE		103
4.1	Conclusion	103
4.2	Perspectives	104
4.2.1	A model for IFITM3 antiviral mechanism.....	104
4.2.2	Future studies	106

REFERENCES..... 117

LIST OF FIGURES

Figure 1. Different types of fatty-acylated proteins.....	2
Figure 2. Function of protein fatty-acylation.....	3
Figure 3. Protein S-fatty-acylation regulates multiple steps in the life cycle of membrane and peripheral membrane proteins.....	6
Figure 4. Detection of protein fatty-acylation using chemical reporters.	14
Figure 5. Methods for analysis of fatty-acylated proteins.	18
Figure 6. Visualization and identification of S-palmitoylated proteins in dendritic cells.	29
Figure 7. Topology model of IFITM3.	35
Figure 8. Sequence alignment and predicted topology of IFITM proteins.....	37
Figure 9. S-fatty-acylation of murine IFITM3 and Cys mutants.....	39
Figure 10. S-fatty-acylation of human IFITM3 and Cys mutants in A549 cells.....	40
Figure 11. S-fatty-acylation of human IFITMs in HEK293T cells.	41
Figure 12. Endogenous mIFITM3 S-palmitoylation assessed by APE.	43
Figure 13. Endogenous human IFITM3 S-fatty-acylation in A549 cells.	44
Figure 14. APE analysis of overexpressed mIFITM3 and Cys mutants.....	46
Figure 15. APE of overexpressed human IFITM3 and mutants.	47
Figure 16. Antiviral activity of WT and IFITM3 Cys mutants.	49
Figure 17. Imaging of HA-mIFITM3 in NIH3T3 fibroblasts.....	51
Figure 18. Protein turnover of IFITM3 WT, C72A, and Palm Δ in HeLa IFITM2/3 $-/-$ cell line.....	54
Figure 19. Cycloheximide-chase analysis of IFITM3 turnover.....	55
Figure 20. Determination of rate constant and protein degradation half-life.	56

Figure 21. Cycloheximide with inhibitors chase experiment.	57
Figure 22. Analysis of protein degradation with inhibitors.	58
Figure 23. Site-specific incorporation of UAAs using amber codon suppression.....	77
Figure 24. Site-specific protein labeling.....	79
Figure 25. Using UAA to study GPCR.....	81
Figure 26. Bioorthogonal ligations.	82
Figure 27. Unnatural amino acids used for bioorthogonal labeling.....	86
Figure 28. Analysis of murine IFITM3 amber codon mutants with BocLys.....	87
Figure 29. Profiling sites of amber suppression of human IFITM3 using BocLys.	89
Figure 30. Relative expression level of human IFITM3 expression level.....	90
Figure 31. Site-specific bioorthogonal labeling of IFITM3 <i>in vitro</i>	92
Figure 32. Incorporation DiZPK into IFITM3 for photocrosslinking studies.	94
Figure 33. Incorporation of UAA in Caveolin 1 (Cav1).....	95
Figure 34. IFITM3 antiviral working models.	105
Figure 35. Scheme of site-specific live cell imaging using IED-DA reaction.....	107
Figure 36. Screening for an optimal pair of unnatural amino acids and tetrazine dye. ..	108
Figure 37. Live cell imaging of IFITM3 F8TAG with Si-Rh-Tz.	109
Figure 38. Summary of HA-IFITM3-F8-DiZPK double-SILAC X-proteomics.....	112
Figure 39. <i>In vitro</i> alkylation with hexadecylmaleimide (Mal-C16:0).....	114

LIST OF TABLES

Table 1. List of fatty acylation prediction sites.....	12
Table 2. List of chemical reporters for fatty-acylation.	15
Table 3. Summary of literature on proteomics study of fatty-acylated proteins	27
Table 4. List of viruses suppressed by IFITMs.....	33
Table 5. Summary of post-translational modifications on IFITM3.....	35
Table 6. Rate constant and half-life of CHX chase experiment.	55
Table 7. Determination of rate constant using one phase decay model.....	59
Table 8. Sequences of primers for site-directed mutagenesis of IFITM3 cysteine mutations.	70
Table 9. Sequences of primers for site-directed mutagenesis of amber mutants.....	98

LIST OF ABBREVIATIONS

ϕ p-Pyl	Cyclopropene
ABE	Acyl-biotin exchange
APE	Acyl-PEG exchange
BCNK	Bicyclo[6.1.0]nonyne-lysine
BONCAT	Bioorthogonal non-canonical amino acid tagging
β -ME	β -mercaptoethanol
BocK	N ϵ -Boc-L-lysine
CHX	Cycloheximide
CuAAC	Copper-Catalyzed Azide-Alkyne Cycloaddition
FUNCAT	Fluorescent non-canonical amino acid tagging
FFA	Free fatty acid
GOAT	Ghrelin O-Acyltransferase
GPCR	G protein-coupled receptors
IAV	Influenza A virus
IEDDA	Inverse-electron-demand Diels-Alder cycloaddition
IFITM	Interferon-inducible-transmembrane protein
IFN	Interferon
IFNAR	IFNB receptor
IFNGR	IFNH receptor
IFNLR	IFNM λ receptor
IL-10R2	Interleukin-10 receptor 2
IpaJ	Invasion plasmid antigen J
ISG15	IFN-stimulated protein of 15 kDa
HDR	Homology directed repair
HIV-1	Human immunodeficiency virus 1
HSV	Herpes simplex virus
NEM	N-ethylmaleimide
NHEJ	Non-homologous end joining

NMT	N-myristoyltransferase
MMTS	Methyl methanethiosulfonate
MetRS	Methionyl-tRNA synthetase
MGST3	Microsomal glutathione-S-transferase 3
Mx	Myxovirus resistance protein
OAS	2',5'-oligoadenylate synthetase
PAT	Protein acyltransferase
PKR	Protein Kinase R.
PSD95	Postsynaptic density protein of 95 kDa
PTM	Post-translational modification
RAC	Resin-assisted capture
Rps11	Ribosomal protein S11
Sec61b	β -subunit of the protein translocating system
SILAC	Stable isotope labeling by amino acids in cell culture
SILAM	Stable Isotope Labeling of Mammals
SNARE protein receptor	Soluble N-ethylmaleimide-sensitive factor attachment
STAT	Signal transducer and activators of transcription
TBTA	tris[(1-benzyl-1H-1,2,3-triazol-4-yl)methyl] amine
TCEP	tris(2-carboxyethyl)phosphine hydrochloride
TCOK	Trans-cyclooctene lysine
TLR	Toll-like receptor
TNF- α	Tumor necrosis factor alpha
TTSS	Type III secretion system
TYK2	Tyrosine kinase 2
UAA	Unnatural amino acid
zDHHC	Zinc finger DHHC

Chapter One: Biochemical methods for analyzing protein fatty-acylation

1.1 Introduction to protein fatty-acylation

Of the numerous protein modifications in bacteria and eukaryotes (Walsh et al., 2005), lipidation is especially intriguing due to its ability to directly regulate protein hydrophobicity and membrane trafficking. Lipidation refers to the covalent attachment of lipid or lipid-like groups onto proteins (Hang and Linder, 2011; Resh, 2006). Fatty-acylation and prenylation are the most common types of protein lipidation found in mammalian cells (Hang and Linder, 2011; Resh, 2006). While prenylation primarily occurs at the C-terminus of proteins through a thioether bond, protein fatty-acylation can be attached through S-, O-, or N-linkages at different sites throughout proteins. Protein fatty-acylation occurs co- or post-translationally and plays an essential role in regulating protein function and localization. Specifically, during the protein modification, lipid moieties with varying chain length, such as myristate (14 carbons) and palmitate (16 carbons), covalently attach to proteins under the regulation of a set of enzymes like acyltransferases and deacylases. Furthermore, lipidated proteins can have distinct interactions with signaling proteins and specific membrane domains. In this introduction, we will focus on protein fatty-acylation and will present a summary of chemical tools used for detecting these modifications *in vitro* and *in vivo*.

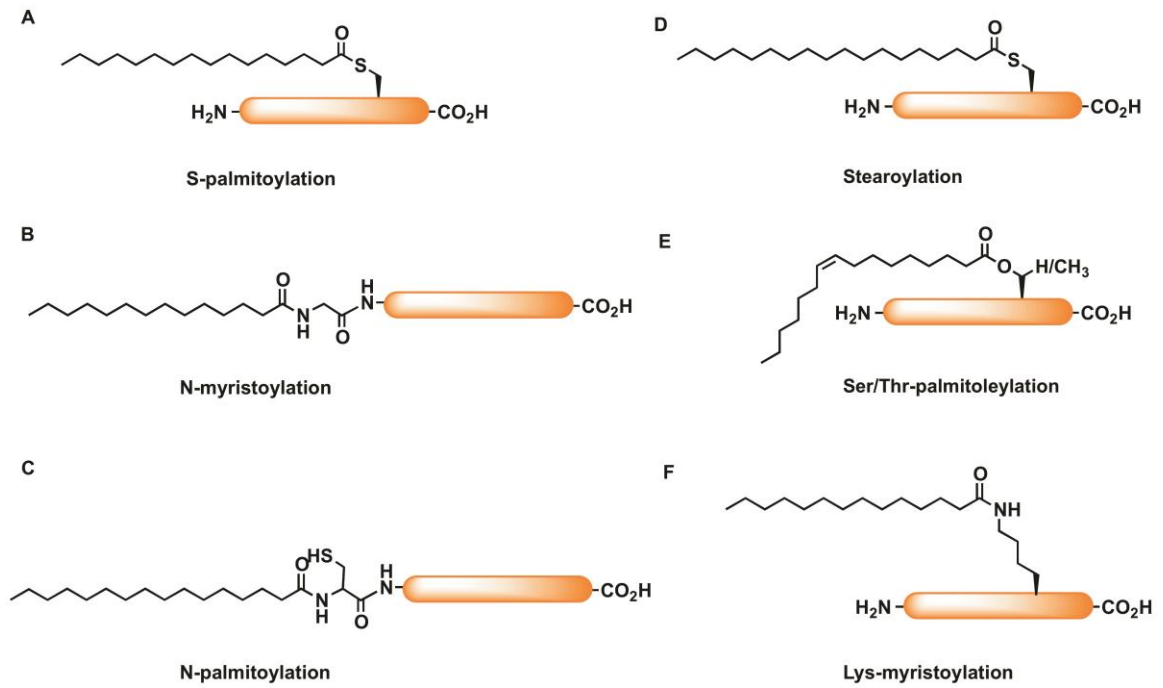


Figure 1. Different types of fatty-acylated proteins A) S-palmitoylation. B) N-myristoylation. C) N-palmitoylation. D) Stearoylation. E) Palmitoylation on Ser or Thr. F) Lys-myristoylation.

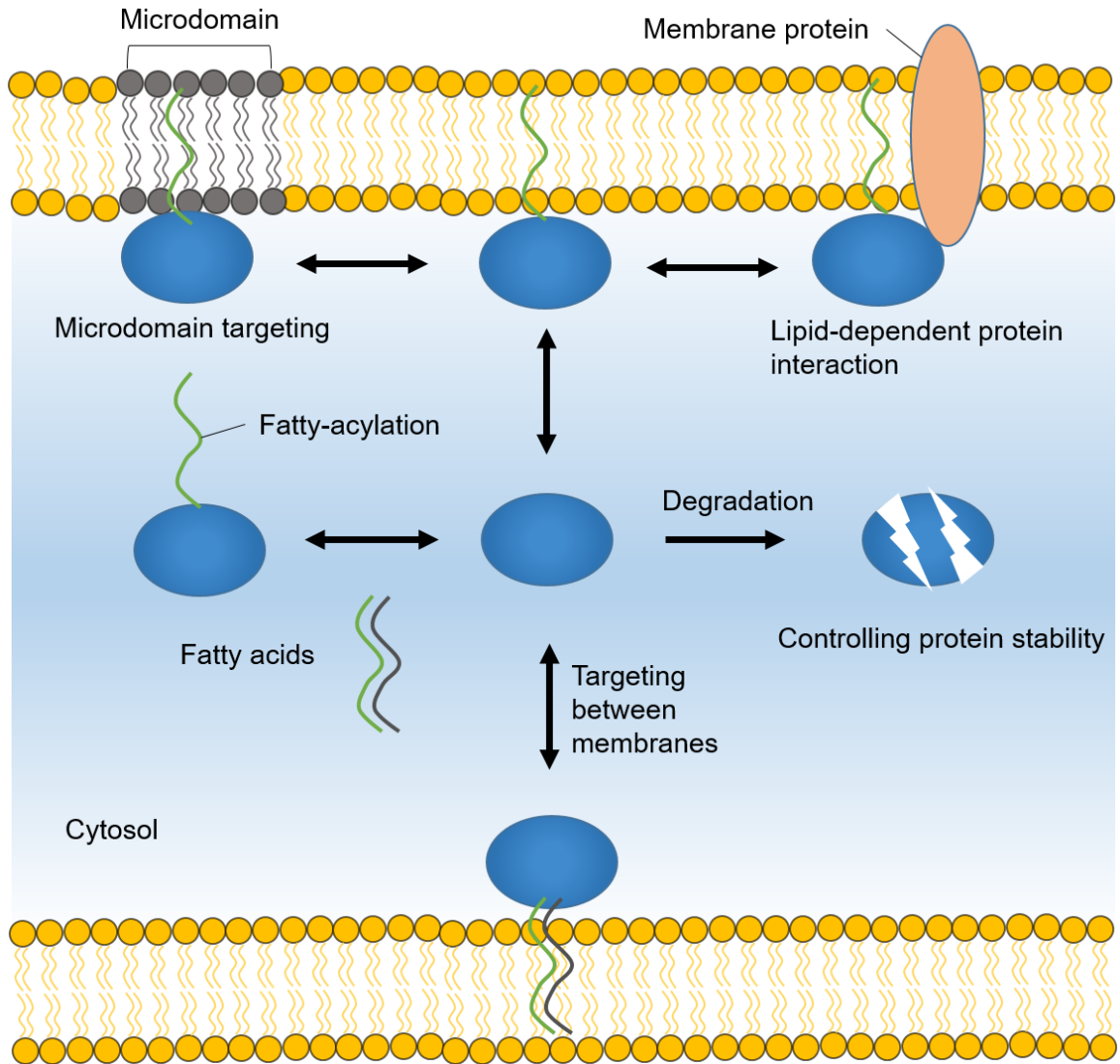


Figure 2. Function of protein fatty-acylation. Protein fatty-acylation regulates the interaction of the modified proteins with cellular membrane. The presence or absence of fatty-acylation also regulates protein stability, degradation and complex formation. Specific fatty-acylation might determine the cellular microdomain targeting and cellular vesicle shuttle.

1.1.1 S-fatty-acylation

Protein S-fatty-acylation, or frequently referred to as S-palmitoylation, is the post-translational modification of fatty acids onto Cys residues via a thioester linkage (Chamberlain and Shipston, 2015) (Figure 1A). S-palmitoylation is often used to describe this modification because palmitate is the predominant fatty acid in this process. However, other long chain fatty acids have also been observed (Liang et al., 2001). Protein S-palmitoylation was first documented more than 30 years ago (Schmidt and Schlesinger, 1979), but the enzymes responsible for this modification took over 20 years to identify (Bartels et al., 1999; Deschenes and Broach, 1987). Historically, radioactive labeling using [³H]palmitate had been the major method to study palmitoylation. G protein-coupled receptors (GPCR) (O'Brien and Zatz, 1984), G α subunits (Linder et al., 1993), Src family kinases (Paige et al., 1993), Ras proteins (Buss and Sefton, 1986), and soluble N-ethylmaleimide-sensitive factor attachment protein receptor (SNARE) (Hess et al., 1992) are among the list of proteins that were identified using this approach. S-fatty-acylation is enzymatically mediated by a family of zinc finger DHHC (zDHHC) motif-containing protein acyltransferases (DHHC-PATs) that catalyze S-palmitoylation. There are seven DHHC proteins in budding yeast (Mitchell et al., 2006), five in fission yeast (Zhang et al., 2013a) and more than 20 DHHC genes in mammalian species, all of which are multi-pass transmembrane proteins. Early work on DHHC enzymatic activity towards postsynaptic density protein of 95 kDa (PSD-95), which was the first comprehensive analysis of the mammalian DHHC, identified that DHHC 2, 3, 7 and 15 were the most active (Fukata et al., 2004).

Protein S-fatty-acylation is a reversible process, a key property that distinguishes it from other lipid modifications. Pulse-chase experiments on N-Ras with [³H] palmitate highlighted the reversibility of S-fatty-acylation (half-life ~20 min) (Magee et al., 1987). That deacylation of N-Ras may occur 10–20 times faster than calculated by pulse-chase analysis (Rocks et al., 2005, 2010). However, marked differences can exist in the turnover rates of different S-fatty-acylation sites in the same protein (Zuckerman et al., 2011). Indeed, rates of palmitate turnover at each cysteines are dramatically different. For example, although S-palmitoylation at the proximal site of the β -adrenergic receptor is remarkably stable, S-palmitoylation at the distal site is rapidly turned over. Thus, the dynamics of acylation/deacylation is an outstanding question in the S-fatty-acylation research: how the dynamics of lipid turnover of S-fatty-acylated proteins is regulated and why different proteins display distinct turnover rates. Notably, recent enrichment and mass-spectrometry-based proteomics approaches have significantly accelerated the characterization of S-fatty-acylated proteins and reignited the interest in the poorly characterized dynamics of protein S-fatty-acylation (Peng et al., 2016; Zhou et al., 2014).

Major functions of protein S-fatty-acylation include targeting proteins to discrete intracellular membrane compartments, control of protein stability and modulation of protein-protein interactions (Chamberlain and Shipston, 2015) (Figure 2). Furthermore, the reversibility of S-fatty-acylation offers spatial and temporal control of protein function, for example, stable association, and release of peripheral membrane proteins from lipid bilayers (Figure 3).

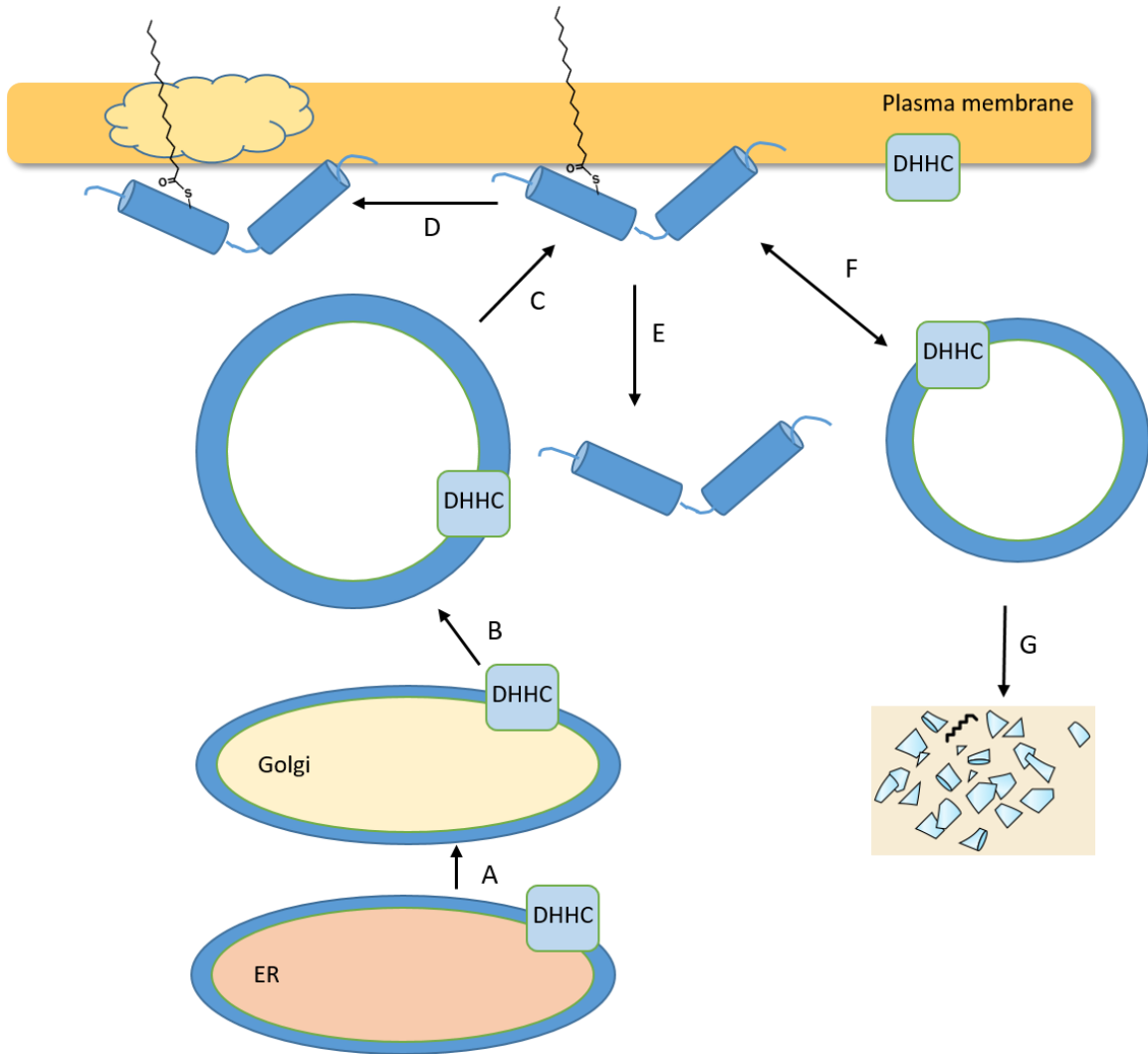


Figure 3. Protein S-fatty-acylation regulates multiple steps in the life cycle of membrane and peripheral membrane proteins. Protein S-fatty-acylation can happen at multiple locations including ER, Golgi, endosomes, as well as the plasma membrane. A) Protein synthesis and ER exit. B) Maturation and Golgi exit. C) Sorting and trafficking to the plasma membrane. D) Clustering into membrane microdomains. E) Partitioning of peripheral membrane proteins between the cytosol and membranes. F) Internalization. G) Recycling and degradation.

1.1.2 N-myristoylation

Protein N-myristoylation describes the covalent modification of N-terminal Gly residues with a 14 carbon fatty acid (myristate) (Farazi et al., 2001) (Figure 1B). This fatty acid is transferred from myristoyl-CoA to substrate proteins by N-myristoyltransferase (NMT). N-myristoylation is necessarily preceded by proteolysis to reveal an N-terminal glycine, the only completely conserved motif across all known NMT substrates. N-myristoylation can also occur posttranslationally during apoptosis upon proteolytic cleavage, thereby exposing an N-terminal glycine residue within a myristoylation consensus sequence (Martin et al., 2011). Recent chemical proteomics approaches identified N-myristoylated proteins during normal cellular growth and apoptosis (Martin et al., 2008; Thinon et al., 2014). The wide scope of substrates with diverse functions that undergo co-translational or post-translational N-myristoylation, such as c-Abl (Nagar et al., 2003), c-Src (Patwardhan and Resh, 2010), Bid (Zha et al., 2000), PAK2 (Vilas et al., 2006), and gelsolin (Sakurai and Utsumi, 2006), to name a few, underscores the critical role that N-myristoylation plays not only in proper localization of proteins but also regulating their activity. Notably, atomic crystal structures of c-Abl show that the N-terminal myristoyl modification of c-Abl 1b binds to the kinase domain and induces conformational changes that allow the SH2 and SH3 domains to dock onto it (Nagar et al., 2003). These approaches should help uncover potential roles of N-myristoylation in cancer and neurodegenerative disease.

The 50-60 kDa monomeric enzyme NMT catalyzes the transfer of myristate from myristoyl-CoA to suitable peptides and proteins. The structure of the yeast *Saccharomyces cerevisiae* NMT1p was solved as a ternary complex and reveals how myristoyl-CoA and peptide substrates bind to the enzyme (Bhatnagar et al., 1998). Although usually non-

eukaryotic species lack NMT that is required for this modification, there are instances of pathogen-host interaction around N-myristoylation. Indeed, since first discovered in the early eighties, many viral proteins has been found to be myristoylated by NMTs of their eukaryotic hosts (Maurer-Stroh and Eisenhaber, 2004). N-myristoylation of viral proteins has roles in assembly, structure, budding, viral entry and intracellular host interactions. Furthermore, bacteria effectors injected into host cells through type III secretion system (TTSS) can also be myristoylated (Nimchuk et al., 2000). A recent study found that *Shigella flexneri* virulence factor invasion plasmid antigen J (IpaJ) cleaves N-myristoylated glycines of eukaryotic proteins as a pathogenic mechanism in host cells (Burnaevskiy et al., 2013, 2015). Specifically, mass spectrometry showed that IpaJ cleaved the peptide bond between N-myristoylated Gly2 and Asn3 of human ARF1, thereby providing a new mechanism for host secretory inhibition by a bacterial pathogen (Burnaevskiy et al., 2013, 2015).

1.1.3 O-acylation

Protein O-acylation is a less common form of fatty-acylation at serine or threonine residues. A notable example of O-acylation is O-palmitoleoylation on Wnt proteins (Figure 1E). Wnts are secreted signaling molecules that are covalently modified with palmitoleic acid (16:1) at a serine residue (Gao and Hannoush, 2014; Takada et al., 2006). Other O-acylated proteins include ghrelin (Gutierrez et al., 2008; Yang et al., 2008), PLTX-II (Branton et al., 1993), and histone H4 protein (Zou et al., 2011). Serine-3 of ghrelin is acylated with an eight-carbon fatty acid, octanoate, which is required for its endocrine actions. Notably, Wnt has been studied extensively because first of all, Wnt protein family is one of the largest secreted protein families that are responsible for extracellular signaling in virtually all animal development stages, and secondly post-translational fatty acylation is essential for its activity. Interestingly, mass spectrometry studies and recent bioorthogonal fatty acid labeling on Wnt3a have shown that Ser209 is O-palmitoleoylated rather than Cys77 (Gao and Hannoush, 2014; Takada et al., 2006). The enzyme that is responsible for the modification is called Porcupine, a member of membrane-bound O-acyl transferase (MBOAT). Chemical reporter methods also demonstrated that Porcupine is S-palmitoylated, which negatively regulates Wnt signaling (Berthiaume, 2014).

1.1.4 ϵ -N-Lys acylation

Fatty-acylation on Lys side-chain via formation of an amide bond is another potentially regulated lipid modification (Figure 1F). Tumor necrosis factor alpha (TNF- α) precursor and Interleukin-1- α were shown to undergo myristoylation on specific inner lysine residues (Stevenson et al., 1992, 1993). ϵ -N-Ly acylation has been long thought to be non-hydrolysable due to the irreversible nature of amide bond linkage, but the recent discovery of SIRT6, a sirtuin family NAD⁺-dependent protein deacetylase that can also remove long-chain fatty acids on Lys side chains reignites interests on dynamics regulation of fatty N-acylation. SIRT6 promotes the secretion of TNF- α by removing the fatty acyl modification on K19 and K20 of TNF- α (Jiang et al., 2013). Subsequently, *in vitro* studies of all sirtuins to hydrolyze 13 different acyl groups have revealed the specificity of sirtuin enzymes for deacylating Lys modified with a broad range of fatty acids (Feldman et al., 2013; Teng et al., 2015). Interestingly, free fatty acids (FFAs) could stimulate deacetylation activity of SIRT6 towards long-chain acylated peptides. Crystal structure of SIRT6 reveals that, different from the other four members of mammalian sirtuins family, there is a large hydrophobic pocket that can accommodate long-chain fatty acyl groups rather than shorter acetyl groups. The new findings of protein deacylation enzyme activity provide a roadmap to uncover the biological functions of protein ϵ -N-Lys-fatty-acylation modifications with previously unknown functions.

1.2 Methods for analyzing fatty-acylated proteins

Due to the importance of protein fatty-acylation in regulating protein function, there have been significant interests in detecting and characterizing these modifications in cells. Unlike phosphorylation and other post-translational modifications, no robust antibodies specific to lipid-modified peptides or proteins are readily available. Bioinformatic predictions of fatty-acylation are also limited since some modifications do not have clear consensus motifs (Table 1). Traditionally, the analysis of protein fatty-acylation relied on radioactive lipid labeling, followed by immune precipitation and lengthy film exposure (Berthiaume et al., 1995; Schlesinger et al., 1980). However, this classical method suffers the risks associated with radioactivity, as well as low sensitivity and long exposure time, from days to months. Other methods like acyl-biotin exchange (ABE) (Drisdell and Green, 2004) and acyl-resin-assisted capture (acyl-RAC) (Forrester et al., 2011) are useful to detect and enrich S-acylated proteins since the thioester bond can be readily cleaved with hydroxylamine and replaced by other functional groups.

Bioorthogonal chemistry developed in the recent years has permitted improved detection and large-scale proteomic analysis of fatty-acylated proteins (Hang and Linder, 2011; Hang et al., 2011). The two-step strategy involves metabolic labeling with chemical reporters and then detection using bioorthogonal chemistry (Grammel and Hang, 2013; Prescher and Bertozzi, 2005). The advantages of separating incorporation and detection are that 1) sterically-demanding fluorophores or affinity tags would not interfere with chemical reporter incorporation and 2) chemical reporters provide direct detection of the modified substrate.

Table 1. List of fatty acylation prediction sites.

Myristoylation predictor	http://mendel.imp.ac.at/myristate/	(Maurer-Stroh and Eisenhaber, 2004)
	http://web.expasy.org/myristoylator/	(Bologna et al., 2004)
	http://plantsp.genomics.purdue.edu/myrist.html	(Podell and Gribskov, 2004)
Palmitoylation predictor	http://doc.aporc.org/wiki/CKSAAP-Palm	(Wang et al., 2009)
	http://csspalm.biocuckoo.org/	(Ren et al., 2008)
	http://nbapalm.biocuckoo.org/	(Xue et al., 2006)
	http://14.139.227.92/mkumar/palmpred/	(Kumari et al., 2014)
	http://bioinfo.ncu.edu.cn/WAP-Palm.aspx	(Shi et al., 2013)
Prenylation site predictor	http://mendel.imp.ac.at/sat/PrePS/	(Maurer-Stroh and Eisenhaber, 2005)

1.2.1 Detection of fatty-acylation by radiolabeling

The traditional method for detecting fatty-acylation study used radio-active ^3H -, ^{14}C -labeled or iodinated fatty acids, which are converted into fatty-acyl-CoA in cells and incorporated into proteins. Compared to ^3H -, ^{14}C -labeling methods, use of radioiodinated fatty acids is advantageous, because it reduces the exposure times and allows the use of phosphorimager technology (Berthiaume et al., 1995; Peseckis et al., 1993).

1.2.2 Bioorthogonal detection of fatty-acylation using chemical reporters

By first incorporating fatty acid chemical reporters that contain bioorthogonal handles, we can then label modified proteins with secondary detection tags such as fluorophores or affinity tags (Charron et al., 2009a). The chemical reporter is usually of similar size with natural fatty acid (azide- or alkyne- reporter) to facilitate recognition by acyltransferase inside cells (Table 2). *In vitro* labeling can also be done using fatty acyl-CoA reporter analogs. Although both azide and alkyne reporters have been used in the past, alkyne reporters are preferred for detection of protein fatty-acylation due to its better efficiency and specificity (Figure 4) (Thinon and Hang, 2015). Our lab has successfully detected protein N-myristoylation (Charron et al., 2009a), S-palmitoylation (Charron et al., 2009a; Yount et al., 2010; Zhang et al., 2010), S-prenylation (Charron et al., 2011) and Lys-acetylation (Yang et al., 2010b) using alkynyl-chemical reporters in the past. Alkyne-tagged reporters have been used in specific and efficient two-step labeling with Cu(I)-catalyzed azide-alkyne cycloaddition (CuAAC) for fluorescence visualization or quantitative proteomics methods such as stable isotope labeling by amino acids in cell culture (SILAC) (Figure 4). Specifically, SILAC enables the evaluation of

signal/background ratios to identify fatty-acylated proteins with high confidence as well as the comparison of the protein acylation level (Peng et al., 2016).

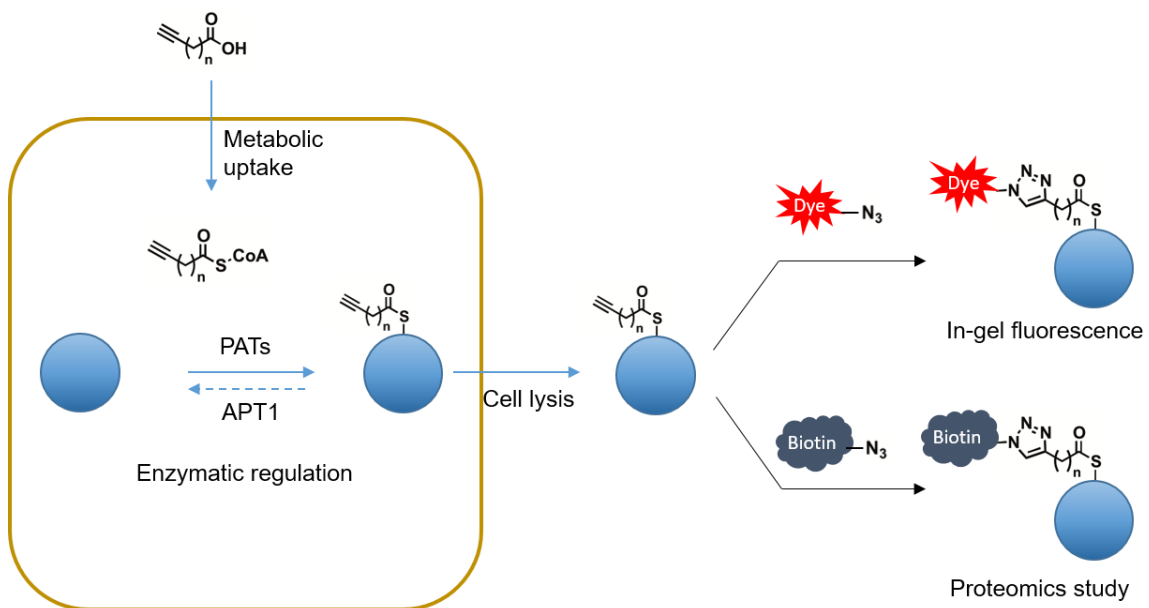


Figure 4. Detection of protein fatty-acylation using chemical reporters. Alkyne-bearing chemical reporters are fed to the cells. After uptake and metabolic incorporation into proteins, cells are lysed and subjected to subsequent CuAAC ligation with either a fluorophore for imaging or biotin for proteomics study.

One of the advantages of using chemical reporters is the ability to apply to versatile lipid modifications on proteins, including S-fatty-acylation, N-myristoylation and S-prenylation. They also offer more sensitive and immediate detection compared to radioactive methods. After probes have been incorporated into proteins, samples can be processed and reacted through bioorthogonal chemistries with fluorophore conjugates for visualization or biotin conjugates for enrichment. Furthermore, dynamic S-fatty-acylation

can be readily monitored using pulse-chase analysis with fatty acid reporters (az-16 or alk-16) (Martin et al., 2012; Zhang et al., 2010).

Table 2. List of chemical reporters for fatty-acylation.

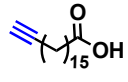
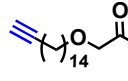
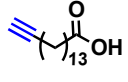
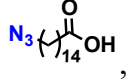
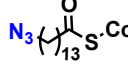
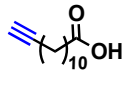
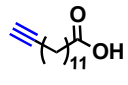
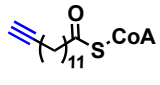
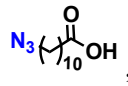
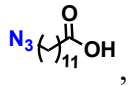
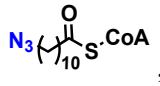
Acylation	Reporter chemical structure	References
S-palmitoylation	 C_{15}OH , Alk-16 or ODYA	(Charron et al., 2009b; Hannoush and Arenas-Ramirez, 2009)
	 HDYOA	(Yount et al., 2011a)
	 Alk-14	(Charron et al., 2009a; Hannoush and Arenas-Ramirez, 2009)
	 AZ-15	(Charron et al., 2009a; Hang et al., 2007)
	 AZ-14-CoA	(Kostiuk et al., 2008)

Table 2. List of chemical reporters for fatty-acylation (continued).

Acylation	Reporter chemical structure	References
N-myristoylation	 <chem>C#CCCCCCCC(=O)O</chem> , Alk-11	(Hannoush and Arenas-Ramirez, 2009)
	 <chem>C#CCCCCCCCC(=O)O</chem> , Alk-12	(Charron et al., 2009a; Hannoush and Arenas-Ramirez, 2009; Heal et al., 2008a)
	 <chem>C#CCCCCCCCC(=O)S.COA</chem> , Alk-12-CoA	(Heal et al., 2008a)
	 <chem>[N-]=[N+]=NCCCCCCCC(=O)O</chem> , Az-11	(Heal et al., 2008a)
	 <chem>[N-]=[N+]=NCCCCCCCCC(=O)O</chem> , Az-12	(Charron et al., 2009a; Hang et al., 2007; Martin et al., 2008)
	 <chem>[N-]=[N+]=NCCCCCCCC(=O)S.COA</chem> , Az-11-CoA	(Heal et al., 2008a, 2008b)

1.2.3 Acyl-biotin exchange method for S-fatty-acylation detection and enrichment

Unlike N-/O- acylation, thioester linkage is sensitive to nucleophilic reagents that can be exploited for detection and enrichment. Drisdell and Green developed acyl-biotin exchange (ABE) chemistry to take advantage of the free thiol that is liberated by hydroxylamine (NH_2OH) to be labeled with a Cys-reactive reagent (Drisdel and Green, 2004). In the first step, cell extracts are treated with N-ethylmaleimide (NEM) to block free Cys residues. One-half of the sample is then treated with NH_2OH to remove fatty acids from Cys residues, whereas the other half is the control sample. Reactive biotin reagents like HPDP-Biotin (N-[6-(Biotinamido)hexyl]-3'-(2'-pyridyldithio)propionamide) can then be used to label newly liberated Cys residues. Biotinylated proteins are then captured on a streptavidin column and eluted. Eluted proteins can be either visualized by SDS-PAGE or analyzed by proteomics (Figure 5A). A S-palmitoylated protein should be present in the NH_2OH -treated sample, but absent from the control sample.

Compared to the chemical reporters method, ABE does not require metabolic labeling so it can be used to analyze S-acylated proteins in native cells, tissues, and biofluids (Zhou et al., 2014). ABE has been used to analyze global protein palmitoylation in the yeast, which identified thirty five new S-palmitoyl proteins including many SNARE proteins and amino acids permeases as well as other participants in cellular signaling and membrane trafficking pathway (Roth et al., 2006). While ABE has the potential to capture the full S-acylproteome, chemical reporters only capture proteins that are dynamic and turnover during the metabolic labeling window, which indicates that metabolic labeling method is potentially biased towards the enrichment of proteins with fast S-fatty-acylation turnover.

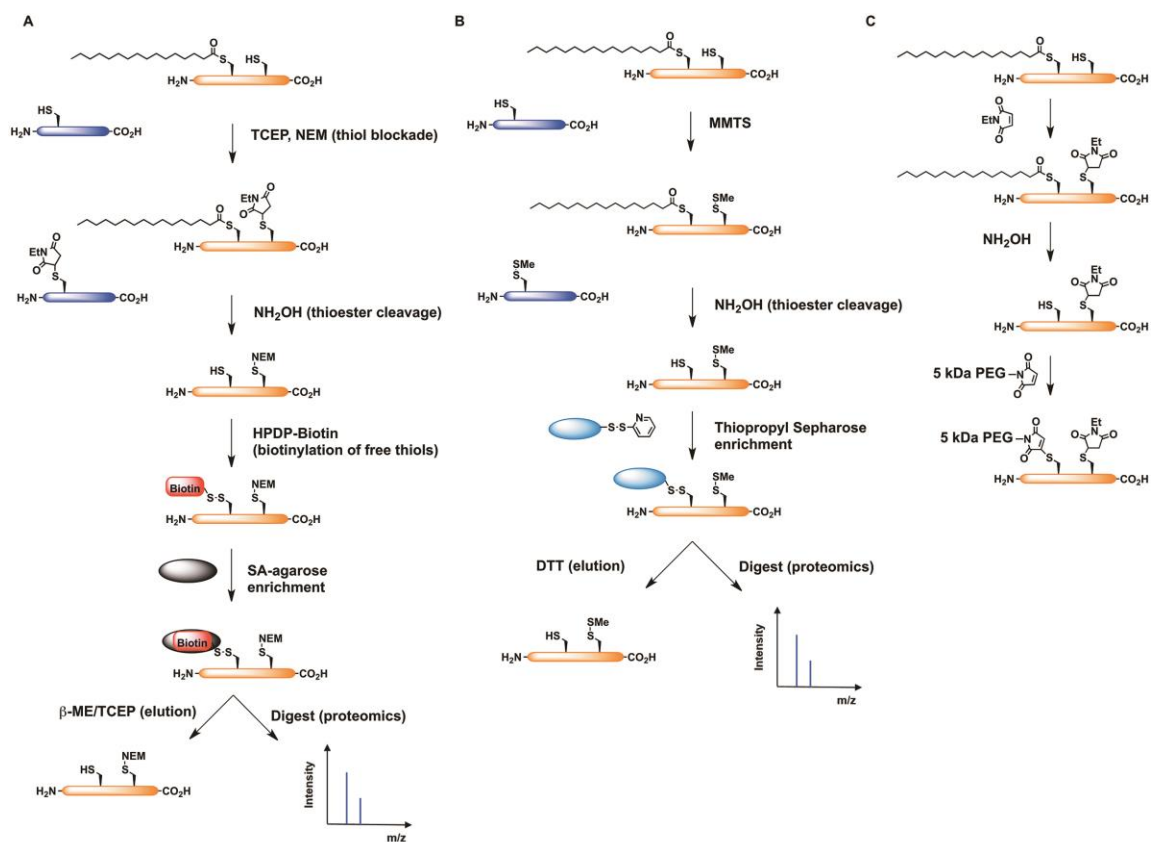


Figure 5. Methods for analysis of fatty-acylated proteins. A) Acyl-biotin exchange (ABE). B) Acyl-RAC. C) Acyl-PEG exchange (APE).

1.2.4 Acyl-RAC method for S-fatty-acylation detection and enrichment

ABE is readily adapted to immunoblotting techniques and is also adaptable to mass spectrometric-based identification of individual S-acylated proteins (Kang et al., 2008; Roth et al., 2006; Yang et al., 2010a). However, the detection of biotinylated proteins requires repeated protein precipitations, SDS neutralization, and streptavidin pull-down. An alternative to ABE that uses the detection of S-acylated proteins via resin-assisted capture (acyl-RAC) instead of biotinylation was proposed (Forrester et al., 2009, 2011; Ren et al., 2013). Specifically, acyl-RAC method was initially described as a methodology to identify S-nitrosylation sites in proteins and later developed to apply on S-fatty-acylation. Coupled with mass-spectrometry proteomics, acyl-RAC can be also used to enrich and identify S-acylproteome (Figure 5B). Compared with ABE, which involves multiple steps of precipitation and resolubilization of samples, acyl-RAC method use thiolpropyl sepharose to eliminate the biotin enrichment steps so the purification scheme is relatively simplified (Zhou et al., 2014). This method can also be generalized to study other cysteine-based reversible modifications, including disulfide formation, S-nitrosylation (SNO), and S-glutathionylation (SSG), by varying reducing reagents such as ascorbate, glutaredoxin, DTT, or NH_2OH , respectively (Guo et al., 2014).

Acyl-RAC has been used to detect S-fatty-acylation of overexpressed and endogenous H-Ras in mammalian cell system in an NH_2OH -dependent manner. Double mutants C181,184S, which are not S-acylated, were not detected, which further validate the specificity of acyl-RAC method. Coupled with mass spectrometry and isobaric labeling method, acyl-RAC was able to identify new S-acylated substrates, such as the β -subunit of the protein translocating system (Sec61b), ribosomal protein S11 (Rps11), and microsomal glutathione-S-transferase 3 (MGST3) (Forrester et al., 2011).

1.2.5 Acyl-PEG exchange method for S-fatty-acylation detection and enrichment

To evaluate endogenous levels of S-fatty-acylation, our laboratory developed a mass-shift labeling method that exploits the NH_2OH -sensitivity of thioesters and selective reactivity of Cys residues for site-specific alkylation with maleimide-functionalized polyethylene glycol reagents, termed acyl-PEG exchange (APE) (Figure 5C). APE induces a mass-shift on S-acylated proteins that can be readily monitored by western blot analysis of target proteins and circumvents the need for metabolic labeling or affinity enrichment of proteins. More importantly, acyl-PEG exchange method reveals the ratio of unmodified versus S-fatty-acylated proteins or multiple sites of S-fatty-acylation, which is critical for understanding how quantitative differences in S-fatty-acylation level control protein function and associated cellular phenotypes. APE provides a sensitive and readily accessible method of evaluating endogenous S-fatty acylation levels and should facilitate the quantitative analysis of this dynamic lipid modification in diverse cell types and tissues (Percher et al., 2016).

1.2.6 Comparison of different methods for protein S-fatty-acylation detection and enrichment

In general, two major methods exist for S-fatty acylation: first is metabolic chemical reporter labeling method, in which synthetic fatty acids analogs with bioorthogonal handles are incorporated into proteins on cysteine residues; the second is to use reversible modifications of cysteine thiols to label S-acylated residues. The two methods complement each other and are best used together to avoid some of the biases.

Firstly, ABE, acyl-RAC, or APE does not require metabolic labeling so it can be used to analyze S-acylated proteins in native cells, tissues, and biofluids. In comparison, chemical reporters metabolic labeling requires feeding and uptake of chemical reporters beforehand. Secondly, ABE, acyl-RAC, APE have the potential to capture the full S-acylproteome, while chemical reporters theoretically only capture proteins that become S-acylated during the metabolic labeling window, which tends to label proteins with fast turnover (Zhou et al., 2014). However, metabolic labeling has considerable advances in the past decade. Development of bioorthogonal reactions enables versatile chemical reporters for various kinds of modifications. The ability to pulse reporters at a specific time into cell culture, tissue or animals provides information about the dynamics of the modification (Martin et al., 2012; Zhang et al., 2010).

1.3 Discovery of new fatty-acylated proteins from chemical proteomics

1.3.1 Summary of proteomics studying using chemical reporter and ABE method

It has been challenging to study protein fatty acylation due to lack of specific antibody and limited methods. However, some of the methods developed as mentioned above enabled specific enrichment and large-scale analysis using mass spectrometry. Metabolic chemical reporters introduce alkyne or azide tag into fatty-acylated proteins, which allows bioorthogonal reactions with affinity tags (e.g., biotin) for selective enrichment and large-scale proteomic identification (Peng et al., 2016). This chemical reporter strategy has been widely employed for the global analysis of N-myristoylated and S-palmitoylated proteins, and can in principle be used for other fatty-acylated proteins. Alternatively, NH_2OH -mediated ABE or acyl-RAC methods utilize HPDP-biotin or thiolpropyl sepharose to capture and enrich S-acylated proteins for mass spectrometry analysis (Thinon and Hang, 2015).

Those selective methods have allowed the large-scale analysis of fatty-acylated proteins in different cell types and animals and more than 300 fatty-acylated proteins have been identified to date, suggesting broader roles of fatty-acylation in regulating eukaryotic biology than previously appreciated (Thinon and Hang, 2015). To label N-myristoylation proteins, alk-12 is preferred reporters because comparative analysis of different analogs like alk-11, alk-12, az-11 and az-12 showed that alk-12 in combination with azide-tagged fluorophores gives minimal background labeling. Alk-12 also labels N-myristoylated proteins better than other longer-chain fatty acid reporters (Charron et al., 2009a; Wilson et al., 2011). However, it becomes complicated when chemical reporters enter the cell and are metabolized to other alkyne containing molecules. It should be also noted that some of

the fatty-acylation process is highly promiscuous which tolerates chemical reporters labeling non-specifically (Jiang et al., 2013). To mediate the artifact effects of false positive candidates, several strategies have been used. First one is to use NMT inhibitors to test whether the enriched proteins are dependent on NMT inhibitors or not to reliably identify NMT substrates. Wright et al. quantitatively profiled N-myristoylation in malaria parasites using chemical reporters, NMT inhibitors and validated NMT as a potential drug target (Wright et al., 2014). Further analysis of global co-translationally and post-translationally N-myristoylated proteome in human cells has identified over 100 NMT substrates, including 40 proteins that are post-translationally N-myristoylated, following caspase cleavage, during apoptosis (Thinon et al., 2014). Further application of this strategy in parasites such as *Leishmania donovani*, revealed 30 high confidence NMT substrates with more than half uncharacterized previously (Wright et al., 2015). However, due to the toxicity of NMT inhibitors, not all the systems will work with this strategy. Another way to differentiate N-myristoylation from other forms of fatty acylation is to use the criteria of possession of N-terminal glycine. Studies on global profiling of host N-myristoylated proteins in cells infected by herpes simplex virus (HSV) or human immunodeficiency virus 1 (HIV-1) revealed protein fatty-acylation during infection (Colquhoun et al., 2015; Serwa et al., 2015). Another N-myristoylation study in the context of bacterial infection was focused on Gram-negative bacteria *Shigella* effector protein IpaJ (Burnaevskiy et al., 2015). IpaJ specifically demyristoylates Golgi-associated ARF/ARL family GTPases during *Shigella* infection which suggests important concerted mechanism of proteolytic demyristoylation.

Proteomics studies on S-fatty-acylation using ABE, acyl-RAC or chemical reporters methods have made a tremendous contribution to our understanding of this reversible modification (Thinon and Hang, 2015). Indeed, there were over 20 proteomics profiling studies on identification of dynamic S-acylated proteins and substrates of DHHC or deacylation enzyme (Table 3). The palmitoyl acyltransferases (PATs) encoded by ZDHHC genes (5 in fission yeast, 7 in budding yeast, 23 in human, 24 in mouse and *Arabidopsis*) are responsible for catalyzing the formation of thioester bond on cysteine residue with fatty acyl-CoA. Since there are redundant genes for this enzymatic activity, one important question that remains to be solved is the function and specificity of each DHHC-PAT enzyme. In cells, DHHC-PATs are localized to different compartments such as the endoplasmic reticulum, the Golgi apparatus, plasma membrane, and endocytic vesicles. The first global study in *Saccharomyces cerevisiae* by Roth et al. compared the differences in the S-fatty-acylation levels of 30 abundant S-acylated proteins before and after the deletion of one to six DHHC-PATs (Roth et al., 2006). They were able to identify 35 new S-palmitoylated proteins and reveal the diverse enzymatic specificities of individual DHHC-PATs. A global analysis of rat neural S-palmitoylome using the ABE method identified most of the known neural palmitoyl proteins and more than 200 new S-palmitoylated protein candidates with diverse functions, including neurotransmitter receptors, transporters, scaffolding proteins, as well as vesicular trafficking proteins (Kang et al., 2008).

S-palmitoylome study using chemical reporters in dendritic cells (DC2.4) identified more than 150 candidate S-palmitoylated proteins and revealed that S-palmitoylation is crucial for the antiviral activity of IFITM3 as well as the activity of Toll-like receptor 2

(TLR2), both of which are crucial immune-related proteins, highlighting the importance of S-fatty-acylation in control of immune response (Chesarino et al., 2014a; Yount et al., 2010). Quantitative proteomics with ABE and Stable Isotope Labeling of Mammals (SILAM) has also enabled protein S-palmitoylation profiling in more complex biological samples (Wan et al., 2013) (Table 3).

The advances that have been made on understanding of protein fatty-acylation and the scale of proteome that is regulated by these modifications enable us to design new drug targets deepen our understanding of the biological function. Though we should also recognize that there are limitations of current methods. The first one is to understand the native S-fatty-acylation of endogenous proteins. Both ABE or metabolic labeling methods ignore or presume the fatty acid to be palmitate. However, other long chain fatty acids like palmitoleate, stearate, oleate, arachidonate, and eicosapentaenoic acid can also modify proteins on cysteine residues. Mass spectrometry analysis of intact S-acylated peptides can provide direct evidence of the fatty acids composition.

Table 3. Summary of literature on proteomics study of fatty-acylated proteins

Species	Method	References
Saccharomyces cerevisiae	ABE	(Roth et al., 2006),
Embryonic rat neurons	ABE	(Kang et al., 2008)
Jurkat T cells	Chemical reporter	(Martin and Cravatt, 2009), (Wilson et al., 2011)
Macrophage	ABE	(Merrick et al., 2011)
Human B cells	ABE	(Ivaldi et al., 2012)
Plasmodium falciparum	ABE/Chemical reporter	(Jones et al., 2012)
Neuronal stem cell	Chemical reporter	(Li et al., 2012)a
Endothelial cell	ABE	(Marin et al., 2012)a,
Mouse brain	ABE	(Wan et al., 2013)

1.3.2 Discovery of IFITMs S-fatty-acylation

Proteomic analysis of fatty-acylated proteins in murine dendritic cell line (DC2.4) using a palmitic acid reporter (alk-16) and bioorthogonal ligation methods by our laboratory recovered known S-palmitoylated proteins (i.e. NRas, CANX) as well as many new candidate S-fatty-acylation proteins such as IFITMs that are directly involved in host immunity to pathogens (Yount et al., 2010) (Figure 6). The S-fatty-acylation on IFITM3 is NH_2OH -sensitive, and loss of S-fatty-acylation by mutagenesis of all three Cys residues inactivates IFITM3. The first two Cys residues are at the edge of the first helical domain while the third Cys is near the second helical domain. The two helical domains are predicted to be transmembrane, but the exact topology of IFITM3 remained to be determined.

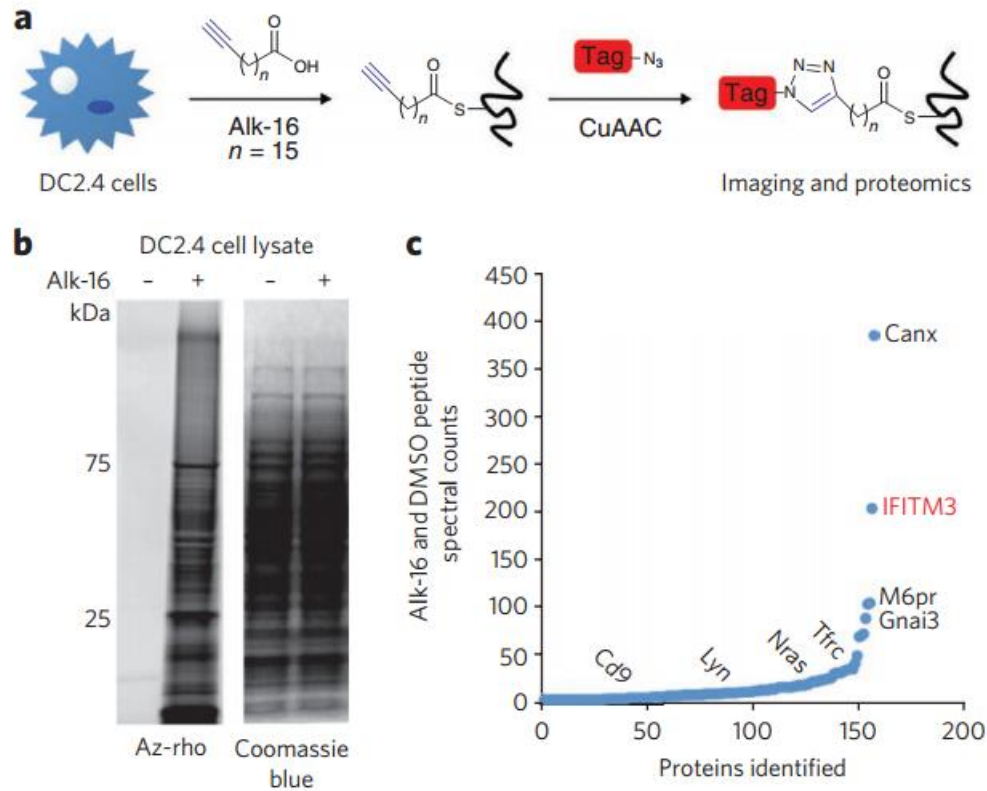


Figure 6. Visualization and identification of S-palmitoylated proteins in dendritic cells. A) Metabolic labeling of cells with alk-16 palmitate reporter and subsequent CuAAC ligation with bioorthogonal detection tags for imaging or proteomics. B) and C) DC2.4 cells were incubated for two hours with 50 mM alk-16 or DMSO as a control. In B), cell lysates were reacted with az-rho by CuAAC, and proteins were separated by SDS-PAGE for visualization by fluorescence gel scanning. Coomassie blue staining demonstrates equal loading. In C), cell lysates were reacted with az-diazo-biotin by CuAAC for the enrichment of alk-16-labeled proteins with streptavidin beads and identification by mass spectrometry. For each identified protein, the ratio of peptide spectral counts from the alk-16 and DMSO samples was plotted. Several known palmitoylated proteins are shown in black. IFITM3, the highest-ranked candidate S-palmitoylated protein, is shown in red. Figure is taken from (Yount et al., 2010).

Chapter Two: Characterization of IFITM3 S-palmitoylation

2.1 Summary

Interferon-induced transmembrane protein (IFITM) family proteins are unique interferon-induced proteins that restrict the infection of multiple pathogenic viruses. Our laboratory discovered that S-palmitoylation and ubiquitination of IFITM3 are critical for its antiviral activity. While overexpression of wild-type mouse or human IFITM3 in mammalian cell lines significantly reduced influenza A virus (IAV) infection, overexpression of the S-palmitoylation deficient (Palm Δ) IFITM3 mutant had no antiviral activity. Notably, mutation of Cys72 to Ala (C72A) in both mouse and human IFITM3 constructs increased the infection level, and additional mutation of Cys71 to Ala (C71A) further reduced the antiviral effect to the level similar to that of Palm Δ IFITM3. Bioinformatics studies on the IFITM family of proteins across 27 vertebrates reveals that CD225 domain and all three cysteines are highly conserved, Especially C72 is more conserved than C71 and C105. To quantify the endogenous levels of IFITM3 palmitoylation, we developed a mass-shift assay based on hydroxylamine-sensitivity of thioesters and selective maleimide-modification of Cys residues, termed the acyl-PEG exchange (APE). Using metabolic chemical reporter labeling and APE methods, we demonstrated that IFITM3 is S-fatty-acylated on three Cys residues, but specific sites and fatty acylation levels are vital for its antiviral activity.

We observed lower protein expression levels of human IFITM3 C72A mutant in HeLa and lung epithelial cells, suggesting S-palmitoylation might regulate the stability of IFITM3. To understand the precise mechanism(s) by which IFITMs prevent virus entry, we generated hIFITM1, 2, 3 deletion cell lines utilizing CRISPR/Cas9 technology. We then performed a cycloheximide (CHX) chase assay in HeLa IFITM2/3 knockout (KO) cell

lines with overexpressed IFITM3 WT and cysteine mutants with or without proteasome/lysosome/p97 inhibitor to identify which pathway is responsible for IFITM3 degradation.

2.2 Introduction

2.2.1 Early findings on IFN-induced effectors

Interferons (IFN) are a group of cytokines made and released from host cells to inhibit pathogen infection by inducing expression of more than 300 IFN-stimulated genes (ISGs) (MacMicking, 2012; Sadler and Williams, 2008). Type I IFNs activate host pathways to inhibit the replication of most viruses. Humans deficient in components of type I IFN signaling are particularly vulnerable to viral disease. This innate system of defense limits viral infections through the induction of ISGs but the antiviral mechanisms for many of these genes remain to be determined.

As early as the 1950s, researchers observed that under certain conditions virus-infected cells are resistant to a second virus infection. It also had been demonstrated that inactivated IAVs can interfere with live IAVs, even though the mechanism or substance that mediates this process was not known (Henle, 1950). In 1957, the term “interferon” was coined by Isaacs & Lindenmann to describe the substance that interferes with IAV (Isaacs and Lindenmann, 1957; Isaacs et al., 1957). By the 1980s, it was shown that IFN is a small protein produced and secreted by cells (Lengyel, 1982). It had been nearly two decades since the initial description of IFN before methods were developed to allow sufficient purification and more rigorous characterization of IFN properties (Pestka, 2007).

2.2.2 Discovery of antiviral activity of IFITMs towards different viruses

IFITM family was recently shown to mediate a significant portion of the IFN-associated response. IFITMs appear to be conserved in vertebrates with 5 homologs in humans (IFITM1, 2, 3, 5 and 10) and 7 in mice (Ifitm1, 2, 3, 5, 6, 7 and 10). Murine embryonic fibroblasts (MEFs) deficient in *Ifitm3* were more readily infected with influenza virus than control cells, before and particularly after treatment with IFN α when compared to wild-type MEFs. In addition, overexpression studies have shown that IFITM3/*Ifitm3* is the most active isoform and also provides antiviral activity against many other pathogenic viruses including, hepatitis C virus (HCV), dengue virus, West Nile virus, vesicular stomatitis virus (VSV), human immunodeficiency virus (HIV), and SARS virus (Bailey et al., 2012; Brass et al., 2009; Everitt et al., 2012; Schoggins et al., 2011; Yount et al., 2010). (Table 4).

Table 4. List of viruses suppressed by IFITMs. Taken from (Perreira et al., 2013)

Virus	Family	Host receptor	Endocytic pathway	Where the virus enters the host cell	pH Requirement ^a
IAV	Orthomyxovirus	α 2,6-linked sialic acid (human)	Clathrin-mediated endocytosis, macropinocytosis	RAB7+ late endosomes	pH 5.5
DENV	Flavivirus	CD14	Clathrin-mediated endocytosis	RAB7+ late endosomes	pH 5.5
West Nile virus	Flavivirus	Unknown	Clathrin-mediated endocytosis	RAB7+ late endosomes	pH 5.5
Yellow fever virus	Flavivirus	Unknown	Clathrin-mediated endocytosis	RAB7+ late endosomes	pH 5.5
Omsk hemorrhagic fever virus	Flavivirus	Unknown	Clathrin-mediated endocytosis	RAB7+ late endosomes	pH 5.5
HCV	Flavivirus	CD81, Occludin, SB-R1, Claudin-1	Clathrin-mediated endocytosis	RAB5+ early endosomes	pH 6.5
SARS CoV	Coronavirus	Angiotensin-converting enzyme 2 (ACE2)	Clathrin-mediated endocytosis	Lysosomes (pH-dependent cleavage: cathepsins B and L)	pH 4.5
MARV	Filovirus	Neimann-Pick C1 (NPC1), T-cell immunoglobulin mucin domain-1 (TIM-1), C-type lectins	Macropinocytosis	NPC1+ lysosomes (pH-dependent cleavage: cathepsins B and L)	pH 4.5
EBOV	Filovirus	Neimann-Pick C1 (NPC-1), T-cell immunoglobulin mucin domain-1 (TIM-1), C-type lectins	Macropinocytosis	NPC1+ lysosomes (pH-dependent cleavage: cathepsins B and L)	pH 4.5
Rift Valley fever virus	Bunyavirus	Unknown	Dynamin II-dependent caveolin-1-mediated endocytosis	RAB7+ late endosomes	pH 5.5
La Crosse virus	Bunyavirus	Unknown	Clathrin-mediated endocytosis	RAB7+ late endosomes	pH 5.5
Andes virus	Bunyavirus	Unknown	Unknown	RAB7+ late endosomes	pH 5.5
Hantaan virus	Bunyavirus	Unknown	Clathrin-dependent endocytosis	RAB7+ late endosomes	pH 5.5
Vesicular stomatitis Indiana virus	Rhabdovirus	LDL receptor	Clathrin-mediated endocytosis	RAB5+ early endosomes	pH 6.5
<i>Scophthalmus maximus</i> rhabdovirus	Rhabdovirus	Unknown	Unknown	Unknown	Stable infectivity between pH 4 and pH 9
HIV-1	Lentivirus	CD4, CXCR4, or CCR5	Unknown	Cell surface, early endosomes	pH Independent
JSRV	Betaretrovirus	Hyaluronidase 2 (Hyal2)	Dynamin-associated endocytosis	RAB5+ early endosomes	pH 6.5
Reovirus	Reovirus	Proteinaceous receptor junction adhesion molecule A (JAM-A)	Clathrin-mediated endocytosis	RAB7+/RAB9+ late endosomes	pH 5.5
<i>Rana grylio</i> virus	Iridoviridae	Unknown	Caveolin-mediated endocytosis	Unknown	pH-dependent

2.2.3 IFITM3 posttranslational modifications, localization and membrane topology

IFITMs are relatively small proteins (133 - 137 amino acids) that were originally predicted to be dual-pass transmembrane proteins based on two hydrophobic domains (Brass et al., 2009). Subsequent biochemical studies from our laboratory revealed that mIFITM3 is also ubiquitinated on four conserved lysines (K24, K83, K88, K104), mostly on K24, which regulates IFITM3 stability, antiviral activity and localization (Yount et al., 2012) (Table 5). Tyr20 was later reported to be phosphorylated (Chesarino et al., 2014b; Jia et al., 2012). The identification of K24 ubiquitination on IFITM3 raised the possibility that the predicted dual-pass transmembrane topology was incorrect since the enzymes responsible for ubiquitin conjugation are localized in the mammalian cytosol (Yount et al., 2012). Subsequent N-linked glycosylation mapping studies and protein lipidation engineering (N-myristoylation and C-prenylation) studies, in conjunction with immunofluorescence analysis and antiviral activity assays from our laboratory suggest that mIFITM3 may be an intramembrane protein where both the N- and C-termini of mIFITM3 have access to the cytoplasm (Yount et al., 2012). In addition to S-fatty-acylation and ubiquitination, phosphorylation of Tyr20 has also been reported to regulate IFITM3 endocytosis from the plasma membrane (Chesarino et al., 2014a; Jia et al., 2014). More recent epitope-mapping studies have also confirmed the cytoplasmic orientation of IFITM3 N-terminus and suggest that the C-terminus may either be luminal or extracellular (Bailey et al., 2013; Weston et al., 2014). These studies collectively suggest that the IFITM proteins may adopt an intramembrane or type II membrane protein topology, or both, in mammalian cells (Figure 7).

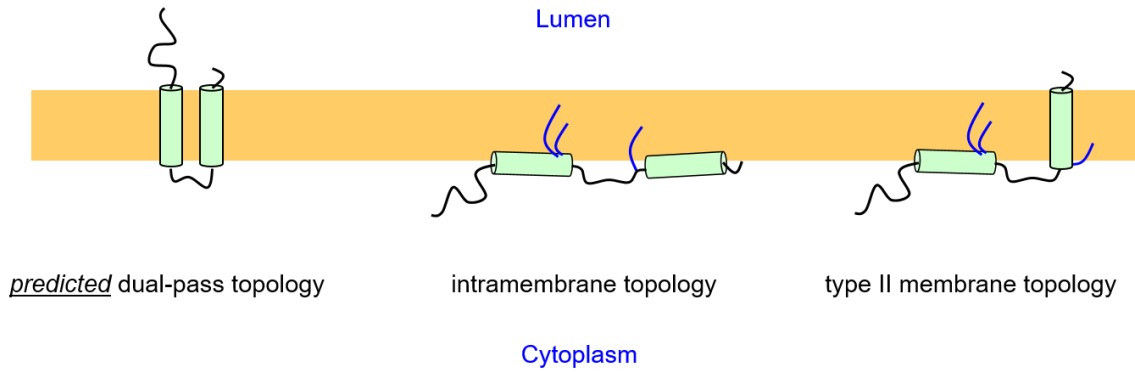


Figure 7. Topology model of IFITM3. From left to right, predicted dual-pass transmembrane topology, intramembrane topology and type II membrane topology models.

Table 5. Summary of post-translational modifications on IFITM3.

Residue	PTM	Function*
Y20	Phosphorylation	Localization
K24	Ubiquitination	Stability, anti-viral activity
C71	S-fatty-acylation	Stability, localization, anti-viral activity
C72	S-fatty-acylation	Stability, localization, anti-viral activity
K83	Ubiquitination	Stability, anti-viral activity
K88	Ubiquitination	Stability, anti-viral activity
K104	Ubiquitination	Stability, anti-viral activity
C105	S-fatty-acylation	Stability, localization, anti-viral activity

- The exact function of each PTM is still not very clear

Our laboratory has further demonstrated the antiviral activity of Ifitm3 is dependent on S-palmitoylation of all three membrane-proximal Cys residues as well as ubiquitination of conserved Lys residues that regulate IFITM3 protein turnover and localization to endolysosomes. However, the precise mechanisms of how S-fatty-acylation of IFITM3 controls its antiviral activity, and protein stability are still unclear. Sequence alignment of IFITM family from human, mouse, and chicken revealed highly conserved cysteine residues across all species (Figure 8), which highlights the importance of S-fatty-acylation during the evolution of IFITM family. To follow up on our previous study of mouse IFITM3, we focused on human IFITM3.

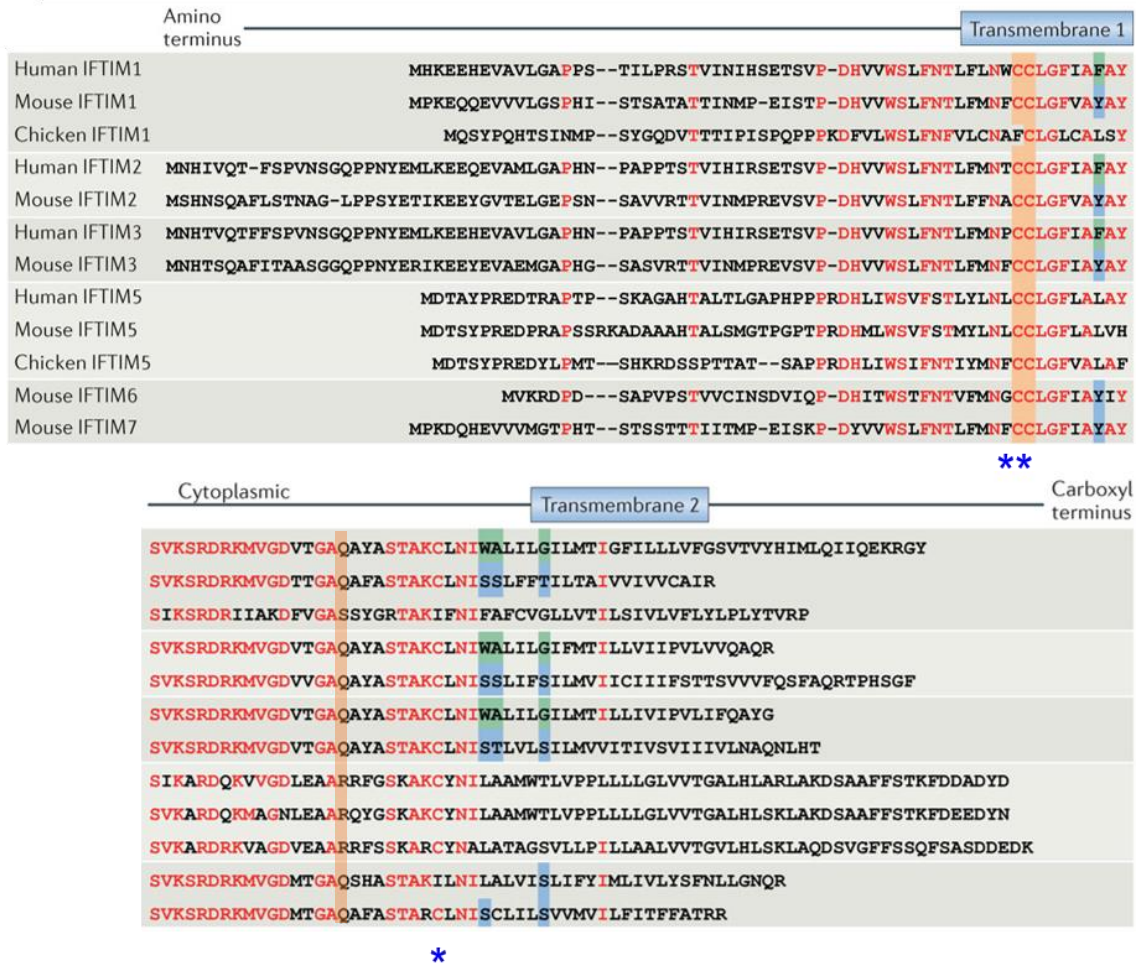


Figure 8. Sequence alignment and predicted topology of IFITM proteins. Human, mouse, and chicken IFITM protein family sequences are aligned. Red residues indicate that at least nine of twelve IFITM proteins are conserved. The site of palmitoylation is highlighted in orange. Green and blue highlighting indicate species-specific signature residues of humans and mice, respectively, possibly suggesting interaction with a cofactor that similarly diverged in each species. Blue stars indicate conserved cysteines position. B) Membrane topology models of IFITM3.

2.3 Results

2.3.1 S-fatty-acylation of human IFITMs

Our lab previously discovered that S-fatty-acylation of membrane-proximal Cys on murine IFITM3 enhances its clustering and is crucial for its inhibitory activity toward influenza virus infection (Yount et al., 2010). However S-fatty-acylation does not appear to influence the protein levels of overexpressed murine IFITM3 in human HeLa cells, as judged by western blot, immunofluorescence, and flow cytometry analysis (Yount et al., 2010), (Figure 9). For our studies of human IFITM3, expression of Cys-to-Ala mutants in A549 revealed that all three Cys residues are S-acylated, indicating a conserved pattern of S-fatty-acylation (Figure 10). Alkynyl palmitate reporter alk-16 was used to detect IFITM3 S-fatty-acylation as shown in Figure 9 and Figure 10. Specifically, 50 μ M Alk-16 was pulsed for one hour after transfection with respective IFITM3 constructs. Cells were then harvested and immunoprecipitated using α -HA antibody conjugated resin. On-bead click chemistry was then performed and the in-gel fluorescence level was measured using Typhoon biomolecule imager. Interesting, the human IFITM3 C72A mutant affects not only its S-palmitoylation but also protein expression levels (Figure 10). C71A has lower expression level compared to the wild-type and but still higher than C72A. We then performed a similar analysis on human IFITM1 and IFITM2 (Figure 11). All three IFITMs orthologues were S-acylated on the conserved Cys. Interestingly, IFITM2 and IFITM3 showed doublet bands in in-gel fluorescence results while IFITM1 only showed a single band. Sequence alignment showed IFITM1 has a shorter N-terminal domain, but all three proteins have conserved CD225 domain including three Cys at similar positions near the helical domain (Figure 9). Mutagenesis analysis of single Cys to Ala showed that the

middle Cys expressed consistently lower level proteins, which suggests a conserved function of this key Cys residue on IFITM protein stability (Figure 11)

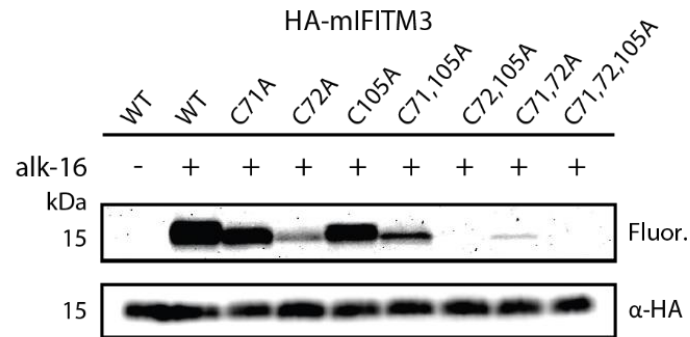


Figure 9. S-fatty-acylation of murine IFITM3 and Cys mutants. NIH3T3 cells transfected with HA-mIFITM3 constructs were metabolically labeled for two hours with 50 μ M alk-16. Cell lysates prepared with 1% Brij 97 were subjected to immunoprecipitation with anti-HA agarose beads, reacted with az-rho by CuAAC, separated by SDS-PAGE and visualized by fluorescence gel scanning. Comparable protein loading was confirmed by anti-HA western blotting (Data from Jacob Yount).

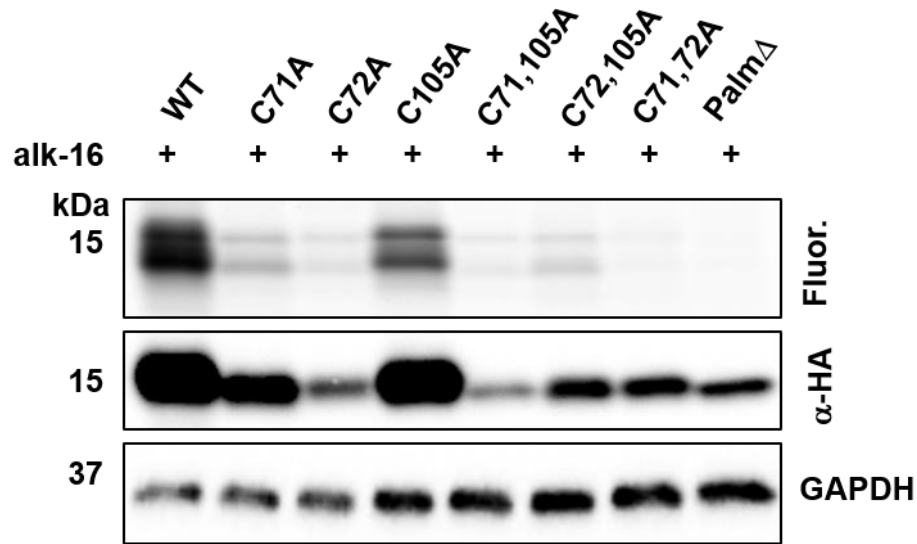


Figure 10. S-fatty-acylation of human IFITM3 and Cys mutants in A549 cells. Human IFITM3 plasmid was subcloned into N-HA vector to create pCMV-HA-hIFITM3 plasmid. Single, double and triple (Palm Δ) mutations were made using QuikChange II XL Site-Directed Mutagenesis Kit (Agilent). A549 cells were plated in growth medium without antibiotics the day before the experiment and then transfected with indicated plasmids using Lipofectin® 2000 (Invitrogen). After 18 hours of incubation, cells were labeled with alk-16 reporter for one hour. Cells were then lysed in 1% Brij97 buffer with EDTA-free protease inhibitors. After centrifugation to get rid of cell debris, the supernatant was immunoprecipitated with EZview™ anti-HA agarose (Sigma-Aldrich). After washing with RIPA buffer for three times, on beads click chemistry was then performed and incubated for one hour at room temperature. Beads were washed again with RIPA buffer for three times before adding loading buffer and subject to SDS-PAGE. Two identical gels are subjected to western blot analysis and in-gel fluorescence respectively.

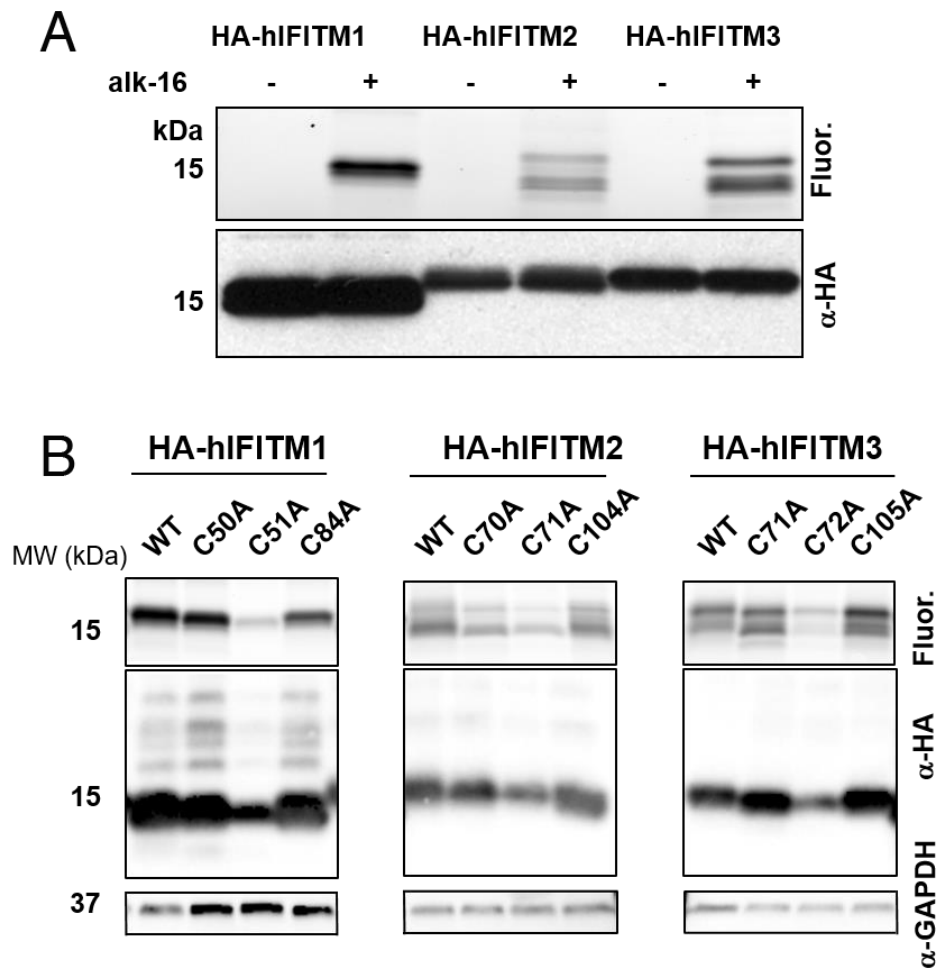


Figure 11. S-fatty-acylation of human IFITMs in HEK293T cells. In-gel fluorescence detection of alk-16 labeled proteins and α -HA western blot of the same gel were performed to show protein expression and S-fatty-acylation. A) Wild-type pCMV-HA-IFITM1, pCMV-HA-IFITM2, and pCMV-HA-IFITM3 were transfected into HEK293T cells before labeling with Alk-16. B) Single cysteine mutations IFITM1 C50A, C51A, C84A, IFITM2 C70A, C71A, C104A and IFITM3 C71A, C72A, C105A, were labeled with alk-16 and S-palmitoylation was measured using in-gel fluorescence.

2.3.2 Characterization of endogenous and site-specific S-fatty-acylation levels of IFITM3 in mammalian cells

Our site-directed mutagenesis studies and alk-16 labeling revealed that all three Cys residues can be S-acylated. However, mutation of Cys to Ala may affect properties other than S-fatty-acylation and does not reveal the endogenous levels of IFITM3 S-fatty-acylation. To address these challenges, our laboratory has developed a mass-shift detection method based on NH_2OH -sensitivity of thioesters and selective maleimide-modification of Cys, termed acyl-PEG exchange (APE). The protocol of APE is discussed in Chapter 1.2. We first tested APE for detection of S-fatty-acylation of endogenous IFITM3 from NIH3T3 and Raw264.7 cell lines (Figure 12), which revealed three slower migrating PEGylated polypeptides in SDS-PAGE that likely correspond to the mono-, di-, and tri-S-fatty-acylated isoforms of mIFITM3. Unmodified IFITM3 is far less abundant than the PEGylated proteins, which indicated that most of the endogenously expressed mIFITM3 in IFN-stimulated cells are S-acylated on one or more Cys residues. The analysis of endogenous human IFITM3 in A549 cells also revealed similar results to mouse IFITM3 (Figure 13). Endogenous Calnexin 1 (CANX) that is dually S-palmitoylated was used as a control for protein loading and APE (Lakkaraju et al., 2012).

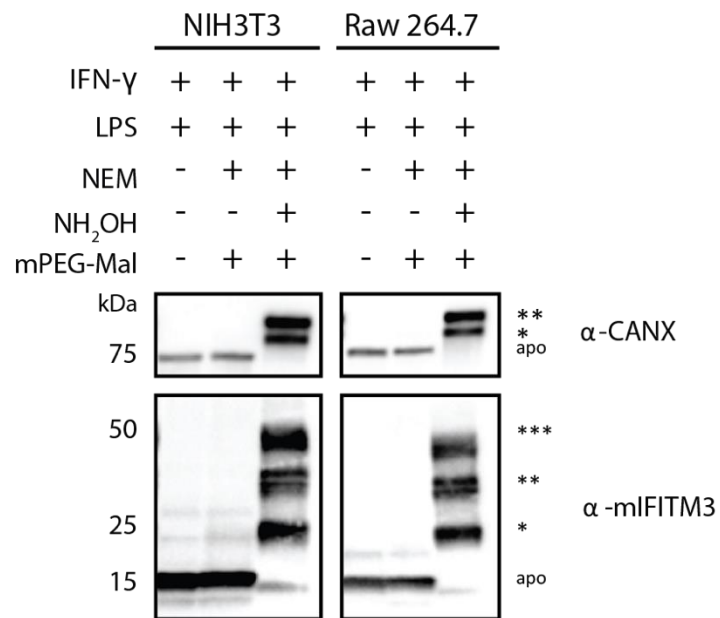


Figure 12. Endogenous mIFITM3 S-palmitoylation assessed by APE. NIH3T3 or RAW264.7 cells were activated with 500 ng /mL LPS, 100 U/mL IFN- γ for 16 hours, subjected to APE, separated by SDS-PAGE and analyzed by western blot (Data from Percher et al., 2016)

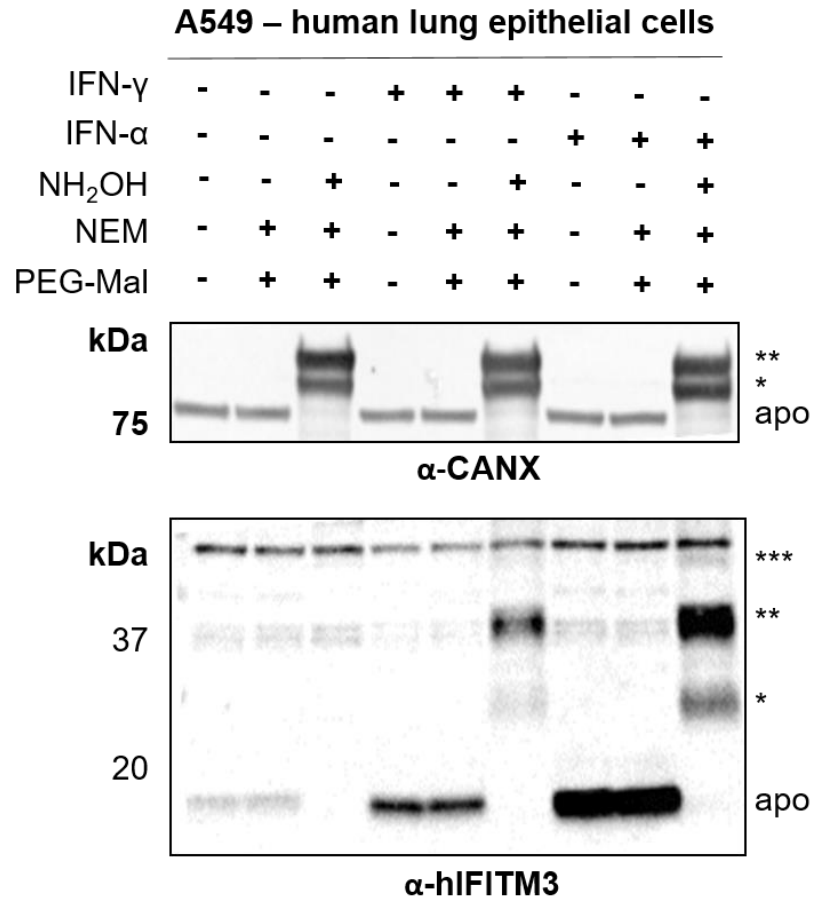


Figure 13. Endogenous human IFITM3 S-fatty-acylation in A549 cells. A549 cells were activated with 500 ng/mL LPS, 100 μ g/mL IFN- γ or IFN- α for 16 hours, subjected to APE, separated by SDS-PAGE and analyzed by western blot. (Data from Percher et al., 2016)

To evaluate the contribution of individual Cys residues on IFITM3 S-fatty acylation levels, we generated single and double Cys mutants and analyzed their levels of S-fatty acylation by APE and metabolic labeling methods. APE analysis of the wild-type and the individual Cys to Ala HA-mIFITM3 mutants transfected into unstimulated murine NIH3T3 fibroblasts showed that mutation of Cys71 and 105 to Ala eliminated the tri-S-acylated fraction and decreased the levels of the mono- and di-S-acylated mIFITM3. In contrast, the C72A mutant or multiple Cys mutants containing C72A abrogated the tri- and di-S-acylated IFITM3 and even lost the mono-S-acylated fraction for C72,105A mutant (Figure 14). A similar trend was also observed for human IFITM3 APE experiment (Figure 15). The comparison of APE and alk-16 labeling suggests that while the C72A IFITM3 mutant is still significantly mono-S-fatty-acylated, the majority of fatty acid metabolic labeling is abrogated (Figure 10 and Figure 15). These data suggested that quantitative differences of dynamic S-fatty-acylation may contribute to the function of IFITM3.

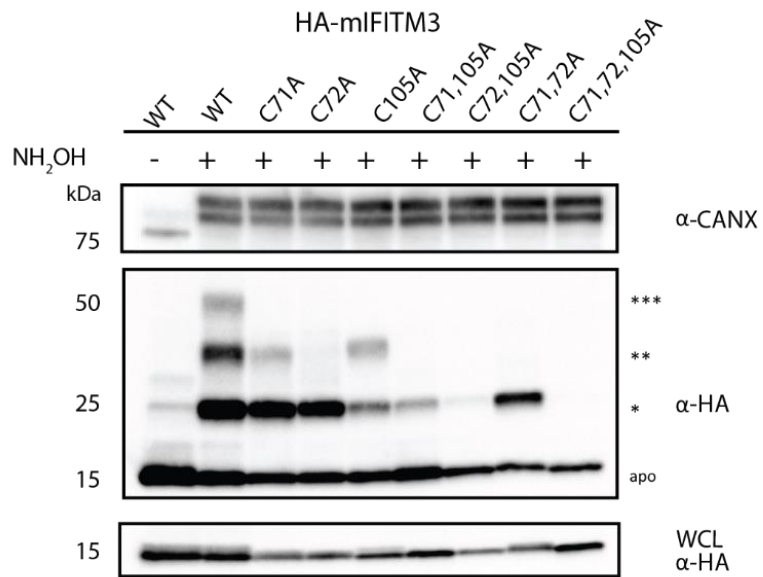


Figure 14. APE analysis of overexpressed mIFITM3 and Cys mutants. NIH3T3 cells transfected with WT HA-mIFITM3 or Cys to Ala mutant constructs were subjected to APE, separated by SDS-PAGE and analyzed by western blot. Analysis of whole cell lysate (WCL) indicates levels of protein expression without APE.

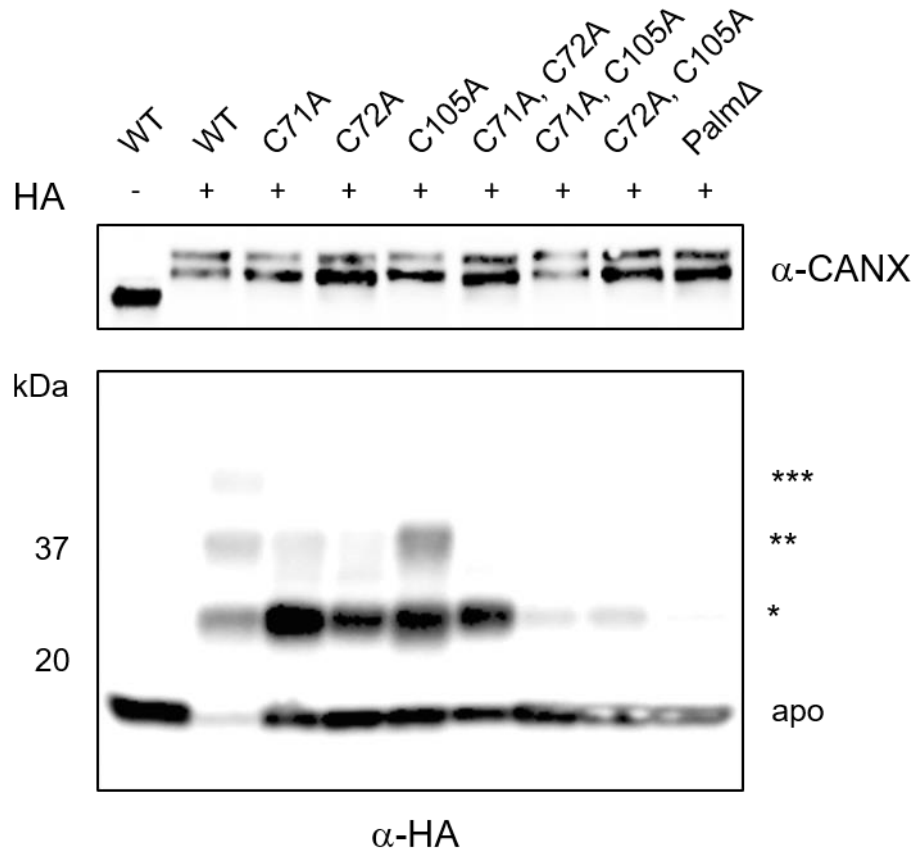


Figure 15. APE of overexpressed human IFITM3 and mutants. HEK293T cells transfected with WT and mutant HA-IFITM3 constructs were analyzed using APE protocol. For the wild-type sample, with or without hydroxylamine (HA) controls were both used. Star indicated the mono-, di-, and tri-S-palmitoylated species.

2.3.3 Anti-influenza virus activity of IFITM3 S-palmitoylation mutants

We next evaluated the antiviral activity of IFITM3 Cys mutants using flow cytometry staining with influenza virus NP-specific antibodies, as previously described by our laboratory (Yount et al., 2010, 2012). The analysis of HA-IFITM3-Palm Δ mutant activity against H1N1 influenza virus (type A, PR8 strain) infection confirmed this S-palmitoylation deficient has decreased antiviral activity. Interestingly, both mouse and human IFITM3 C72A had significantly less activity compared to C71A (Figure 16). Moreover, C71, 72A double mutant showed loss of activity similar to the level of Palm Δ , which suggested that C71 and/or C72 are necessary for the activity of IFITM3. On the other hand, C71A hardly affected antiviral activity, which suggests a crucial role of Cys72 S-fatty-acylation for the full antiviral activity of IFITM3. Note that single C105A mutant also had decreased activity to a very low level especially for mouse IFITM3, however IFITM3 double mutants C71,72A with only one Cys105 was inactive (Figure 16) indicating Cys105 is essential but not sufficient for the activity of IFITM3.

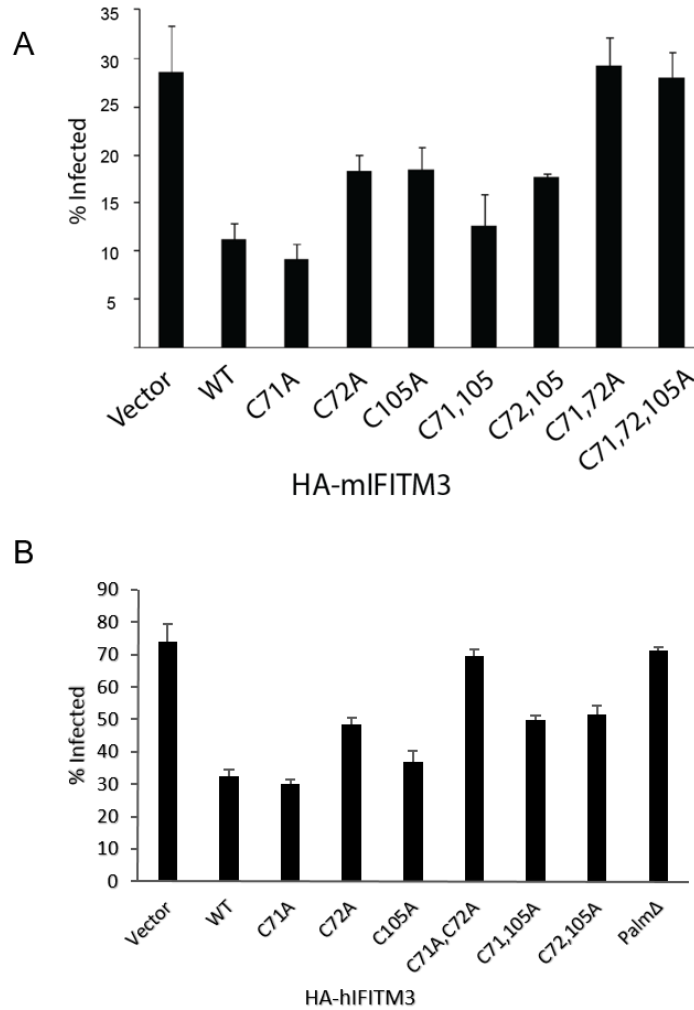
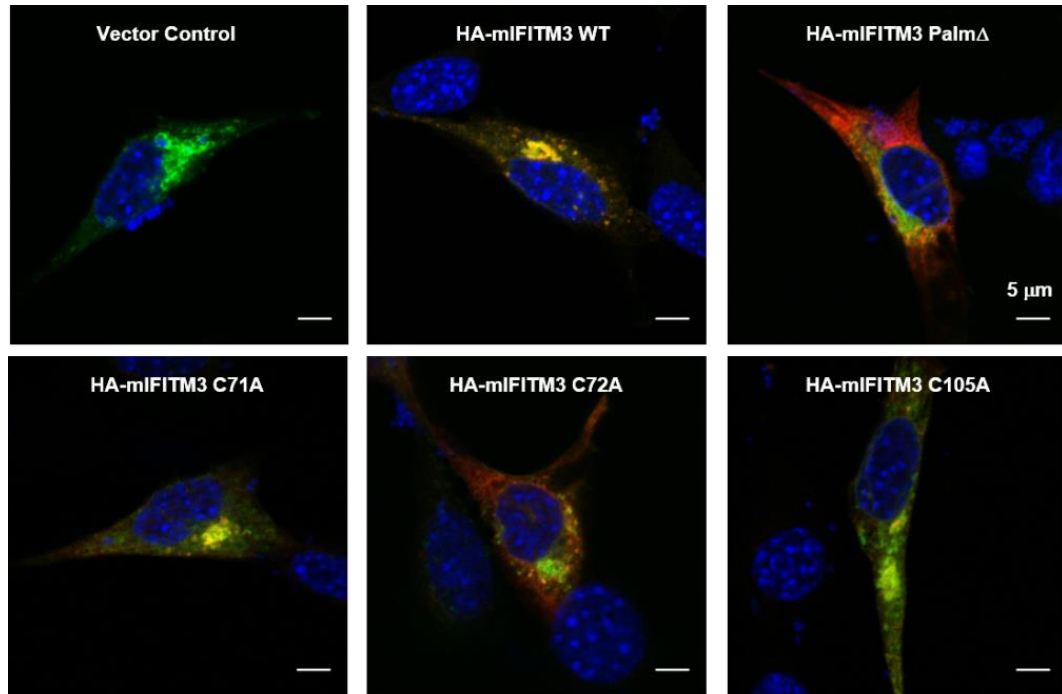


Figure 16. Antiviral activity of WT and IFITM3 Cys mutants. A) NIH3T3 fibroblasts were transfected with vector or HA-mIFITM3 plasmids, then infected with influenza A virus (PR8 strain) for six hours and analyzed by flow cytometry using α -HA antibody to identify HA-mIFITM3 expressing cells and α -NP to analyze the number of IAV-infected cells. B) HEK293T cells were transfected overnight with indicated plasmids before a 6-h infection with influenza virus at a multiplicity of infection of 2.5 and analyzed by flow cytometry. Cells expressing IFITM3 constructs were analyzed for the percentage of cells that were infected using influenza specific anti-NP antibodies.

2.3.4 Immunofluorescence analysis of IFITM3 Cys mutants in mammalian cells.

To understand the mechanism of action of IFITM3 S-fatty-acylation, we investigated the influence of S-palmitoylation on IFITM3 expression and distribution in cells. Immunofluorescence analysis revealed that mIFITM3 is distributed into punctate clusters. Loss of S-palmitoylation led to decreased co-localization with lysosome marker LAMP1 (Figure 17). However, the quantitative analysis did not show enough statistical difference between IFITM3 WT and C72A mutant. Similarly, we transfected human IFITM3 WT and Cys mutants in HeLa cells and analyzed their colocalization with GFP-LAMP1 (data not shown). Even though we initially observed altered colocalization of hIFITM3 C72A and PalmD with GFP-LAMP1, these differences were not still not statistically significant.



Staining: Nuclear (DAPI), Lysosome (LAMP1-GFP), HA-mIFITM3 (α -HA)

Figure 17. Imaging of HA-mIFITM3 in NIH3T3 fibroblasts. NIH3T3 cells grown on coverslips in 12-well plates were transfected with one μ g pCMV-HA-mIFITM3 WT, C71A, C72A, C105A and Palm Δ and stained with anti-HA (red) and DAPI (blue). Scale bars represent five μ m. Cells were also co-transfected with lysosomal markers, LAMP1-GFP (green).

2.3.5 Protein turnover of human IFITM3 and Cys mutants

To understand how Cys mutation affects IFITM3 protein stability, we investigated whether S-fatty-acylation affected IFITM protein stability in cycloheximide (CHX) chase experiments. For these experiments, CHX is added to cells, and the decay in the steady-state level of a target protein is monitored by immunoblotting. Normalized protein expression data is then fitted into protein decay model to calculate rate constant and half-life. I then compared the differences between wild-type IFITM3 and Cys mutants. To avoid the complication of endogenous IFITM3, our lab has generated IFITM3 knockout HeLa and A549 cell lines, using CRISPR-Cas9 gene targeting technology (Ruina He).

For the IFITM3 turnover experiments, IFITM2/3 $-/-$ knockout HeLa cells were used to avoid heterotypic interaction with endogenous IFITMs. Transient expression of IFITM3 WT, C72A, and Palm Δ plasmids was performed in IFITM2/3 $-/-$ knockout cells, which were then treated with inhibitors at different concentrations for 12 hours before analysis using immunoblotting (Figure 18). Quantification of normalized proteins level showed that proteasome, lysosome, and p97 inhibitors can increase protein expression. Interestingly, the p97 inhibitor ML240-treated sample showed the highest expression level and stability. ML240 is a selective, ATP-competitive inhibitor of p97/VCP. VCP has been shown to mediated turnover of ubiquitin-labeled proteins for recycling or degradation by the proteasome but also has functional relevance to lysosomal degradation for similar proteins to IFITM3 such as caveolin (Meyer et al., 2012).

After I identified working concentration for different inhibitors at a single time point, I profiled dynamic changes of protein expression at various time points (Figure 19). IFITM2/3 $-/-$ HeLa cells were transfected with hIFITM3 WT, C72A, and Palm Δ constructs.

After transfection for 16 hours, 25 $\mu\text{g/ml}$ CHX was added to the cell culture to inhibit protein synthesis. Cells were harvested at designated time points and snap-frozen for further analysis. After lysis with 4% SDS buffer, protein expression level in homeostasis was detected using α -HA and α -GAPDH immunoblotting. Triplicates of the same experiment were performed and the normalized IFITM3 expression level was plotted. I then fit the data using one-phase decay from Graphpad Prism (Figure 20). Rate constants of IFITM3 WT, C72A, and Palm Δ were calculated (Table 6).

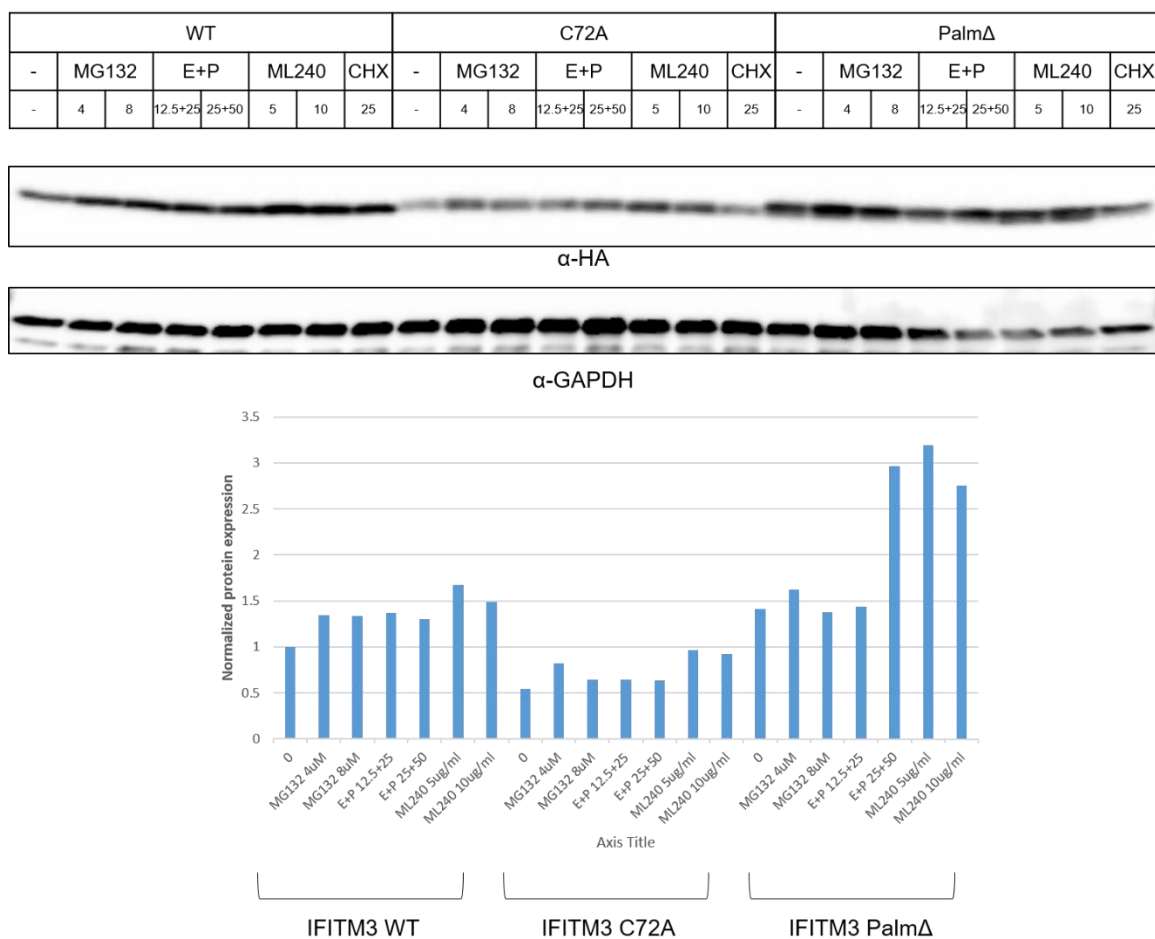


Figure 18. Protein turnover of IFITM3 WT, C72A, and PalmΔ in HeLa IFITM2/3 ^{-/-} cell line. HeLa IFITM2/3 ^{-/-} cells were plated into 12-well plates before transfection. pCMV-HA-IFITM3 WT, C72A, and PalmΔ were transfected respectively followed by treatment with proteasome and lysosome inhibitors. Cells were harvested after 12-hour incubation and were analyzed for α-HA and α-GAPDH. Normalized protein level

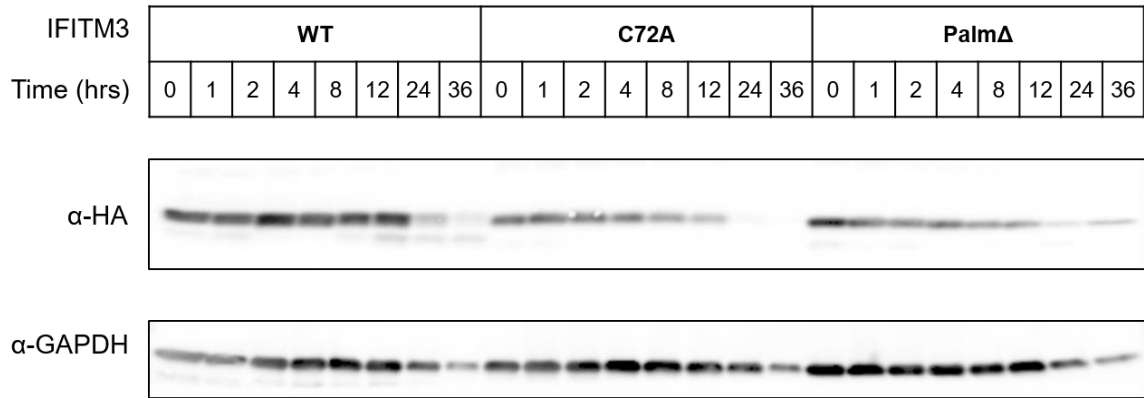


Figure 19. Cycloheximide-chase analysis of IFITM3 turnover. HeLa IFITM2/3 $-/-$ cells were plated into 12-well plates before transfection. pCMV-HA-IFITM3 WT, C72A, and PalmΔ were transfected respectively and were treated with cycloheximide (CHX) after 18 hours. Cells were harvested at indicated hours and were analyzed for immunoblotting α -HA and α -GAPDH. Cycloheximide is an inhibitor of protein biosynthesis in eukaryotic organisms, produced by the bacterium *Streptomyces griseus*. Due to the inhibition of overall protein synthesis, by measuring the degradation rate of existing IFITM3 proteins, we can measure the half-life of each construct.

Table 6. Rate constant and half-life of CHX chase experiment.

	WT	C72A	PalmΔ
K (hr⁻¹)	~ 7.857e-005	0.1643	0.03655
Half-Life (hr)	~ 22	4.22	18.97

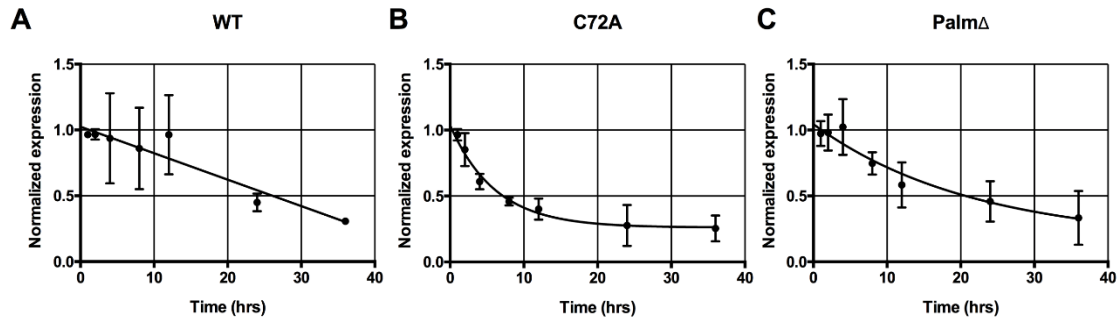


Figure 20. Determination of rate constant and protein degradation half-life. Data of cycloheximide chase experiments. Triplicates of the degradation experiments were performed and the normalized data was fit with one phase decay model using GraphPad Prism.

Triplicates of the cycloheximide chase experiments were fitted with the non-linear curve model. Best-fit values of the curve showed that WT IFITM3 was relatively stable at half-life of ~22 hours, while the half-life of C72A mutant is 4.22 hours and PalmΔ 18.97 hours. The rate of protein degradation of IFITM3 was increased to ~5-fold with C72A mutation. Interestingly, PalmΔ IFITM3 with three Cys residues mutated is relatively more stable than C72A, which is consistent with the western blotting data (Figure 10). The loss of stability associated with Cys72 mutation also partly contributed to the lower antiviral activity of this construct compared to other Cys mutants during the antiviral assay (Figure 16). We then want to understand the mechanism of action of how IFITM3 is degraded and why C72 is essential to keep IFITM3 stable.

2.3.6 Effects of protein degradation pathway inhibitors

To understand which degradation pathway was responsible for IFITM3 degradation, we used specific inhibitors of proteasome, lysosomal protease and p97 to measure the dynamics under those inhibitor treatments. Similar to cycloheximide-chase experiment, HeLa IFITM2/3 *-/-* cells were transfected with IFITM3 C72A construct and were treated the CHX and respective inhibitors for designated hours (Figure 21). After immunoblotting with α -HA and α -GAPDH, protein expression level was then normalized to plot on the non-linear model.

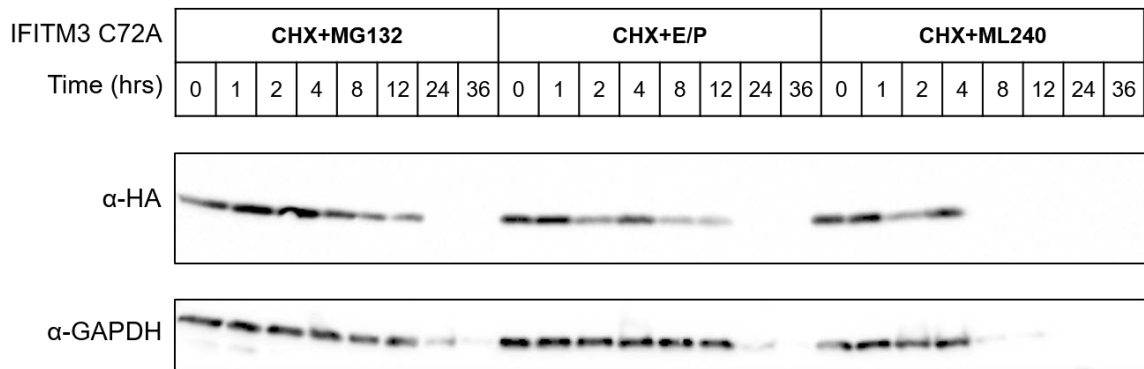


Figure 21. Cycloheximide with inhibitors chase experiment. HeLa IFITM2/3 *-/-* cells were transfected with IFITM3 C72A and were treated with CHX plus proteasome (MG132), lysosome (E/P), or p97 (ML240) inhibitors. Cells were harvested at indicated time points and snap-frozen. Samples were analyzed by immunoblotting of α -HA antibody and α -GAPDH antibody. Cells were mostly dead after 24 hr incubation with CHX+MG132 or E/P. CHX+ML240 was much more toxic to cells as most cells were dead after 8 hours.

Because of the toxicity of cycloheximide with degradation inhibitors, most cells died after 12 hours, especially for CHX plus ML240 samples. So I only use the data from the first 12 hours. After plotting with Graphpad Prism, we were able to get the half-life of inhibitor-treated samples (Table 7). Interestingly, all three inhibitors increased the stability of IFITM3, with ML240 having the most effect. The half-life of C72 was increased from 4.22 hours to 7.95, 6.38, and 20.26 hours respectively. Since p97/VCP is involved in both endosome-lysosome membrane fusion and proteasome degradation pathway, the prominent effect of p97 inhibition might suggest that IFITM3 is degraded through both proteasome and lysosomal pathway.

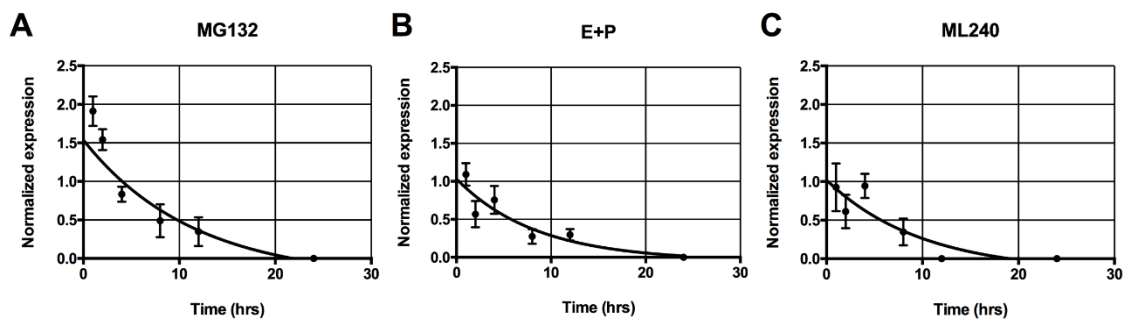


Figure 22. Analysis of protein degradation with inhibitors. Triplicates of the degradation experiments were performed and the normalized data was fit with one phase decay model using GraphPad Prism.

Table 7. Determination of rate constant using one phase decay model.

	CHX+MG132	CHX+E/P	CHX+ML240*
K (hr⁻¹)	0.08723	0.1086	~ 0.03421
Half Life (hr)	7.946	6.381	~ 20.26

2.4 Discussion

2.4.1 Key sites of human IFITM3 S-fatty-acylation

Bioinformatics analysis of IFITM isoforms from 27 vertebrate genomes representing from diverse animals (reptiles, amphibian, fish, birds, primates and other mammals) shows that these three S-fatty-acylated Cys residues (C71, 72 and 105 in mIFITM3) are amongst the most highly conserved amino acids within this family of membrane proteins (Figure 8) (Hickford et al., 2012; Zhang et al., 2012). All three Cys residues of IFITM3 are S-palmitoylated, APE and alk-16 experiment showed that endogenous IFITM3 is mostly S-fatty-acylated in IFN-stimulated cells and that S-fatty acylation of specific Cys residues and levels are crucial for IFITM3 antiviral activity against influenza virus. In murine and human IFITM3, even though Cys71 is highly conserved this residue is dispensable for dual-S-fatty acylation and antiviral activity. In contrast, Cys72 in IFITM3 is the most prominent site of S-fatty-acylation and results in the loss of antiviral activity when mutated to Ala. The S-fatty-acylation and antiviral activity of Cys105 may depend on the IFITM isoform, expression levels, and cell-type, as the mutation of this Cys residue decreases murine IFITM3 antiviral activity but is not required for human IFITM3 activity. From CHX chase experiments, C72A and Palm Δ mutants dramatically decreased protein stability of IFITM3, while protein degradation inhibitors restored some but not all of C72A stability. In summary, antiviral activity results from our laboratory and others (John et al., 2013; Yount et al., 2010), S-fatty-acylation assay, and protein turnover experiments suggests Cys72 in IFITM3, at the edge of the first helical domain, plays a critical role in IFITM3 function.

Protein hydrophobicity analysis using Kyte & Doolittle plot with nine amino acids as a window shows that IFITM3 protein contains two major hydrophobic regions. Experimental results with in vitro recombinant expression of IFITM3 without S-palmitoylation also showed insolubility without detergent solubilization. So without lipidation IFITM3 is also intrinsic membrane protein. However, ultracentrifugation experiment showed there is a higher percentage of IFITM3 Palm Δ in soluble fraction compared to IFITM3 wide type purified from mammalian cell lysate, indicating an enhanced membrane attachment ability with S-palmitoylation. Indeed, multiple other membrane proteins are also S-palmitoylated at the same time such as Calnexin, GPCRs. The reasons for such addition lipidation are multi-fold. First of all, attachment of palmitate acids increases the membrane affinity of the membrane protein. Secondly, S-palmitoylation in many cases specifies the membrane subdomain to which modified proteins are localized.

2.4.2 Lipid composition of IFITM3 S-fatty-acylation

A key drawback of chemical reporter labeling method is its inability to distinguish the fatty acid species that are incorporated into the candidate proteins. Although palmitate is the major modification, other long chain fatty acids like palmitoleate, stearate, oleate, arachidonate, and eicosapentaenoic acid can also modify proteins on cysteine residues (Liang et al., 2001). To determine the composition of fatty acids attached to a particular S-fatty-acylation site, mass spectrometry analysis of intact S-acylated peptides can provide direct evidence. It has been shown that at least singly or dually S-palmitoylated peptides can be separated by C18 reversed-phase liquid chromatography and sequenced by mass spectrometry (Ji et al., 2013). It is important to know about the lipid composition because the levels and composition of fatty acids *in vivo* can determine the strength and specificity of immune responses that are essential for host resistance to pathogens and inflammatory metabolic diseases such as type 2 diabetes (Stienstra et al., 2012).

2.4.3 Protein stability regulated by S-fatty-acylation

S-fatty-acylation has been implicated in regulating proteins stability in multiple proteins (Linder and Deschenes, 2007). For example, the viral membrane glycoprotein of Rous sarcoma virus and two G-protein-coupled receptors, the A₁ adenosine receptor and the chemokine receptor CCR5 showed reduced stability when S-palmitoylation is defective (Gao et al., 1999; Percherancier et al., 2001). S-palmitoylation of SNARE complex in *S. cerevisiae* and anthrax-toxin receptor trafficking in mammalian cells protects proteins from degradation by preventing their ubiquitination (Abrami et al., 2006; Valdez-Taubas and Pelham, 2005) The SNARE complex protein Tlg1 was recently shown to have opposing roles of palmitoylation and ubiquitination in regulating its half-life. Tlg1 is an essential target-membrane SNARE in *S. cerevisiae* that mediates the fusion of vesicles with the late Golgi compartment (Siniossoglou and Pelham, 2001; Valdez-Taubas and Pelham, 2005).

Similarly, IFITM3 was shown to be regulated by ubiquitination and S-palmitoylation (Yount et al., 2012). Previously ubiquitination was shown to control IFITM3's stability while S-fatty-acylation affects its anti-viral activity but not its protein level. From the CHX chase experiments, C72A and Palm Δ dramatically decreased the protein half-life of IFITM3 which suggested that S-fatty-acylation, especially, on Cys72 residue indeed affect IFITM3's stability. We also observed that the loss of stability associated with Cys72Ala was more prominent in A549 cells than HEK 293T cells. Since transfection efficiency is much higher in HEK293T cells, more episomal IFITM3 was expressed in HEK293T cells than A549 cells, which may cause overwhelming of normal protein degradation pathway.

Another point worth noted regarding the methodology used for analyzing protein stability is the toxicity with CHX plus protein degradation inhibitors. Cells treated with either CHX or protein degradation inhibitors showed less cell death than combined. Cell death caused by drugs treatment might interfere with the results. One way to lower the toxicity is to use radioactive pulse-chase approach. First, radioactive labeling with (35)S-methionine is carried out to label newly synthesized proteins (pulse). Subsequently, the dynamics of the decay of these proteins is monitored in the absence of labeled amino acids over a defined time period (chase). CHX is not needed for this method, thus may reduce the cell death rate. A systematic analysis using radioactive pulse-chase with protein degradation inhibitor might provide a more conclusive results on the protein degradation pathway.

2.4.4 Differences between murine and human IFITM3

The effect about lower protein expression level was only observed in human but not murine IFITM3 Cys72Ala mutants, probably because of the differences between two species and there is added complicated regulatory mechanism for human IFITM3. Sequence alignment of murine and human IFITM3 showed that the central domains are highly conserved with overall 66% identity. The amino acids from Ser53 to Ile108 are basically same between human and mouse except position 70, where it is Pro in human, but Phe in mouse. Proline is sometimes known as "helix breakers" because they disrupt the regularity of the α helical backbone conformation. Since Pro is close to Cys71 and Cys72, it might be possible that the change from mouse Phe70 to human Pro70 causes disparity on Cys72Ala mutation protein stability.

2.4.5 Effect of S-fatty-acylation on protein localization

To understand the functional significance of IFITM3 S-fatty-acylation, we wanted to investigate whether the loss of fatty acylation will affect its localization inside the cell. Study of mIFITM3 transiently expressed in HeLa cells showed S-fatty-acylation controls clustering of IFITM3 in membranes rather than its trafficking to distinct cellular compartments (Yount et al., 2010). In another study, single Cys mutation C72A of human IFITM3 in A549 cells exhibited a more centralized expression pattern, although no colocalization marker was shown in the image (John et al., 2013). Our study on the murine and human IFITM3 WT, single Cys mutants, and palmitoylation-deficient mutant in either NIH3T3 cells or HeLa cells confirmed the previous observation that WT IFITM3 is colocalized with lysosomal marker LAMP1 and partly with Rab5 and Rab7. However, no significant effects on protein localization for Cys mutants were observed. The reason for no change in localization of Cys mutations might be due to the fact that IFITM3 has different S-fatty-acylation states inside the cell. Some of them are functional against virus infection while the others are relatively inactive. The subtle change of the proper S-fatty-acylated species may not be obvious among all IFITM3 population. New site-specific lipidation methods and imaging in live cells as well as more detailed biophysical methods will be required to evaluate how S-fatty-acylation controls IFITM3 antiviral activity.

2.5 Materials and methods

2.5.1 Materials

E. coli DH5 α (Invitrogen) was used for plasmid propagation and isolation. Oligonucleotides were obtained from Integrated DNA Technology. Nucleotides were synthesized from Integrated DNA Technologies (IDTdna). Plasmid DNA was purified using Qiagen Mini and Maxi prep kits. Metabolic chemical reporter (alk-16) and fluorescent dye were synthesized in the lab. QuikChange site-directed mutagenesis kit from Agilent was used for mutation experiments. HEK293T cells, HeLa cells were obtained from ATCC.

2.5.2 Metabolic incorporation of chemical reporters of protein fatty acylation in living cells

Serum-containing complete cell culture medium (DMEM, invitrogen) was replaced with cell culture medium, supplemented with 2% charcoal/dextran-filtered FBS. Cells were labeled with either DMSO as a solvent control or 20 to 100 μ M (final concentration) alkyne-fatty acid chemical reporter (Alk-16) for one hour at 37 $^{\circ}$ C. Cell pellets were then lysed with 4% SDS buffer with EDTA-free protease inhibitors and 1 μ l (250 U) of Benzonase (Sigma-Aldrich). Protein concentration was determined using a standard BCA assay (Olson and Markwell, 2001). Aliquots of equal amounts of protein (~50 μ g) were dispensed into 1.5-ml microcentrifuge tubes, and were brought to 44.5 μ l with 4% SDS buffer with EDTA-free protease inhibitors.

2.5.3 Copper(I)-catalyzed alkyne-azide cycloaddition labeling of cell lysates

5.5 μ l click chemistry master mix (1 μ l of 5 mM azido-rhodamine in DMSO, 1 μ l of 50 mM TCEP, 2.5 μ l of 2 mM TBTA in 1:4 (v/v) DMSO/butanol, 1 μ l of 50 mM CuSO₄) was added to the protein sample (44.5 μ l) from method 2.5.2, and vortex to mix. Samples are incubated for 1 hour at room temperature, followed by a chloroform/methanol precipitation of protein to remove unreacted azido-rhodamine by adding the following ice-cold reagents to each tube: 200 μ l methanol, 75 μ l chloroform, and 150 μ l water. Mixture was vortexed and centrifuged for 15 min at 20,000 \times g, at 4 $^{\circ}$ C. The solution in the tube was separated into three phases: the clear upper aqueous layer, the pink-colored lower organic layer, and a white layer of protein between the two layers. Remove and discard the upper aqueous phase, leaving the lower organic phase and the white layer of protein between the two layers. 1 ml of ice-cold methanol was added to each sample and mix gently, causing the protein pellet to sink to the bottom of the tube. Centrifuge 10 min at 20,000 \times g, 4 $^{\circ}$ C. All of the liquid was removed by pipetting, being careful not to disturb the pellet and then wash the protein pellet by adding 1 ml of ice-cold methanol and inverting the tube. Centrifuge 10 min at 20,000 \times g, 4 $^{\circ}$ C. After carefully removing the methanol, the remaining methanol was dried by leaving the sample tubes open on the bench for 20 min at room temperature. Protein pellets were then dissolved in 50 μ l of 4% SDS buffer with EDTA-free protease inhibitors to dissolve the protein pellets. 4 \times LDS sample buffer (Invitrogen) and 2-mercaptoethanol were then added and the samples were heated for 5 min at 95 $^{\circ}$ C; 20 μ L of the sample was loaded per gel lane for separation by SDS-PAGE (4–20% Bio-Rad Criterion Tris-HCl gel).

2.5.4 Immuno-precipitation using antibody-conjugated resin for click chemistry reaction

Cells were lysed in Brij97 buffer (1% Brij 97, 50 mM TEA, 150 mM NaCl, pH 7.4) and protein concentration was determined using the BCA assay. Add 500-1000 mg protein in 100 uL Brij97 buffer to a dolphin tube. Prewashed α -HA-conjugated agarose (Sigma) in Brij97 buffer (Use 15 uL Sigma agarose per sample) was added to protein sample and incubate over the nutating mixer at 4 °C for 1h. Agarose was spun down for 1 min at 9000x g to remove the supernatant. Agarose resin was then washed three times with 500 uL RIPA wash buffer (50 mM TEA, 150 mM NaCl, 1% Na-Deoxycholate, 1% Triton X 100, 0.1% SDS). Beads were resuspended in 22.5 uL 4% SDS buffer and 2.5 uL click chemistry master mix was added to the beads to incubate for 1 h. 4x blue buffer/BME (165 uL blue buffer with 35 uL BME) was added after incubation followed by vortexing and boil for 5 min. Samples were spin down beads and load gel. After running SDS-PAGE, gels were imaged by TyphoonTM scanner (GE Healthcare).

2.5.5 Site mutagenesis using QuikChange methods for Cysteine mutants

Site-directed mutagenesis was done using Agilent QuikChange II Site-Directed Mutagenesis Kit (<http://www.agilent.com>). Primers used in the experiments are listed in Table 8.

Table 8. Sequences of primers for site-directed mutagenesis of IFITM3 cysteine mutations.

Primer name	Sequence
mIFITM3-C71A-F	acacttctcatgaactcgcctgcctgggcttcatagc
mIFITM3-C71A-R	gctatgaagcccaggcaggcgaagttcatgaagagtgt
mIFITM3-C72A-F	ctcttcatgaacttctgcgcctgggcttcatagccta
mIFITM3-C72A-R	taggctatgaagcccaggcgcagaagttcatgaagag
mIFITM3-C105A-F	cgcctccaactgctaaggcctgaacatcagcacc
mIFITM3-C105A-R	ggtgctgatgttcaggccttagcagtggaggcg
hIFITM1-C50A-F	ccctcttctgaactgggcctgtctgggcttcatag
hIFITM1-C50A-R	ctatgaagcccagacaggcccagttcaagaagagg
hIFITM1-C51A-F	cctcttctgaactggtgcgctctgggcttcatagcattc
hIFITM1-C51A-R	gaatgctatgaagcccagagcgcaccagttcaagaagagg
hIFITM1-C84A-F	cctccaccgccaaggcctgaacatctggg
hIFITM1-C84A-R	cccagatgttcaggccttggcggtggagg
hIFITM2-C70A-F	cccttctcatgaacaccgctgcctgggcttcatag
hIFITM2-C70A-R	ctatgaagcccaggcaggcgggttcatgaagagg
hIFITM2-C71A-F	ctcttcatgaacacctgcgcctgggcttcatagcatt
hIFITM2-C71A-R	aatgctatgaagcccaggcgcaggtgttcatgaagag
hIFITM2-C104A-F	cctccaccgccaaggcctgaacatctggg
hIFITM2-C104A-R	cccagatgttcaggccttggcggtggagg
hIFITM3-C71A-F	cctcttcatgaaccccgcctgcctgggcttcata

hIFITM3-C71A-R	tatgaagcccaggcaggcgggggttcatgaagagg
hIFITM3-C72A-F	cttcatgaaccctgcgccctgggcttcatagca
hIFITM3-C72A-R	tgctatgaagcccaggcgcaggggttcatgaag
hIFITM3-C105A-F	cctccaccgccaaggccctgaacatctggg
hIFITM3-C105A-R	cccagatgttcaggccttggcggtggagg

2.5.6 Transfection of mammalian cell lines

Cells were seeded to be 70–90% confluent at transfection. Medium was changed to Opti-MEM® for transfection. DNA-lipid complexes were made by mixing Lipofectamine® Reagent with DNA plasmids in Opti-MEM® Medium. After 10 min incubation, DNA and Lipofectamine® 2000 reagent mixture was added to cells for 16 hours and then check for expression.

2.5.7 S-fatty-acylation detection using acyl-PEG exchange

Cell samples were lysed with 4% sodium dodecyl sulfate (SDS, Fischer) in TEA buffer (pH 7.3, 50 mM triethanolamine (TEA), 150 mM NaCl) containing 1x protease inhibitor cocktail (Roche), 5 mM PMSF (Sigma), 5 mM EDTA (Fischer) and 1500 units/mL benzonase (EMD). The protein concentration of the cell lysate was then measured using a BCA assay (Thermo), and adjusted to 2 mg/mL with lysis buffer. Typically, 200 µg of total protein in 92.5 µL of lysis buffer was treated with 5 µL of 200 mM neutralized tris(2-carboxyethyl)phosphine (TCEP, Thermo) for final concentration of 10 mM TCEP for 30 minutes with nutation. N-ethylmaleimide (NEM, Sigma), 2.5 µL from freshly made 1 M stock in ethanol, was added for a final concentration of 25 mM and incubated for 2 hours

at room temperature. Reductive alkylation of the proteins was then terminated by methanol-chloroform-H₂O precipitation (4:1.5:3) with sequential addition of methanol (400 μ L), chloroform (150 μ L) and distilled H₂O (300 μ L) (all pre-chilled on ice). The reactions were then mixed by inversion and centrifuged (Centrifuge 5417R, Eppendorf) at 20,000 g for 5 minutes at 4° C. To pellet the precipitated proteins, the aqueous layer was removed, 1 mL of pre-chilled MeOH was added, the eppendorf tube inverted several times and centrifuged at 20,000 g for 3 minutes at 4° C. The supernatant was then decanted, and the protein pellet washed once more with 800 μ L of pre-chilled MeOH, centrifuged again and dried using a speed-vacuum (Centrivap Concentrator, Labconco) To ensure complete removal of NEM from the protein pellets, the samples were resuspended with 100 μ L of TEA buffer containing 4% SDS, warmed to 37° C for 10 minutes, briefly (~5 seconds) sonicated (Ultrasonic Cleaner, VWR) and subjected to two additional rounds of methanol-chloroform-H₂O precipitations as described above.

For hydroxylamine (NH₂OH) cleavage and mPEG-maleimide alkylation, the protein pellet was resuspended in 30 μ L TEA buffer containing 4% SDS, 4 mM EDTA and treated with 90 μ L of 1 M neutralized NH₂OH (J.T. Baker) dissolved in TEA buffer pH 7.3, containing 0.2% Triton X-100 (Fisher) to obtain a final concentration of 0.75 M NH₂OH. Protease inhibitor cocktail or PMSF should be omitted, as these reagents can interfere with the NH₂OH reactivity. Control samples not treated with NH₂OH were diluted in 90 μ L TEA buffer with 0.2% Triton X-100. Samples were incubated at room temperature for 1 hour with nutation. The samples were then subjected to methanol-chloroform-H₂O precipitation as described above and resuspended in 30 μ L TEA buffer containing 4% SDS, 4 mM EDTA, warmed to 37° C for 10 minutes and briefly (~5 seconds)

sonicated and treated with 90 μ L TEA buffer with 0.2% Triton X-100 and 1.33 mM methoxypolyethylene glycol-maleimide (mPEG-Mal, 5 or 10 kDa, Sigma) for a final concentration of 1 mM mPEG-Mal. Samples were incubated for 2 hours at room temperature with nutation before a final methanol-chloroform-H₂O precipitation. Dried protein pellets were resuspended in 50 μ L 1 X Laemmli buffer (BioRad) and then heated for 5 minutes at 95° C. Typically, 15 μ L of the sample was loaded in 4-20% Criterion-TGX Stain Free polyacrylamide gels (Bio-Rad), separated by SDS-PAGE and analyzed by western blot. For western blots, primary antibodies used were anti-calnexin (1:2000 ab22595, Abcam), anti-Pan Ras (1:500, Ras10, Millipore), anti-mouse IFITM3 (1:1000, ab15592, Abcam) anti-FLAG (1:1000, F1804, Sigma) anti-HA (1:1000, ab9134, Abcam), and HRP-conjugated anti-HA (3F10, Roche). Secondary antibodies used were HRP-conjugated goat anti-rabbit (DC03L, Calbiochem), and goat-anti-mouse (ab97023, Abcam). Protein detection was performed with ECL detection reagent (GE healthcare) on a BioRad ChemiDoc MP Imaging System.

2.5.8 Microscopy

For determination of IFITM3 localization, transfected HeLa cells were fixed with 3.7% (w/v) paraformaldehyde, permeabilized with 0.2% (w/v) saponin or 1% (v/v) Tween and blocked with 2% (v/v) FBS in PBS. Cells were incubated with individual antibodies for 30 min in sequence starting with mouse anti-HA (1/1,000, 16B12, Covance), then goat anti-mouse antibodies conjugated to rhod- amine red (1/1,000, Invitrogen), then rabbit antibodies against specific cellular markers or cholera toxin B conjugated to Alexa-488 (Invitrogen) followed by sec- ondary goat anti-rabbit antibodies conjugated to Alexa-488

(1/1,000, Invitrogen). All antibodies were diluted in PBS and 0.2% (w/v) saponin, except for cholera toxin B staining in which PBS and 1% (v/v) Tween 20 was used in all steps. Antibodies against calreticulin (1/500, ab2907, Abcam), LAMP1 (1/500, ab24170, Abcam), EEA1 (1/100, 2411, Cell Signaling) and golgin-97 (1/100, ab33701, Abcam) were used. Cells were incubated with TOPRO-3 (1/1,000, Invitrogen) as a final step.

2.5.9 Infections, fluorescence microscopy, and flow cytometry

Influenza virus A/PR/8/34 (H1N1) was propagated in 10-day embryonated chicken eggs for 40 h at 37° C and titrated using Madin-Darby canine kidney cells. Cells were infected at a multiplicity of infection of 2.5 for 6 h before fixation and staining. For Salmonella typhimurium infections, strain IR715 was used, and infections were performed as previously described (18). For both flow cytometry and microscopy, cells were fixed with 3.7% paraformaldehyde in PBS for 10 min followed by a 10-min permeabilization with 0.2% saponin in PBS and a 10-min blocking step with 2% FBS in PBS. Cells were stained using anti-HA anti-antibody (Covance, clone 16B12) directly conjugated to Alexa-488, -555, or -647 using kits for 100 µg of antibody available from Invitrogen. Anti-NP (Abcam, ab20343) was directly conjugated to Alexa-647 using a similar kit. Likewise, anti-myc (Clontech, 631206) was conjugated to Alexa-488. All conjugated antibodies were used at a 1:200 dilution in 0.2% saponin in PBS for 30 min at room temperature for both microscopy and flow cytometry. Anti-calreticulin (Abcam, ab2907) was used at a 1:1000 dilution followed by a goat anti-rabbit secondary conjugated to Alexa-488 (Invitrogen). TOPRO-3 (Invitrogen) was used at a 1:1000 dilution in PBS for 10 min to stain nuclei as a final step in some experiments before glass slide mounting in ProLong Gold Antifade Reagent (Invitrogen).

Chapter Three: Site-specific incorporation of unnatural amino acid into IFITM3 in mammalian cells

3.1 Summary

To understand IFITM3 function and regulation in mammalian cells, I explored the site-specific incorporation of unnatural amino acids (UAAs) using amber codon suppression for potential live-cell imaging and protein crosslinking studies. We chose the pyrrolysyl-tRNA synthetase (PylRS)/Pyl tRNA_{CUA} system from *Methanosarcina* species due to its ability to incorporate structurally diverse UAAs. Using this technology, I systematically evaluated sites in mouse and human IFITM3 for the incorporation of UAAs. By screening amber codon (TAG) mutants, I identified several IFITM3-TAG mutants that showed with high expression levels and no truncation products. Notably, both mouse and human IFITM3 F8TAG mutant (Phe8 mutated to the amber codon TAG) showed consistent expression in mammalian cells. The full length IFITM3 amber codon mutants labeled with UAAs were S-fatty-acylated and showed antiviral activity similar to wild type. Notably, these IFITM3 amber codon mutants could be site-specifically labeled with lysine analogs for bioorthogonal labeling studies *in vitro* and living cells. Furthermore, we showed that IFITM3 amber codon mutants could also be labeled with photo-crosslinkable UAA, DiZPK, for site-specific protein crosslinking in living cells. These studies demonstrate IFITM3 can be site-specifically labeled with UAAs for potential live cell imaging and protein crosslinking studies.

3.2 Introduction

3.2.1 Overview of site-specific protein labeling

Amber codon suppression technology has enabled the site-specific incorporation of unnatural amino acids bearing uniquely reactive functional groups into proteins in yeast (Hancock et al., 2010), bacteria (Liu and Schultz, 2010), mammalian cells (Gautier et al., 2010; Lang et al., 2012; Mukai et al., 2008), and animals (Bianco et al., 2012; Greiss and Chin, 2011) via the evolution of orthogonal aminoacyl-tRNA synthetase/tRNA pairs (Figure 23). Site-specific labeling of the proteins with unnatural amino acid containing unique chemical reactivity has provided scientists with new tools for understanding basic biology and drug development (Krall et al., 2015). Notably, the incorporation of unnatural amino acids containing bioorthogonal chemical handles and photocrosslinkers are providing new opportunities for imaging studies and protein-protein interaction studies, respectively.

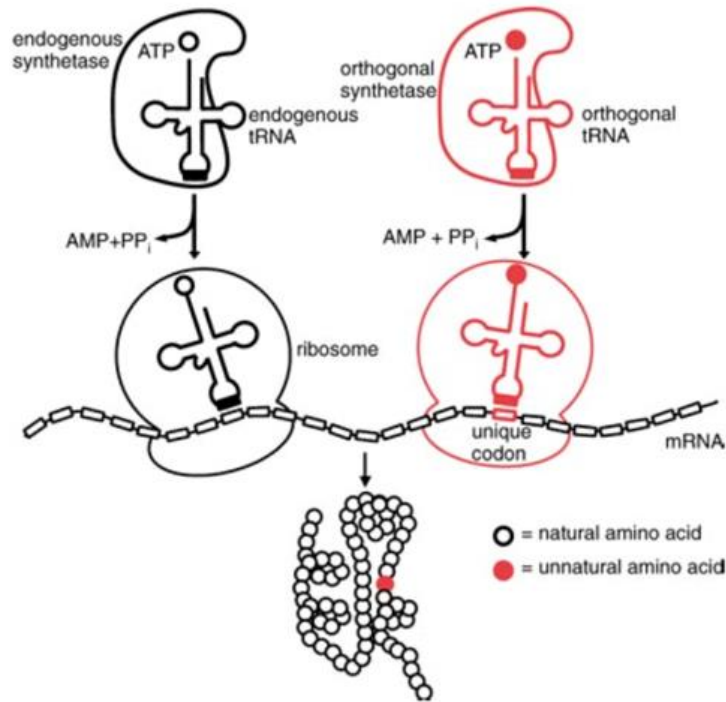


Figure 23. Site-specific incorporation of UAAs using amber codon suppression.

Orthogonal synthetase and tRNA are introduced to the host cells. After adding unnatural amino acids that are compatible with the orthogonal pair but not with endogenous machinery, they will be incorporated into specific positions (unique codon, such as amber codon). Figure is taken from (Wang et al., 2001).

3.2.2 Application of unnatural amino acids for imaging

The site-specific incorporation of unnatural amino acids enables powerful new approaches to control and image proteins of interest at a site-specific level. While genetic fusion of fluorescence protein (GFP, RFP) to the protein of interest is the most common method to do imaging, because it is easy to implement and has greatly advanced our understanding of protein localization and function, GFP fusion may disturb the structure and function of the protein and can be only placed at the N- or C- terminus. The size of GFP is ~27 kDa, which may be too big for the purpose of protein labeling, and may disturb the structure or localization of the fused proteins, especially if the protein has a small size. By using unnatural amino acids, we are able to genetically incorporate fluorescent amino acids or bioorthogonal amino acids that can ligate with a fluorophore later. With respect to established methods for fluorescently labeling proteins, the incorporation of unnatural amino acids has minimal perturbations to protein structure and is therefore unlikely to interfere with the function and localization of proteins as approaches using fusions or tagging can.

The ability to introduce amino acids with functional side chains combined with bioorthogonal chemistry greatly expands available toolbox to study protein structure and function (Liu and Schultz, 2010). Progress on discovery and invention of bioorthogonal reactions that do not react with natural entities inside the cell but selectively react with each other greatly promoted the development of new methods to visualize, identify, and analyze different classes of biomolecules (Figure 24) (Prescher and Bertozzi, 2005; Sletten and Bertozzi, 2009). The combination of site-specific labeling and bioorthogonal chemistry provides new opportunities for precise imaging studies *in vitro* and in cells.

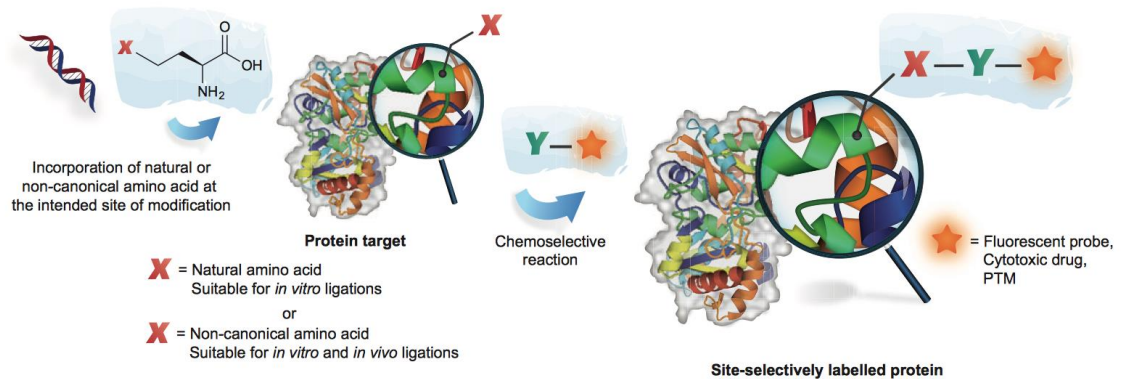


Figure 24. Site-specific protein labeling. To label protein of interest, the first step is to incorporate a natural or unnatural amino acid to the intended site of modification. The inserted molecule would be chemoselectively reacted with a fluorescent probe, an affinity tag, or PTM analog. The resulting molecule can be either visualized by fluorescence imaging, analyzed by proteomics or modulated as a “gain/loss of function” (PTM, antibody-drug conjugate, or *in situ* activation).

The two-step method used by bioorthogonal chemistry involves 1) incorporation of unnatural amino acids with tailor-made side chain and 2) bioorthogonal reaction with the externally added chemical probe. For the first step, an orthogonal synthetase/tRNA pair is required for incorporation. An orthogonal aminoacyl-tRNA synthetase does not recognize any endogenous tRNAs in the host cell, but specifically aminoacylates its cognate orthogonal tRNA. On the other hand, endogenous aminoacyl-tRNA synthetases do not accept an orthogonal tRNA. Translational incorporation of amino acid substrates of the orthogonal aminoacyl-tRNA synthetase responds to a blank codon, most commonly the amber stop codon.

One example using unnatural amino acids strategy to investigate previous intractable protein is G-protein coupled receptors (GPCRs) (Figure 25). GPCR is a

particularly important class of cell-surface receptors that represent targets for more than a quarter of all therapeutic drugs (Daggett and Sakmar, 2011). Amber codon suppression method allows site-specific labeling of GPCRs with various molecular probes to facilitate cell-based studies of protein–protein or protein–ligand interactions and the visualization of conformational changes using fluorescence spectroscopy or single-molecule imaging. UAAs such as p-benzoyl-L-phenylalanine (BzF), p-acetyl-L-phenylalanine (AcF), and p-azido-L-phenylalanine (azF) into heterologously were able to be expressed in GPCRs in mammalian cells (Grunbeck et al., 2011; Huber et al., 2013; Tian et al., 2013).

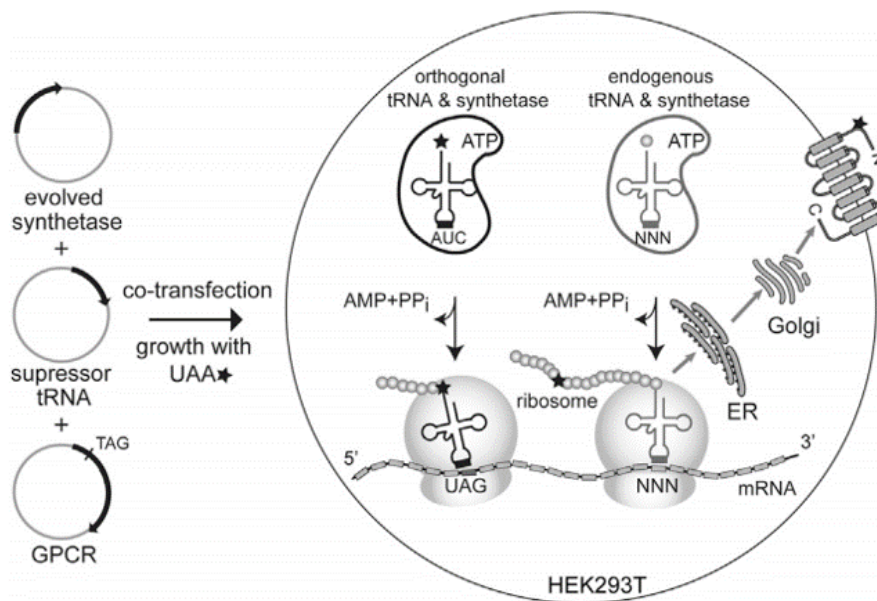


Figure 25. Using UAA to study GPCR. Amber stop codon (UAG) suppression technology has been used to study GPCR functions. HEK293T or HEK293F cells are cotransfected with three different plasmids encoding the evolved synthetase gene, the suppressor tRNA gene, and the gene encoding the GPCR with an in-frame TAG mutation at a desired position. Culturing the transfected cells in the presence of the UAA results in protein translation, with suppression of the amber stop codon and site-specific incorporation of the UAA at a desired position to give a full-length protein. Figure taken from (Huber and Sakmar, 2014)

Live-cell imaging using amber suppression requires rapid and compatible bioorthogonal ligation with fluorophores (Figure 26). Cu^I-azide-alkyne cycloaddition (CuAAC) reaction has a reasonable reaction rate, but the toxicity of Cu^I makes it hard to use this method to label live cells (Figure 26A). To solve this problem, strain-promoted, copper-free azide-alkyne cycloaddition was developed to provide alternatives for live-cell

imaging. The tagging of azide-containing glycan with cyclooctyne conjugates has been explored previously (Figure 26B) (Agard et al., 2004). Strained cyclooctynes enabled rapid labeling of cell-surface azides for dynamic cell imaging. However, the dynamic rate of cyclooctyne-azide ligation is still low with the first generation around $0.0012 \text{ M}^{-1}\text{S}^{-1}$. Further development of more reactive cyclooctyne compounds includes dibenzycyclooctynes and biarylazacyclooctynone compounds. Even with these modifications, the most reactive version showed rate constants from ~ 0.1 to $1 \text{ M}^{-1}\text{S}^{-1}$. Moreover, synthesis of the cyclooctyne probes is demanding and often low-yielding.

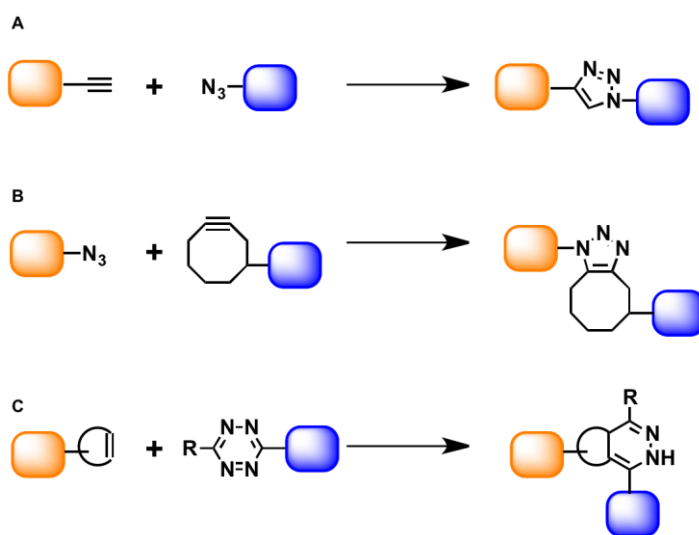


Figure 26. Bioorthogonal ligations. A) Cu^{I} -azide-alkyne cycloaddition (CuAAC). B) Strain-promoted alkyne-azide cycloadditions (SPAAC). C) inverse-electron-demand Diels-Alder cycloaddition (IEDDA).

The recent development of unnatural amino acids bearing components of the inverse-electron-demand Diels-Alder cycloaddition (IEDDA) can react exceptional fast with fluogenic dyes with second-order rate constants in the range of 10^2 – $10^4 \text{ M}^{-1} \text{ s}^{-1}$ (Figure 26C) (Lang and Chin, 2014). UAAs that contain strained alkene Bicyclo[6.1.0]nonyne-

lysine and *trans*-cyclooctene-lysine (BCNK and TCOK) have been incorporated into epidermal growth factor receptor (EGFR) to demonstrate the specific labeling. Membrane permeable fluogenic dye-tetrazine conjugate is then ligated to the protein for live-cell and super-resolution imaging (Uttamapinant et al., 2015).

3.2.3 Application of unnatural amino acids for photocrosslinking

To capture the transient protein interaction inside a complex system, chemical crosslinking has been used to covalently bind partners that are close in space. Crosslinking has also been utilized to stabilize protein tertiary and quaternary structure (Sinz, 2006), lipidated protein interaction (Peng and Hang, 2015) or conjugate an enzyme or tag to purified protein. However, it has been challenging to crosslink specific protein *in vivo* using traditional method. The development of photoreactive UAA has enabled us to study specific protein-protein interactions in mammalian cells (Davis and Chin, 2012). For example, the photoreactive UAAs, BzF and azF, enabled the mapping of ligand-binding sites on chemokine receptors (CXCR4 and CCR5) and on the substance P receptor NK1 (Grunbeck et al., 2011, 2012; Valentin-Hansen et al., 2014). An alkyl diazirine-containing unnatural amino acid, DiZPK, developed by Chen lab was introduced site-specifically onto HdeA, which in conjunction with gel-based proteomics permitted the substrate-profiling of HdeA in *E. coli* cells under very low pH conditions (Zhang et al., 2011).

3.3 Results

3.3.1 Unnatural amino acids incorporation in IFITM3

It has not been possible to image IFITM3 trafficking during virus entry, as N- and C-terminal translational fusions with fluorescent proteins (GFP or mCherry) aggregate in lysosomes and are inactive in antiviral assays (unpublished results Hang laboratory). These observations have precluded us from live-cell imaging experiments to directly visualize whether IFITM3 is recruited to virus-containing vesicles and shuttles this exogenous cargo into lysosomes for degradation or exports these particles through exosomes. However, as mentioned above, unnatural amino acid introduced by amber codon suppression provides a minimal perturbation to the structure of IFITM3 while introducing a bioorthogonal handle that is capable of ligation with fluorophore or affinity tag that is specific to the protein. As shown in Figure 27, unnatural amino acids with different functionality could be made and incorporated into IFITM3.

To develop a robust amber codon suppression system for studying IFITM3, we first started from screening optimal expression positions for murine IFITM3. I chose sites based on several criteria. First, the residue should not affect protein functions, like post-translational modification, protein-protein interaction or disulfide bond. Second, ideally the residue should have similar side chain size to minimize the impact of unnatural amino acids on protein folding and structure. We explored amber codon suppression through different domains of IFITM3 (N-terminus, IMD-1, cytosolic domain, I/TMD-2 and C-terminus) and focused on hydrophobic (Leu, Val, Ile) or aromatic amino acids (Phe, Trp). As shown in Figure 28A, N-terminal HA-tagged and C-terminal FLAG-tagged IFITM3 construct was made to detect both N- and C- terminal epitope to make sure full-length

IFITM3 was expressed. I then use BocLys (Figure 27) as an initial UAA to test the expression profile of different positions (Figure 28). Full length IFITM3 was expressed with the addition of BocLys for several TAG mutants. However, truncation products of several TAG mutants near C-terminal were observed, highlighting potential limitations for site-specific IFITM3 labeling. Nonetheless, several IFITM3 mutants (F8TAG) showed very consistent expression that could be used for the future studies.

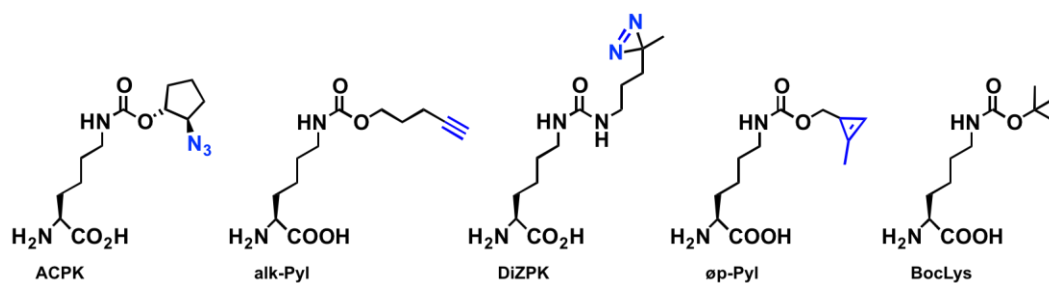


Figure 27. Unnatural amino acids used for bioorthogonal labeling. ACPK and alk-Pyl are used for CuAAC ligation. DiZPK contains photocrosslinkable group which can be used for protein interaction proteomics. øp-Pyl contains cyclopropene group which can be used to do fast IED-DA reaction. BocLys is used for screening and optimization of amber codon positions.

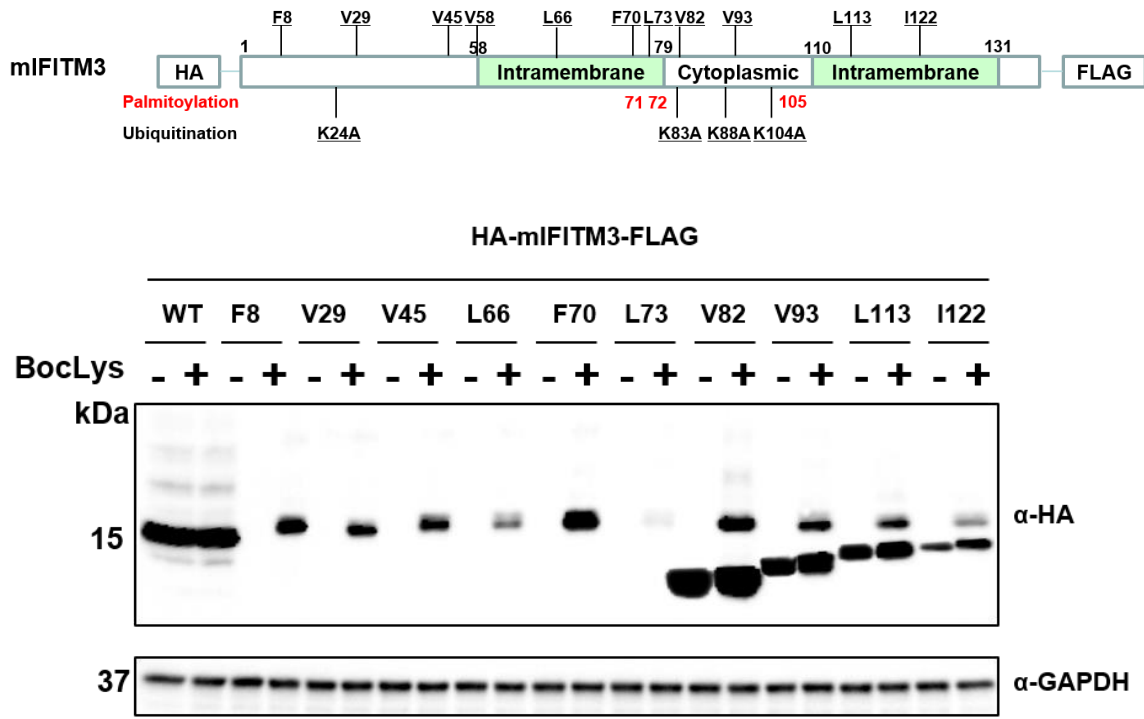


Figure 28. Analysis of murine IFITM3 amber codon mutants with BocLys. Upper panel, schematic illustration of mouse IFITM3 and amber mutations positions. HA- and FLAG-tags were attached to N- and C- terminal of IFITM3 to be able to detect full-length version of the protein. Mutations at different positions across the protein were made. Lower panel, pyrrolysyl-rRNA synthetase PylRS/tRNA_{CUA} pairs from *Methanosarcina* species was transfected along with different amber codon mutation of IFITM3. The residue number on the top of the figure indicates the position of amber codon mutation.

Based on the encouraging results with mIFITM3, I evaluated UAA incorporation into human IFITM3 constructs. Similar to the criteria for selecting amino acids position for mouse version mentioned above, mutations were made across the human IFITM3 (Figure 29). Each mutation was then transfected into HEK293T cells with or without BocLys. After transfection for 18 hours, cells were harvested and lysed. Cell lysates were then immunoblotted for α -HA and α -GAPDH. Protein expression level of each mutant was then normalized to GAPDH level, and triplicates of the results were plotted in Figure 30. The expression level of IFITM3 mutants depends on the position of the amber codon mutation. Some positions exhibited much better protein stability (F8, I74, V93, C105) and expression level while others barely expressed (V29, S61, L73, K88) (Figure 30).

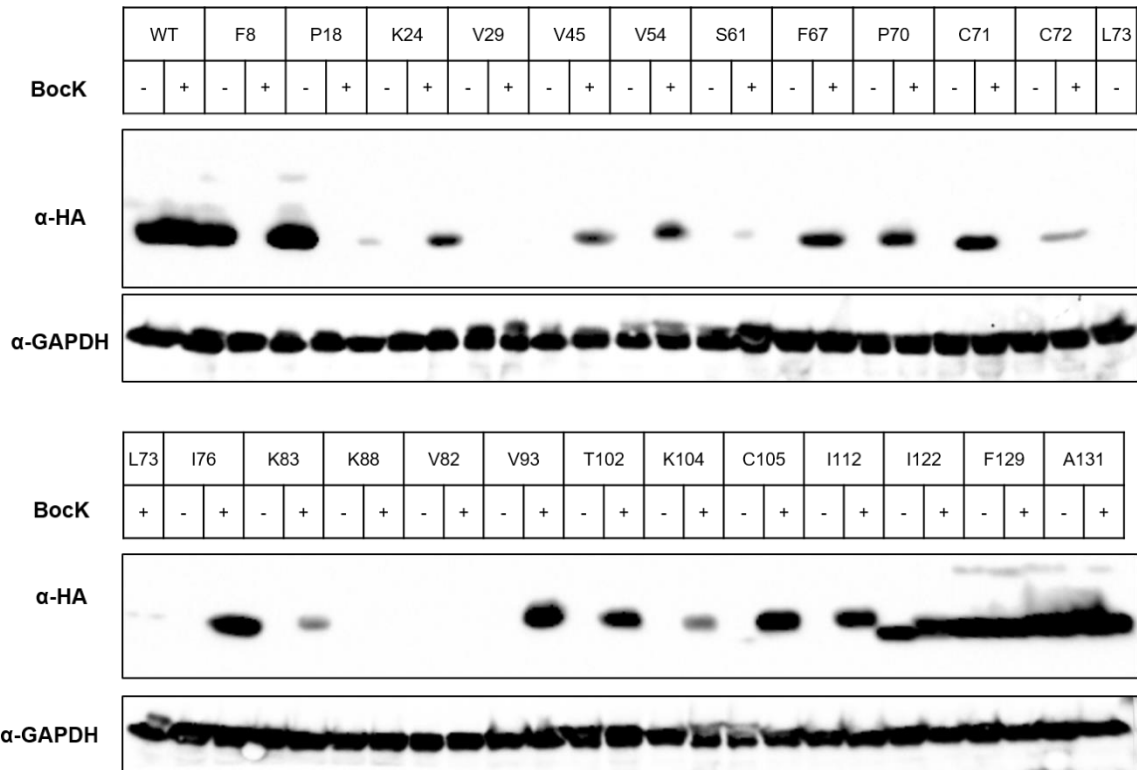


Figure 29. Profiling sites of amber suppression of human IFITM3 using BocLys. We screened human IFITM3 amber mutations at different positions to find the optimal position to introduction unnatural amino acids for imaging and cross-linking purpose. Each mutant was made based on wild type pCMV-HA-IFITM3 plasmid using QuikChange mutagenesis kit. Optimized PylRS/tRNA^{CUA} with respective IFITM3 mutant were co-transfected into HEK293T cells with or without 50 μ M BocK. After incubation for about 16 hours, cells were harvested and tested for IFITM3 expression using immunoblotting against HA epitope.

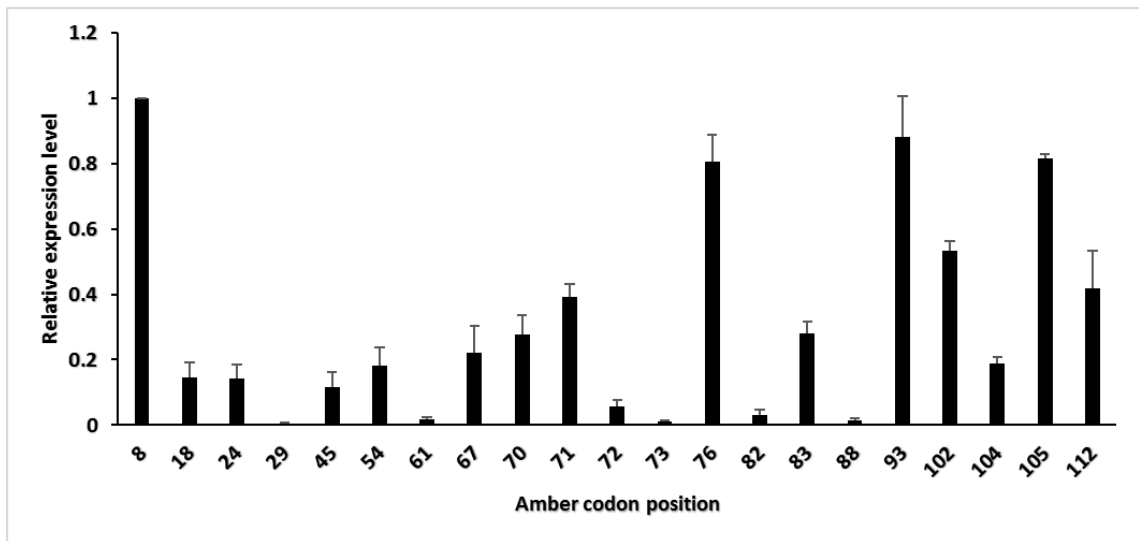


Figure 30. Relative expression level of human IFITM3 expression level. Triplicate experiments of human IFITM3 amber codon expression were plotted as bar graph. Varying positions displayed significant differences in protein expression. The number on the x-axis indicates amber codon mutation position (X to TAG). F8, I76, V93, and C105 were the best-expressed TAG mutants among all the positions.

3.3.2 Site-specific bioorthogonal labeling of IFITM3

To determine if IFITM3 amber codon mutants might be suitable for bioorthogonal imaging studies, I evaluated the incorporation of azide- and alkyne-containing UAAs (Figure 27). Figure 31A describes the initial protocol I used to evaluate bioorthogonal labeling of IFITM3 *in vitro*. Similar to the previous experiments, mIFITM3 F8TAG, F70TAG, V93TAG, I122TAG, L135TAG mutants were transfected individually with PylRS-tRNA^{CUA}, with or without alk-Pyl. Cell lysates were then analyzed for HA-mIFITM3-FLAG expression and click chemistry labeling with fluorescent dyes. The in-gel fluorescence results showed that only in alk-Pyl positive samples, fluorescence signal corresponding to the molecular weight of IFITM3 can be detected. These results showed that *in vitro* fluorescent labeling of IFITM3 amber codon mutants can be achieved, which provides important results for future IFITM3 imaging and membrane topology studies.

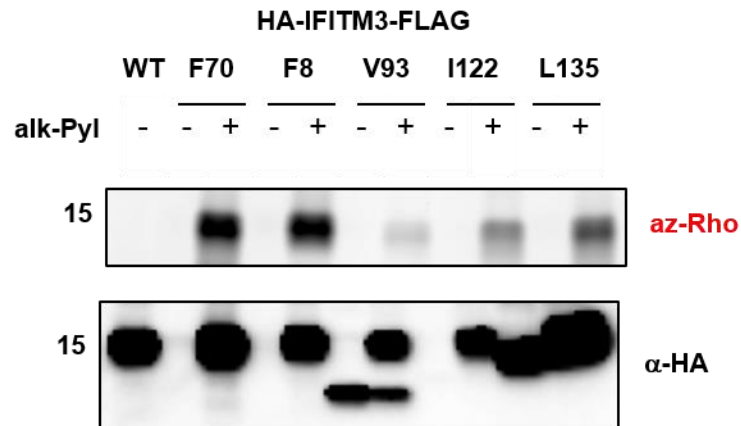
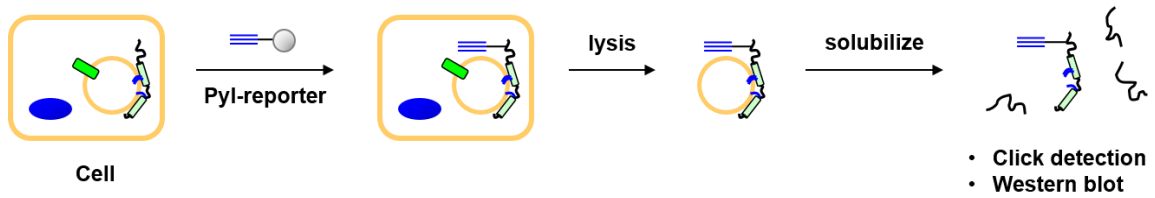
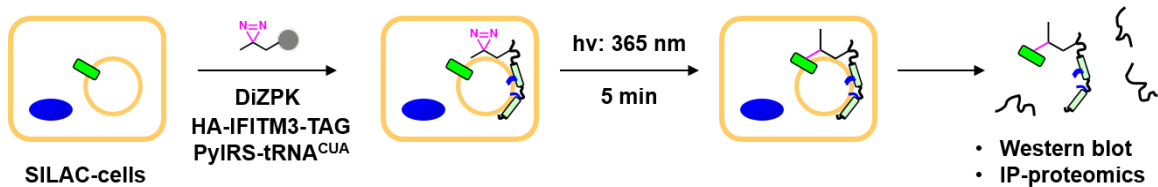


Figure 31. Site-specific bioorthogonal labeling of IFITM3 *in vitro*. Upper panel, IFITM3 amber mutants were transiently transfected into mammalian cells with PylRS/tRNA and unnatural amino acids with bioorthogonal handle (alkyne group in this case). After incubation, cells were lysed and solubilized to do click chemistry detection with azide-fluorophore. Lower panel, mIFITM3 with N-terminal HA tag and C-terminal FLAG mutants were tested for alk-Pyl incorporation and az-rho click chemistry. Fluorescence signal can only be detected in alk-Pyl positive samples, even though some of the constructs showed truncation products.

3.3.3 Photo-crosslinking of DiZPK to study IFITM3 interaction partners

In addition to site-specific fluorescence labeling of IFITM3, we explored the incorporation of DiZPK, a photocrosslinkable amino acid that could be used to covalently trap IFITM3-interacting proteins in mammalian cells. DiZPK contains a diazirine functional group that was previously used to photocrosslink and identify client proteins of the chaperone HdeA in *E. coli* (Zhang et al., 2011). Compared to other photo-activatable chemical groups, diazirine has better photo-stability than phenyl azide groups and it is more easily and efficiently activated with UV light (330 to 370 nm). Figure 32 upper panel shows the scheme for photo-crosslinking DiZPK to identify protein-protein interaction partners. After DiZPK was incorporated into IFITM3, cells were then radiated under UV lamp at wavelength 365 nm to generate active carbene intermediate to covalently trap nearby proteins. Lysates were immunoblotted to check for IFITM3 and its crosslinked products. Multiple crosslinked IFITM3 products were clearly seen after UV radiation when DiZPK was incorporated (Figure 32). These IFITM3 crosslinked products could represent homotypic interactions as well as heterotypic interactions with other key cellular regulators. These preliminary results suggest DiZPK-labeled IFITM3 could be used to discover and validate IFITM3 interacting proteins for future functional studies.



UV-crosslinking of HA-IFITM3-DiZPK

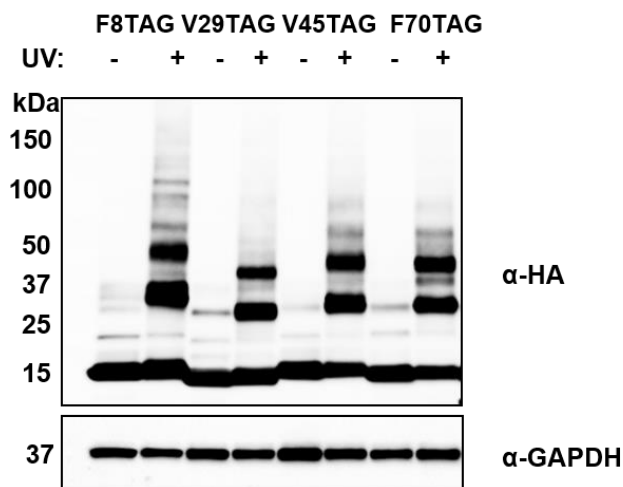


Figure 32. Incorporation DiZPK into IFITM3 for photocrosslinking studies. A) Cells were transfected with HA-IFITM3 plus PylRS-tRNA^{CUA} with DiZPK. After transfection for 18 hours, cells were placed in UV chamber with the lamp at 365 nm wavelength for 5 min. Cells were then lysed and immunoblotted to visualize linked protein complex or immunoprecipitated for proteomics study. B) HA-mIFITM3 F8TAG, V29TAG, V45TAG, and F70TAG were cotransfected with PylRS-tRNA^{CUA} and DiZPK. After UV radiation for 5 min or no UV as control, cells were lysed and immunoblotted for α -HA and α -GAPDH. Compared to the sample with UV induced crosslinking, several more bands higher than MW of IFITM3 were seen.

3.3.4 Application of UAA in other membrane proteins

As we were exploring amber codon suppression technology in IFITM3, I also evaluated other membrane proteins to assess the generality of this system. I initially analyzed caveolin 1 (Cav1) (Dennis J Dietzen et al., 1995), an intramembrane protein involved in vesicle trafficking that has similar biochemical features to IFITMs. I generated several Cav1 amber codon mutants and evaluated their expression with UAAs. Most of Cav1 amber codon mutants can express full-length protein, but V16, V52, V130 TAG mutants appeared to yield the best full length Cav1 expression. I then performed click chemistry ligation with alk-rho, showed that Cav1 can ideally be bioorthogonally labeled by in-gel fluorescence analysis (Figure 33).

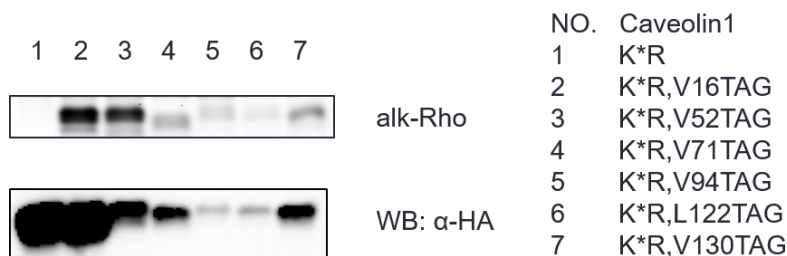


Figure 33. Incorporation of UAA in Caveolin 1 (Cav1). Mutations of Cav1 were chosen using criteria mentioned above. HEK293T cells were transfected with Cav1 plasmids and PylRS-tRNA^{CUA}. ACPK was added during transfection. After transfection, cells lysates were click with alk-Rho for visualization. Immunoblotting and in-gel fluorescence were performed to determine the protein expression level and fluorescence signal.

3.4 Discussion

3.4.1 Optimization of Amber codon suppression in IFITM3

To facilitate imaging and protein-protein interaction studies of IFITM3, we developed amber codon suppression system in IFITM3. Since the incorporation efficiency of UAAs in different residues and proteins can vary, we first needed to systematically profile IFITM3 to find optimal positions for amber codon mutation. As mentioned earlier, we chose positions according to several criteria. First, the residue should not affect protein functions, like post-translational modification, protein-protein interaction or disulfide bond. Second, ideally the residue should have similar side chain size to minimize the impact of unnatural amino acids on protein folding and structure. 15 and 24 mutations were made on mIFITM3 and hIFITM3 respectively. Each mutant was then tested for incorporation of UAA. To make sure full-length proteins were made, N- and C- terminus were tagged with HA and FLAG. Immunoblotting using α -HA or α -FLAG would reveal whether full-length protein is synthesized.

Interestingly, mIFITM3 amber codon positions larger than 80 showed truncated products corresponding to the molecular weight of the protein from first amino acid to amber codon (Figure 28). However, hIFITM3 does not show truncation except a few very C-terminal mutations (I122, F129, A131). Screening of mouse and human IFITM3 amber codon mutants revealed that indeed protein expression level varies from one position to another. mIFITM3 F8, V29, V45, F70 and hIFITM3 F8, I76, V93, C105 mutations exhibited best expression efficiency (Figure 32 and Figure 30). Especially, F8TAG showed great promise for later applications in live-cell imaging and photocrosslinking due to its high expression efficiency with multiple kinds of UAAs.

3.4.2 Bioorthogonal labeling of IFITM3 amber codon mutants with UAAs

UAAs with click chemistry handles (ACPK and alk-Pyl) enabled specific bioorthogonal labeling (Figure 27). To increase the signal-to-noise ratio of the labeling, alkyne-containing UAA was preferred for labeling and azide-conjugated fluorophore or biotin was then used to ligate. Preliminary testing of UAA and dye pairs confirmed that alk-Pyl with az-Rho (Cy3) had the best fluorescent signal-to-noise level. The protocol of click chemistry is similar to the ones we used to identify fatty-acylated proteins with chemical reporter alk-16 (Yount et al., 2011b). Our experiments with mIFITM3 amber codon mutants confirmed that labeled IFITM3 can be specifically ligated to fluorophores *in vitro* (Figure 31).

3.4.3 Application of amber codon suppression in other membrane proteins

Due to the encouraging results from IFITM3 UAA incorporation, we seek to generalize the method to other S-palmitoylated transmembrane proteins. Amber codon mutations on Cav1, CD9, CANX, TLR2 were made and tested for UAA incorporation. However, only Cav1 mutants showed successful expression in several positions (Figure 33) and other mutations of CD9, CANX or TLR2 were either not expressed or truncated (data not shown). Similar to IFITM3, Cav1 is a short intramembrane protein with flexible helical domain. It is possible that flexible intramembrane proteins are more susceptible to amber codon suppression. Transmembrane proteins like CD9, CANX, TLR2 may need more careful analysis of the amber codon position to locate optimal site for incorporation.

3.5 Materials and methods

3.5.1 Materials

The plasmids of Cav1, CANX, CD9 were obtained from Addgene. Anti-HA-Peroxidase, high affinity (clone 3F10) was from Roche life science. Rabbit polyclonal GAPDH Antibody (FL-335) was purchased from Santa Cruz Biotechnology.

3.5.2 Site mutagenesis for amber mutants

Site-directed mutagenesis was done using Agilent QuikChange II Site-Directed Mutagenesis Kit (<http://www.agilent.com>). Primers used in the experiments are listed in Table 9.

Table 9. Sequences of primers for site-directed mutagenesis of amber mutants.

mIFITM3-F8TAG-F	CACACTTCTCAAGCCTAGATCACCGCTGCCAGTG
mIFITM3-F8TAG-R	CACTGGCAGCGGTGATCTAGGCTTGAGAAGTGTG
mIFITM3-V29TAG-F	CAAGGAAGAATATGAGTAGGCTGAGATGGGGGC
mIFITM3-V29TAG-R	GCCCCATCTCAGCCTACTCATATTCTTCCTTG
mIFITM3-V45TAG-F	GCTTCTGTCAGAACTACTTAGATCAACATGCCAGAG
mIFITM3-V45TAG-R	CTCTGGGCATGTTGATCTAAGTAGTTCTGACAGAAGC
mIFITM3-V58TAG-F	GTCGGTGCCTGACCATTAGGTCTGGTCCCTGTTC
mIFITM3-V58TAG-R	GAACAGGGACCAGACCTAATGGTCAGGCACCGAC
mIFITM3-F63TAG-F	CATGTGGTCTGGTCCCTGTAGAATACTCTTCATGAACT
mIFITM3-F63TAG-R	AGTTCATGAAGAGTGTATTCTACAGGGACCAGACCACATG
mIFITM3-L66TAG-F	GTCTGGTCCCTGTTCAATACATAGTTCATGAACTTCTGCTGCCTG

mIFITM3-L66TAG-R	CAGGCAGCAGAAGTTCATGAACTATGTATTGAACAGGGACCAGAC
mIFITM3-F67TAG-F	TCCCTGTTCAATACACTCTAGATGAACTTCTGCTGCCTGG
mIFITM3-F67TAG-R	CCAGGCAGCAGAAGTTCATCTAGAGTGTATTGAACAGGGA
mIFITM3-F70TAG-F	CTGTTCAATACACTCTTCATGAACTAGTGCTGCCTGGGCT
mIFITM3-F70TAG-R	AGCCCAGGCAGCACTAGTTCATGAAGAGTGTATTGAACAG
mIFITM3-L73TAG-F	CATGAACTTCTGCTGCTAGGGCTTCATAGCCTATG
mIFITM3-L73TAG-R	CATAGGCTATGAAGCCCTAGCAGCAGAAGTTCATG
mIFITM3-V82TAG-F	CCTATGCCTACTCCTAGAAGTCTAGGGATCG
mIFITM3-V82TAG-R	CGATCCCTAGACTTCTAGGAGTAGGCATAGG
mIFITM3-V93TAG-F	GAAGATGGTGGGTGATTAGACTGGAGCCCAGGC
mIFITM3-V93TAG-R	GCCTGGGCTCCAGTCTAATCACCCACCATCTTC
mIFITM3-L113TAG-F	CTGAACATCAGCACCTTGGTCTAGAGCATCCTGATGGTTGTTATC
mIFITM3-L113TAG-R	GATAACAACCATCAGGATGCTCTAGACCAAGGTGCTGATGTTTCAG
mIFITM3-I122TAG-F	TCCTGATGGTTGTTATCACCTAGGTTAGTGTCATCATCATTGT
mIFITM3-I122TAG-R	ACAATGATGATGACACTAACCTAGGTGATAACAACCATCAGGA
mIFITM3-L130TAG-F	GTTAGTGTCATCATCATTGTTTAGAACGCTCAAAACCTTCACAC
mIFITM3-L130TAG-R	GTGTGAAGGTTTTGAGCGTCTAAACAATGATGATGACACTAAC
mIFITM3-L135TAG-F	ATTGTTCTTAACGCTCAAACTAGCACACTGATTACAAGGATGAC
mIFITM3-L135TAG-R	GTCATCCTTGTAATCAGTGTGCTAGTTTTGAGCGTTAAGAACAAT
hIfitm3-F8TAG-F	CACACTTCTCAAGCCTAGATCACCGCTGCCAGTG
hIfitm3-F8TAG-R	CACTGGCAGCGGTGATCTAGGCTTGAGAAGTGTG
hIfitm3-V93TAG-F	GAAGATGGTGGGTGATTAGACTGGAGCCCAGGC
hIfitm3-V93TAG-R	GCCTGGGCTCCAGTCTAATCACCCACCATCTTC

hIfitm3-L135TAG-F	ATTGTTCTTAACGCTCAAAACTAGCACACTGATTACAAGGATGAC
hIfitm3-L135TAG-R	GTCATCCTTGTAATCAGTGTGCTAGTTTTGAGCGTTAAGAACAAT
hIfitm3-I122TAG-F	TCCTGATGGTTGTTATCACCTAGGTTAGTGTTCATCATCATTGT
hIfitm3-I122TAG-R	ACAATGATGATGACACTAACCTAGGTGATAACAACCATCAGGA
hIfitm3-I9TAG-F	CACTTCTCAAGCCTTCTAGACCGCTGCCAGTGGAG
hIfitm3-I9TAG-R	CTCCACTGGCAGCGGTCTAGAAGGCTTGAGAAGTG
hIfitm3-T10TAG-F	CTTCTCAAGCCTTCATCTAGGCTGCCAGTGGAGGAC
hIfitm3-T10TAG-R	GTCCTCCACTGGCAGCCTAGATGAAGGCTTGAGAAG
hIfitm3-N131TAG-F	GTGTCATCATCATTGTTCTTTAGGCTCAAAACCTTCACACTG
hIfitm3-N131TAG-R	CAGTGTGAAGTTTTGAGCCTAAAGAACAATGATGATGACAC
hIfitm3-S13TAG-F	CAAGCCTTCATCACCGCTGCCTAGGGAGGACAGCCCCAAACTAC
hIfitm3-S13TAG-R	GTAGTTTGGGGGCTGTCCCTCCCTAGGCAGCGGTGATGAAGGCTTG
Cav1-V16TAG-F	GGACATCTCTACACCTAGCCCATCCGGGAACAG
Cav1-V16TAG-R	CTGTTCCCGGATGGGCTAGGTGTAGAGATGTCC
Cav1-V52TAG-F	GAGATCGACCTGTAGAACCGCGACCCTC
Cav1-V52TAG-R	GAGGGTCGCGGTTCTACAGGTCGATCTC
Cav1-V71TAG-F	CGCATTGACTTTGAAGATTAGATTGCAGAACCAGAAG
Cav1-V71TAG-R	CTTCTGGTTCTGCAATCTAATCTTCAAAGTCAATGCG
Cav1-V94TAG-F	CAGCTTCACCACCTTCACTTAGACGCGCTACTGGTTTTAC
Cav1-V94TAG-R	GTAAAACCAGTAGCGCGTCTAAGTGAAGGTGGTGAAGCTG
Cav1-L122TAG-F	GGCATTACTTCGCCATTTAGTCTTTCCTGCACATCTGG
Cav1-L122TAG-R	CCAGATGTGCAGGAAAGACTAAATGGCGAAGTAAATGCC
Cav1-V130TAG-F	CCTGCACATCTGGGCATAGGTACCATGCATTTCGC

Cav1-V130TAG-R	GCGAATGCATGGTACCTATGCCCAGATGTGCAGG
Cav1-V155TAG-F	CCATCTACGTCCACACCTAGTGTGACCCACTCTTTG
Cav1-V155TAG-R	CAAAGAGTGGGTCACACTAGGTGTGGACGTAGATGG
Cav1-V163TAG-F	GACCCACTCTTTGAAGCTTAGGGGCGCATATTCAGCAATG
Cav1-V163TAG-R	CATTGCTGAATATGCGCCCCTAAGCTTCAAAGAGTGGGTC

3.5.3 Unnatural amino acids incorporation in mammalian cell culture

HEK293T cells were seeded into Corning 6-well plate (Costar, Corning) and grown to 90% confluence in 10% fetal bovine serum DMEM (Invitrogen) in a humidified atmosphere of 5% CO₂. Plasmids encoding RNA synthetase and tRNA, pCMV-Mb-DiZPK-RS, were obtained from Dr. Peng Chen lab (Zhang et al., 2011). When cells reached 80-90% confluency, the media was exchanged to Opti-MEM containing 50 μ M unnatural amino acids (e.g. Bock), and cells were then transfected with pCMV-Mb-DiZPK-RS and pCMV-IFITM3 amber mutants using Lipofectamine® 2000 from Invitrogen. Cells were grown for an additional 12 h before being visualized by a fluorescence microscope.

3.5.4 In-gel fluorescence detection of ligated products

Cells were lysed in Brij97 buffer (1% Brij 97, 50 mM TEA, 150 mM NaCl, pH 7.4) and protein concentration was quantified with BCA assay. 500-1000 mg protein was aliquoted into 100 μ L Brij97 buffer in a dolphin tube. Prewashed α -HA-conjugated agarose (Sigma) in Brij97 buffer (Use 15 μ L Sigma agarose per sample) was added to protein sample and incubated over the nutating mixer at 4 °C for 1h. Agarose beads were spun down for 1 min at 9000x g. Agarose resin was washed three times with 500 μ L RIPA wash buffer (50 mM

TEA, 150 mM NaCl, 1% Na-Deoxycholate, 1% Triton X 100, 0.1% SDS). Beads was resuspended in 22.5 uL 4% SDS buffer and added to 2.5 uL click chemistry master mix for one hour incubation. 4x blue buffer/BME (165 uL blue buffer with 35 uL BME) was added for SDS-PAGE. After running SDS-PAGE, gels were imaged by Typhoon™ scanner (GE Healthcare).

3.5.5 UV-induced photo-crosslinking by DiZPK

Photocrosslinking was performed by irradiation of the mammalian cells with UV light (365 nm) for 0–10 min using a Hoefer UVC 500 Crosslinker installed with 365-nm-wavelength UV lamps (Amersham Biosciences) at a distance of 3 cm at 25 °C. The cells were harvested by Trypsin digestion and centrifuge at 6000g for 2 min and then analyzed by tricine SDS-PAGE and immunoblotting with antibodies against the specified proteins. Gel bands and western blots were scanned and quantified using the ImageJ program (NIH).

Chapter Four: Conclusion and perspective

4.1 Conclusion

New chemical methods for protein fatty-acylation have expanded the number of modified proteins in eukaryotes and highlighted novel roles in biology (Peng et al., 2016) (Chapter 1). Indeed, the discovery of IFITM3 S-palmitoylation by the Hang laboratory identified a new role for protein fatty-acylation in host resistance to virus infection (Yount et al., 2010, 2012). Nonetheless, the precise mechanism of IFITM3 antiviral activity and regulation by S-palmitoylation is not fully understood. To address these outstanding questions of IFITM3 function, I characterized endogenous levels and specific sites of IFITM3 S-palmitoylation in Chapter 2. I demonstrated that IFITM3 is primarily S-palmitoylated on C72, a highly conserved amino acid, which is important for IFITM3 antiviral activity. My additional experiments showed that loss of IFITM3 S-palmitoylation, particularly at Cys72, resulted in enhanced protein turnover through proteasome- and lysosome-mediated degradation pathways.

I also developed new chemical tools and expression systems to explore IFITM3 function and regulation. In particular, I identified IFITM3 amber codon mutants that could be used for site-specific labeling with unnatural amino acids. The ability to incorporate unnatural amino acids into IFITM3 is providing our laboratory new opportunities for live cell imaging studies and photocrosslinking studies, which I will summarize below. In addition, I also explored expression and purification of recombinant IFITM3 in bacteria for *in vitro* site-specific lipidation, which may enable reconstitution of IFITM3 *in vitro* for more precise biochemical and biophysical studies. An updated working model for IFITM3 antiviral activity and future directions is summarized below.

4.2 Perspectives

4.2.1 A model for IFITM3 antiviral mechanism

IFITMs are important IFN-stimulated effectors that control host susceptibility to many viruses, but their mechanisms of action are not understood. Although the complexity of IFITMs antiviral mechanism and the specificity of virus inhibition, there are some proposed mechanisms for IFITMs activity. In the absence of IFITM3, incoming influenza virus particles traffic to acidic endosomes and fuse with host membranes to deposit viral RNA for infection. In IFN-stimulated cells, expression of IFITM3 inhibits virus entry and may divert incoming virus particles for degradation in lysosomes.

IFITM3 does not appear to block the internalization of viruses such as VSV, influenza virus or HCV into host cells but instead prevents deposition of viral contents into the cytosol (Feeley et al., 2011; Huang et al., 2011; Schoggins et al., 2011; Weidner et al., 2010). Additional cell biology studies have suggested that IFITM3, localized to endocytic vesicles and lysosomes, may directly block virus pore formation or indirectly inhibit virus entry by increasing vesicular cholesterol levels and ultimately target incoming viral particles for lysosomal degradation (Amini-Bavil-Olyae et al., 2013; Desai et al., 2014; Feeley et al., 2011; Li et al., 2013). More recent studies have suggested that IFITM3 does not affect virus-host membrane hemifusion but impairs pore formation or alter lipid vesicle composition (Amini-Bavil-Olyae et al., 2013; Desai et al., 2014). The localization of IFITM3 on vesicles has even been proposed to alter membrane curvature and generate “tough membranes” to inhibit virus membrane fusion (Perreira et al., 2013). Beyond viruses, IFITMs have been recently reported to restrict *Mycobacterium tuberculosis* infection (Ranjbar et al., 2015).

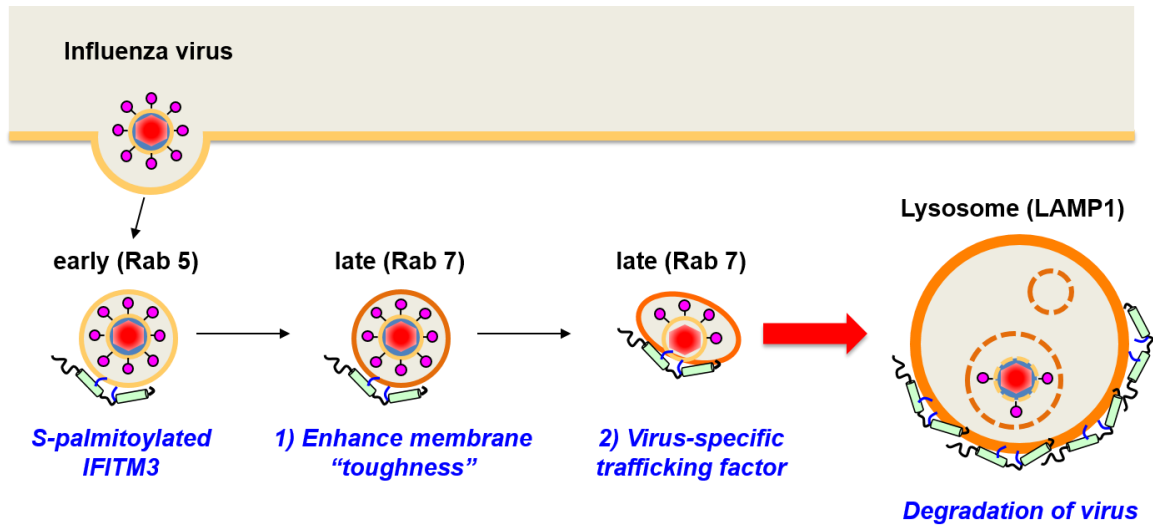


Figure 34. IFITM3 antiviral working models. Incoming viruses are first trapped into early endosome (marker protein Rab5) where some of the IFITM3 population colocalize. As vesicles mature to late endosomes, IFITM3 will first enhance the membrane rigidity to prevent back fusion into the cytosol and secondly direct vesicles into a non-productive pathway for degradation, like lysosome. Immunofluorescence showed IFITM3 strongly colocalized with lysosome marker LAMP1 indicating its role as vesicular trafficking factor for the virus to degrade in the lysosome.

Recent studies in our laboratory suggests that IFITM3 may act like “immune-SNAREs” for pathogens due to its interaction with syntaxin proteins (Q-SNARE) and similarity with VAMP proteins (R-SNARE). VAMPs with similar size to IFITMs are also S-fatty-acylated (unpublished data). Knockdown of VAMPs increased susceptibility to virus infection and are essential for vesicle fusion (Pirooz et al., 2014). VAMPs may thus serve as models to understand how IFITM3 directs pathogen-containing vesicles into degradative cellular compartments. The new chemical tools developed in my thesis studies may help understand IFITM3 mechanism and regulation by S-fatty-acylation.

4.2.2 Future studies

Live-cell imaging to monitor IFITM3 trafficking

The amber codon suppression technology developed for IFITM3 is providing a new system for live-cell imaging (Figure 35). To profile different cell permeable fluorophores, rhodamine, BODIPY or Si-rhodamine (Lukinavičius et al., 2013) were synthesized and tested for three amino acids. Human IFITM3-F8TAG amber mutant was used as a model protein because the previous study had shown that UAA can robustly incorporate into F8TAG mutant. Si-Rho with TCOK showed strong and specific bioorthogonal labeling (Figure 36). The biocompatible near-infrared high permeability and fluorogenic character permit the imaging of proteins in living cells and tissues without washing steps, and its brightness and photostability make it ideally suited for live-cell super-resolution microscopy (Lukinavičius et al., 2013).

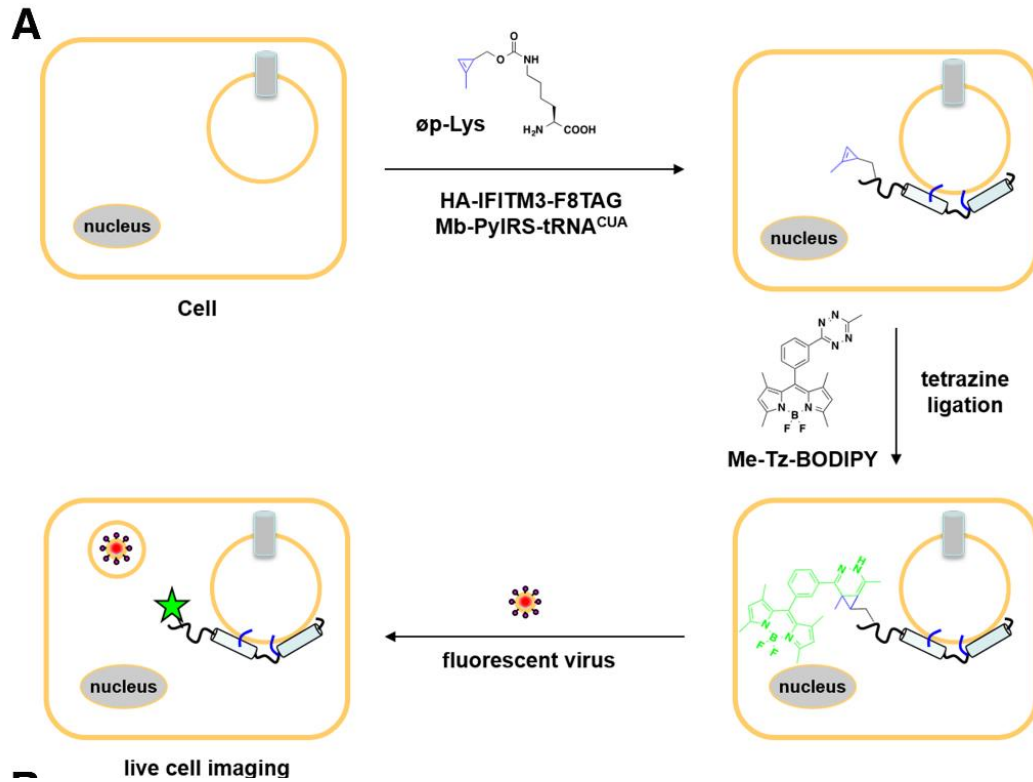


Figure 35. Scheme of site-specific live cell imaging using IED-DA reaction. Amber suppression-mediated incorporation of $\text{\textcircled{ø}p-Lys}$ in IFITM3-TAG mutants enables bioorthogonal ligation with tetrazine-dyes for in-gel fluorescence profiling of cell lysates and live cell labeling for confocal fluorescence imaging studies.

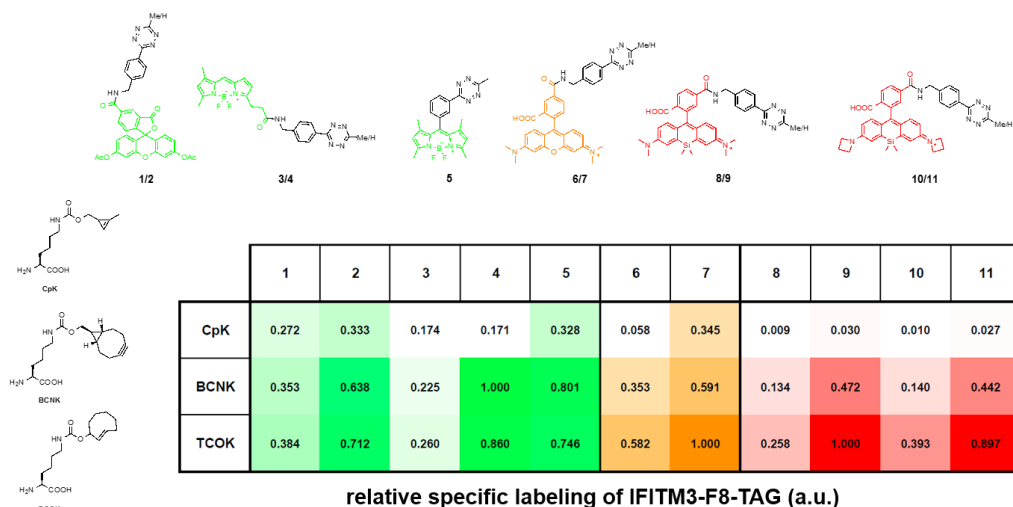


Figure 36. Screening for an optimal pair of unnatural amino acids and tetrazine dye.

Several UAAs, *o*p-Lys, BCNK and TCOK were tested individually with multiple kinds of fluorescent tetrazine dye to screen the optimal pair for labeling IFITM3-F8TAG. Artificial units were used to indicate the relative labeling intensity of each pair. Data from Tao Peng.

Live-cell imaging experiments were then performed using the optimal conditions (Figure 37). IFITM3-F8TAG labeled with Si-Rh-Tz colocalized very well with GFP-LAMP1, which is consistent with the immunofluorescence results. α -HA immunofluorescence of HA-IFITM3 overlapped very well with the Rhodamine fluorescence, which further confirmed the specificity of the UAA labeling. This new technology provides us an exciting opportunity to image IFITM3 trafficking in living cells during virus infection for the first time. We will optimize the multiplicity and kinetics of fluorophore-labeled IAV and then perform live cell imaging studies in IFITM2/3-KO cells coexpressing Si-Rh-Tz-labeled IFITM3 and other GFP-labeled cellular markers. By monitoring the time-lapse imaging of IAV particle infection process, we would be able to know at what step do IFITM3 engages the virus-containing vesicle and the degradation

process. To further understand the specificity of IFITM3 cargo selectivity, other fluorescently-labeled exogenous cargo such as dextran, transferrin, EGF will be tested in parallel with IAV assay.

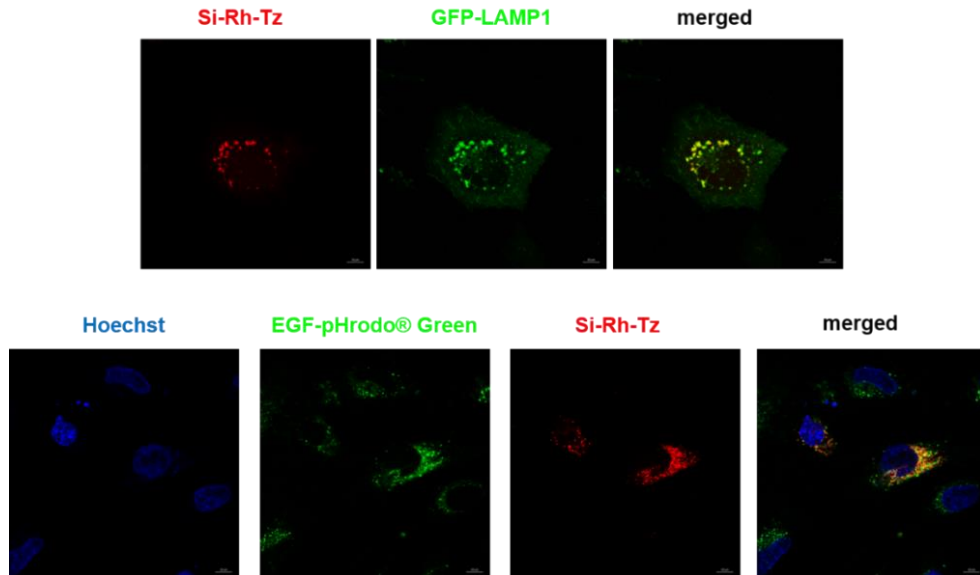


Figure 37. Live cell imaging of IFITM3 F8TAG with Si-Rh-Tz. Upper panel, Si-Rh-Tz labeled IFITM3-F8TAG were cotransfected with GFP-LAMP1. Live-cell imaging were then performed and in consistent with previous observation, Rhodamine signal overlap very well with GFP-LAMP1. Lower panel, pH sensitive EGF-pHrodo® Green is used for the detection of internalized EGF receptor in cells. Data from Tao Peng.

Understanding IFITM3 membrane topology with UAA accessibility methods

The membrane topology of IFITM3 was predicted to be dual transmembrane protein but the identification of K24 ubiquitination on mouse IFITM3 raised the possibility that the predicted dual-pass transmembrane topology was incorrect since the enzymes responsible for ubiquitin conjugation are localized in the mammalian cytosol (Brass et al., 2009; Yount et al., 2012). To further support the N-terminal cytosolic orientation, phosphorylation of Tyr20 has also been reported to regulate IFITM3 endocytosis from the plasma membrane (Chesarino et al., 2014a; Jia et al., 2014). Subsequent N-linked glycosylation mapping studies and protein lipidation site engineering (N-myristoylation and C-prenylation) studies suggest that mIFITM3 may be an intramembrane protein where both the N- and C-termini of mIFITM3 have access to the cytoplasm (Yount et al., 2012). More recent epitope-mapping studies have also confirmed the cytoplasmic orientation of IFITM3 N-terminus and also suggest that the C-terminus may either be luminal or extracellular (Bailey et al., 2013; Weston et al., 2014). Since multiple UAA positions of IFITM3 are available, it creates a new opportunity to study IFITM3 topology with accessibility assay. Basically, membrane impermeable fluorophore conjugates could be used to screen IFITM3 with amber codons at different positions. Only positions that are outside the vesicle membrane should be able to be ligated to the fluorophore. It is especially interesting to figure out whether C-terminus of IFITM3 is luminal or cytosolic or a mix of both (Figure 7).

Identification of cellular factors required for IFITM3 antiviral activity

Development of novel tools to study essential proteins or lipids required for IFITM3 function is vital for us to understand IFITM3 biology. It requires a detailed characterization of lipids and proteins in IFITM3-vesicles, which could provide experimental evidence for two potential mechanisms of action for IFITM3: 1) vesicle-coating protein that enhances membrane integrity by remodeling the lipid or protein composition and or 2) membrane trafficking receptor or adapter that sorts virus-containing vesicles to lysosomes for degradation or export.

As discussed earlier in Chapter 2, the composition of lipids that modify IFITM3 is not known. To characterize IFITM3-associated lipids, IFN-stimulated cells will be mechanically lysed without detergents by Dounce homogenization and IFITM3-vesicles will be purified by α -IFITM3 antibody-conjugated magnetic beads and selectively eluted with low pH buffer. Western blot analysis of these purified vesicles will be performed with antibodies to IFITM3, endocytic markers, and other organelles to ensure specific and efficient enrichment. The immune-purified IFITM3-vesicles will then be extracted with chloroform/methanol, concentrated and analyzed by high-performance thin layer chromatography (HPTLC) and LC-MS/MS along with commercially available lipid standards as previously described (Maeda et al., 2014)

It is often challenging to identify the protein-protein interaction between membrane proteins due to normal co-immunoprecipitations conditions would perturb the cellular lipid environment that is required for proper protein interaction. Amber codon suppression coupled with crosslinkable UAA provides a feasible system for capturing this transient interaction.

To understand the proteins that are interacting with IFITM3 at the N-terminus. Double SILAC experiment was performed by our lab. Stable isotope labeling by amino acids in cell culture (SILAC) is a simple and straightforward approach for *in vivo* incorporation of a label into proteins for mass spectrometry (MS)-based quantitative proteomics. By employing quantitative method, several interesting protein partners were identified such as p97/VCP.

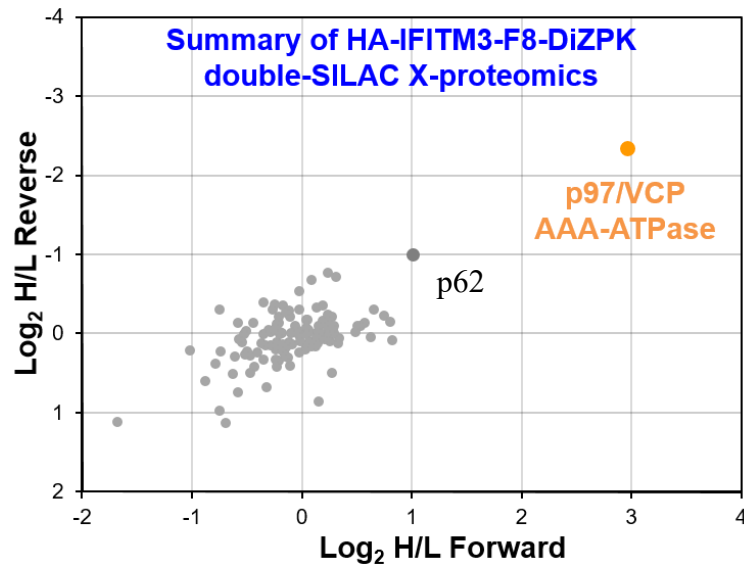


Figure 38. Summary of HA-IFITM3-F8-DiZPK double-SILAC X-proteomics. HeLa cells labeled with heavy- or light-isotope amino acids plus DiZPK, were transfected with HA-IFITM3-Phe8-TAG, subjected to 5 min of UV-crosslinking or not, combined in a 1:1 ratio, subjected to anti-HA immunoprecipitation and then analyzed by LC-MS/MS sequencing using Orbitrap and MaxQuant. For double-SILAC analysis, DiZPK labeling was done with heavy amino acids (Forward) and subsequently performed with light amino acids (Reverse). Quantitative comparison of the samples from forward and reverse (H/L) ratios reveals protein candidates (i.e. p62) that were robustly photocrosslinked to HA-IFITM3-Phe8-DiZPK. Data from Tao Peng.

Reconstitute and analyze lipidated IFITM3 *in vitro*

Reconstitution of IFITM3 antiviral activity using purified proteins and lipids would definitively clarify how IFITM3 works and whether it needs help from other factors. After purifying IFITM3 from bacteria, lipidated or unmodified IFITM3 will be incorporated into synthetic liposome with different compositions to optimize the best system for IFITM3 vesicles. Membrane fractionation experiment would be helpful to understand how S-fatty-acylation changes protein hydrophobicity and lipid preference. Further analysis of how and where IFITM3 participate in the membrane fraction by fluorescent tracking using UAA labeling of IFITM3 and well-established fluorescent membrane probes would provide information on whether S-acylated IFITM3 would prefer ordered membrane fraction.

Several studies have been done on loss of function analysis of IFITM3 S-fatty-acylation through mutagenesis. However, to understand how alterations in S-fatty-acylation controls IFITM3 targeting to membranes and antiviral activity, we need to reconstitute and characterize lipidated IFITM3 *in vitro* and *in vivo*. We have successfully purified codon optimized mouse and human IFITM3 from *E. Coli*. Since S-fatty-acylation machinery is not available in the bacteria, the proteins we've purified have no lipidation. To understand the interaction of IFITM3 with membranes, we will chemically install fatty acid analogs onto the recombinant IFITM3. To introduce defined lipid structures on hIFITM3-His6, we have explored a variety of Cys alkylation methods (maleimide coupling, haloacetamide alkylation, direct acylation, disulfide exchange (Kim et al., 2014) and thiol-ene coupling (TEC) (Valkevich et al., 2012)) and have discovered that maleimide-coupling affords the most selective and efficient method for chemical labeling of the Cys residues of IFITM3 *in vitro*. Lipidation with hexadecyl maleimide (Mal-C16:0) induces a clear

change in purified mouse and human IFITM3 mobility, but not that of IFITM3 palm Δ mutation (Figure 39).

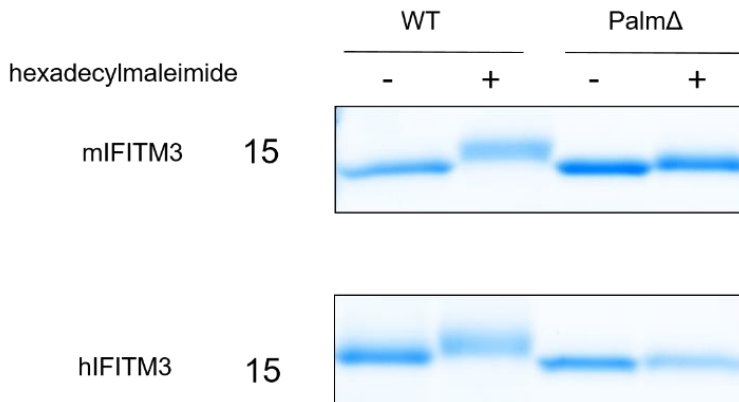


Figure 39. *In vitro* alkylation with hexadecylmaleimide (Mal-C16:0). 30 μ L protein (0.16 mM for mIFITM3 and much lower for hIFITM3) was mixed with 1 μ L 500 mM TCEP (250 eq.) solution. The solution was shaken at room temperature for 30 mins. 60 μ L of a 20 mM (500 eq.) solution of the hexadecyl maleimide (Mal-C16:0) in DMF or DMF control was then added and the reaction shaken at room temperature for another two hours. Chloroform-Methanol precipitation was used to stop the reaction and retrieve proteins.

Even though the maleimide lipidated product is not a natural lipid linkage, this chemical strategy should provide a reasonable approach to generate and reconstitute lipidated IFITM3 variants *in vitro* (Triola et al., 2012). Amber codon mutation could also be introduced into IFITM3 for labeling with fluorescent tags that would facilitate the imaging or membrane fusion assay. To further understand how site-specific lipidation affects IFITM3 function, we can generate proteins with mono-, di- or tri-lipidated isoforms to determine if specific cysteine or cysteine combination is required for proper function. As we mentioned before Cys72 has been proved to be an important site for S-fatty-

acylation, putting back lipidation to Cys72 *in vitro* and *in vivo* will further improve our understand of the function of S-fatty-acylation.

To characterize the activity of the IFITM3-liposome system, we will perform liposome fusion assay and membrane permeability assay to understand how IFITM3 affects vesicle fusion and membrane permeability, which have been suggested as two main mechanisms of IFITM3 antiviral activity (Bailey et al., 2014). More importantly, it is crucial to show that the reconstituted IFITM3-liposome is biologically active. Recent studies have shown that exosomes containing IFITM3 can be added to unstimulated cells and protect them from Dengue virus infection (Zhu et al., 2014). Thus, we can design experiments to compare the antiviral activity of fluorescent lipidated IFITM3-exosomes with nonlipidated version. Importantly, the production of active recombinant lipidated-IFITM3 may provide a well-defined protein-based therapeutic for the prevention or treatment of IAV infections in humans with loss-of-function mutations in IFITM3 (Everitt et al., 2012; Wang et al., 2013; Zhang et al., 2013b).

Summary

My thesis work focused to the development of chemical tools to study the innate immune protein IFITM3, especially focused on the function of S-palmitoylation. The new tools for live-cell imaging, site-specific photocrosslinking and *in vitro* reconstitution system should facilitate future studies on the mechanisms and regulation of IFITM3 antiviral activity. The enhanced understanding of IFITM3 not only helps us figure out how IFITM3 restricts a

broad spectrum of viruses, but may enable the development of new therapeutic approaches against intracellular pathogens in the future.

References

- Abrami, L., Leppla, S.H., and van der Goot, F.G. (2006). Receptor palmitoylation and ubiquitination regulate anthrax toxin endocytosis. *J. Cell Biol.* *172*, 309–320.
- Agard, N.J., Prescher, J.A., and Bertozzi, C.R. (2004). A strain-promoted [3 + 2] azide-alkyne cycloaddition for covalent modification of biomolecules in living systems. *J. Am. Chem. Soc.* *126*, 15046–15047.
- Amini-Bavil-Olyaei, S., Choi, Y.J., Lee, J.H., Shi, M., Huang, I.-C., Farzan, M., and Jung, J.U. (2013). The antiviral effector IFITM3 disrupts intracellular cholesterol homeostasis to block viral entry. *Cell Host Microbe* *13*, 452–464.
- Bailey, C.C., Huang, I.-C., Kam, C., and Farzan, M. (2012). Ifitm3 Limits the Severity of Acute Influenza in Mice. *PLoS Pathog* *8*, e1002909.
- Bailey, C.C., Kondur, H.R., Huang, I.-C., and Farzan, M. (2013). Interferon-Induced Transmembrane Protein 3 is a Type II Transmembrane Protein. *J. Biol. Chem.* jbc.M113.514356.
- Bailey, C.C., Zhong, G., Huang, I.-C., and Farzan, M. (2014). IFITM-Family Proteins: The Cell's First Line of Antiviral Defense. *Annu. Rev. Virol.* *1*, 261–283.
- Bartels, D.J., Mitchell, D.A., Dong, X., and Deschenes, R.J. (1999). Erf2, a Novel Gene Product That Affects the Localization and Palmitoylation of Ras2 in *Saccharomyces cerevisiae*. *Mol. Cell. Biol.* *19*, 6775–6787.
- Berthiaume, L.G. (2014). Wnt acylation: Seeing is believing. *Nat. Chem. Biol.* *10*, 5–7.
- Berthiaume, L., Peseckis, S.M., and Resh, M.D. (1995). Synthesis and use of iodo-fatty acid analogs. *Methods Enzymol.* *250*, 454–466.
- Bhatnagar, R.S., Fütterer, K., Farazi, T.A., Korolev, S., Murray, C.L., Jackson-Machelski, E., Gokel, G.W., Gordon, J.I., and Waksman, G. (1998). Structure of N-myristoyltransferase with bound myristoylCoA and peptide substrate analogs. *Nat. Struct. Mol. Biol.* *5*, 1091–1097.
- Bianco, A., Townsley, F.M., Greiss, S., Lang, K., and Chin, J.W. (2012). Expanding the genetic code of *Drosophila melanogaster*. *Nat. Chem. Biol.* *8*, 748–750.
- Bologna, G., Yvon, C., Duvaud, S., and Veuthey, A.-L. (2004). N-Terminal myristoylation predictions by ensembles of neural networks. *Proteomics* *4*, 1626–1632.
- Branton, W.D., Rudnick, M.S., Zhou, Y., Eccleston, E.D., Fields, G.B., and Bowers, L.D. (1993). Fatty acylated toxin structure. *Nature* *365*, 496–497.

- Brass, A.L., Huang, I.-C., Benita, Y., John, S.P., Krishnan, M.N., Feeley, E.M., Ryan, B.J., Weyer, J.L., van der Weyden, L., Fikrig, E., et al. (2009). The IFITM Proteins Mediate Cellular Resistance to Influenza A H1N1 Virus, West Nile Virus, and Dengue Virus. *Cell* *139*, 1243–1254.
- Burnaevskiy, N., Fox, T.G., Plymire, D.A., Ertelt, J.M., Weigele, B.A., Selyunin, A.S., Way, S.S., Patrie, S.M., and Alto, N.M. (2013). Proteolytic elimination of N-myristoyl modifications by the Shigella virulence factor IpaJ. *Nature* *496*, 106–109.
- Burnaevskiy, N., Peng, T., Reddick, L.E., Hang, H.C., and Alto, N.M. (2015). Myristoylome Profiling Reveals a Concerted Mechanism of ARF GTPase Deacylation by the Bacterial Protease IpaJ. *Mol. Cell* *58*, 110–122.
- Buss, J.E., and Sefton, B.M. (1986). Direct identification of palmitic acid as the lipid attached to p21ras. *Mol. Cell. Biol.* *6*, 116–122.
- Chamberlain, L.H., and Shipston, M.J. (2015). The Physiology of Protein S-acylation. *Physiol. Rev.* *95*, 341–376.
- Charron, G., Zhang, M.M., Yount, J.S., Wilson, J., Raghavan, A.S., Shamir, E., and Hang, H.C. (2009a). Robust fluorescent detection of protein fatty-acylation with chemical reporters. *J. Am. Chem. Soc.* *131*, 4967–4975.
- Charron, G., Wilson, J., and Hang, H.C. (2009b). Chemical tools for understanding protein lipidation in eukaryotes. *Curr. Opin. Chem. Biol.* *13*, 382–391.
- Charron, G., Tsou, L.K., Maguire, W., Yount, J.S., and Hang, H.C. (2011). Alkynyl-farnesol reporters for detection of protein S-prenylation in cells. *Mol. Biosyst.* *7*, 67–73.
- Chesarino, N.M., Hach, J.C., Chen, J.L., Zaro, B.W., Rajaram, M.V., Turner, J., Schlesinger, L.S., Pratt, M.R., Hang, H.C., and Yount, J.S. (2014a). Chemoproteomics reveals Toll-like receptor fatty acylation. *BMC Biol.* *12*, 91.
- Chesarino, N.M., McMichael, T.M., Hach, J.C., and Yount, J.S. (2014b). Phosphorylation of the Antiviral Protein IFITM3 Dually Regulates its Endocytosis and Ubiquitination. *J. Biol. Chem.* jbc.M114.557694.
- Colquhoun, D.R., Lyashkov, A.E., Mohien, C.U., Aquino, V.N., Bullock, B.T., Dinglasan, R.R., Agnew, B.J., and Graham, D.R.M. (2015). Bioorthogonal mimetics of palmitoyl-CoA and myristoyl-CoA and their subsequent isolation by click chemistry and characterization by mass spectrometry reveal novel acylated host-proteins modified by HIV-1 infection. *PROTEOMICS* *15*, 2066–2077.
- Daggett, K.A., and Sakmar, T.P. (2011). Site-specific in vitro and in vivo incorporation of molecular probes to study G-protein-coupled receptors. *Curr. Opin. Chem. Biol.* *15*, 392–398.

- Davis, L., and Chin, J.W. (2012). Designer proteins: applications of genetic code expansion in cell biology. *Nat. Rev. Mol. Cell Biol.* *13*, 168–182.
- Dennis J Dietzen, Hastings, W.R., and Lublin, D.M. (1995). Caveolin Is Palmitoylated on Multiple Cysteine Residues PALMITOYLATION IS NOT NECESSARY FOR LOCALIZATION OF CAVEOLIN TO CAVEOLAE. *J. Biol. Chem.* *270*, 6838–6842.
- Desai, T.M., Marin, M., Chin, C.R., Savidis, G., Brass, A.L., and Melikyan, G.B. (2014). IFITM3 Restricts Influenza A Virus Entry by Blocking the Formation of Fusion Pores following Virus-Endosome Hemifusion. *PLoS Pathog* *10*, e1004048.
- Deschenes, R.J., and Broach, J.R. (1987). Fatty acylation is important but not essential for *Saccharomyces cerevisiae* RAS function. *Mol. Cell. Biol.* *7*, 2344–2351.
- Drisdell, R.C., and Green, W.N. (2004). Labeling and quantifying sites of protein palmitoylation. *BioTechniques* *36*, 276–285.
- Everitt, A.R., Clare, S., Pertel, T., John, S.P., Wash, R.S., Smith, S.E., Chin, C.R., Feeley, E.M., Sims, J.S., Adams, D.J., et al. (2012). IFITM3 restricts the morbidity and mortality associated with influenza. *Nature* *484*, 519–523.
- Farazi, T.A., Waksman, G., and Gordon, J.I. (2001). The Biology and Enzymology of Protein N-Myristoylation. *J. Biol. Chem.* *276*, 39501–39504.
- Feeley, E.M., Sims, J.S., John, S.P., Chin, C.R., Pertel, T., Chen, L.-M., Gaiha, G.D., Ryan, B.J., Donis, R.O., Elledge, S.J., et al. (2011). IFITM3 Inhibits Influenza A Virus Infection by Preventing Cytosolic Entry. *PLoS Pathog* *7*, e1002337.
- Feldman, J.L., Baeza, J., and Denu, J.M. (2013). Activation of the Protein Deacetylase SIRT6 by Long-chain Fatty Acids and Widespread Deacylation by Mammalian Sirtuins. *J. Biol. Chem.* *288*, 31350–31356.
- Forrester, M.T., Thompson, J.W., Foster, M.W., Nogueira, L., Moseley, M.A., and Stamler, J.S. (2009). Proteomic analysis of S-nitrosylation and denitrosylation by resin-assisted capture. *Nat. Biotechnol.* *27*, 557–559.
- Forrester, M.T., Hess, D.T., Thompson, J.W., Hultman, R., Moseley, M.A., Stamler, J.S., and Casey, P.J. (2011). Site-specific analysis of protein S-acylation by resin-assisted capture. *J. Lipid Res.* *52*, 393–398.
- Fukata, M., Fukata, Y., Adesnik, H., Nicoll, R.A., and Brecht, D.S. (2004). Identification of PSD-95 Palmitoylating Enzymes. *Neuron* *44*, 987–996.
- Gao, X., and Hannoush, R.N. (2014). Single-cell imaging of Wnt palmitoylation by the acyltransferase porcupine. *Nat. Chem. Biol.* *10*, 61–68.

- Gao, Z., Ni, Y., Szabo, G., and Linden, J. (1999). Palmitoylation of the recombinant human A1 adenosine receptor: enhanced proteolysis of palmitoylation-deficient mutant receptors. *Biochem. J.* *342*, 387–395.
- Gautier, A., Nguyen, D.P., Lusic, H., An, W., Deiters, A., and Chin, J.W. (2010). Genetically Encoded Photocontrol of Protein Localization in Mammalian Cells. *J. Am. Chem. Soc.* *132*, 4086–4088.
- Grammel, M., and Hang, H.C. (2013). Chemical reporters for biological discovery. *Nat. Chem. Biol.* *9*.
- Greiss, S., and Chin, J.W. (2011). Expanding the Genetic Code of an Animal. *J. Am. Chem. Soc.* *133*, 14196–14199.
- Grunbeck, A., Huber, T., Sachdev, P., and Sakmar, T.P. (2011). Mapping the Ligand-Binding Site on a G Protein-Coupled Receptor (GPCR) Using Genetically Encoded Photocrosslinkers. *Biochemistry (Mosc.)* *50*, 3411–3413.
- Grunbeck, A., Huber, T., Abrol, R., Trzaskowski, B., Goddard, W.A., and Sakmar, T.P. (2012). Genetically Encoded Photo-cross-linkers Map the Binding Site of an Allosteric Drug on a G Protein-Coupled Receptor. *ACS Chem. Biol.* *7*, 967–972.
- Guo, J., Gaffrey, M.J., Su, D., Liu, T., Camp Li, D.G., Smith, R.D., and Qian, W.-J. (2014). Resin-assisted enrichment of thiols as a general strategy for proteomic profiling of cysteine-based reversible modifications. *Nat. Protoc.* *9*, 64–75.
- Gutierrez, J.A., Solenberg, P.J., Perkins, D.R., Willency, J.A., Knierman, M.D., Jin, Z., Witcher, D.R., Luo, S., Onyia, J.E., and Hale, J.E. (2008). Ghrelin octanoylation mediated by an orphan lipid transferase. *Proc. Natl. Acad. Sci.* *105*, 6320–6325.
- Hancock, S.M., Uprety, R., Deiters, A., and Chin, J.W. (2010). Expanding the Genetic Code of Yeast for Incorporation of Diverse Unnatural Amino Acids via a Pyrrolysyl-tRNA Synthetase/tRNA Pair. *J. Am. Chem. Soc.* *132*, 14819–14824.
- Hang, H.C., and Linder, M.E. (2011). Exploring protein lipidation with chemical biology. *Chem Rev* *111*, 6341–6358.
- Hang, H.C., Geutjes, E.-J., Grotenbreg, G., Pollington, A.M., Bijlmakers, M.J., and Ploegh, H.L. (2007). Chemical Probes for the Rapid Detection of Fatty-Acylated Proteins in Mammalian Cells. *J. Am. Chem. Soc.* *129*, 2744–2745.
- Hang, H.C., Wilson, J.P., and Charron, G. (2011). Bioorthogonal chemical reporters for analyzing protein lipidation and lipid trafficking. *Acc Chem Res* *44*, 699–708.
- Hannoush, R.N., and Arenas-Ramirez, N. (2009). Imaging the Lipidome: ω -Alkynyl Fatty Acids for Detection and Cellular Visualization of Lipid-Modified Proteins. *ACS Chem. Biol.* *4*, 581–587.

Heal, W.P., Wickramasinghe, S.R., Leatherbarrow, R.J., and Tate, E.W. (2008a). N-Myristoyl transferase-mediated protein labelling in vivo. *Org. Biomol. Chem.* *6*, 2308–2315.

Heal, W.P., Wickramasinghe, S.R., Bowyer, P.W., Holder, A.A., Smith, D.F., Leatherbarrow, R.J., and Tate, E.W. (2008b). Site-specific N-terminal labelling of proteins in vitro and in vivo using N-myristoyl transferase and bioorthogonal ligation chemistry. *Chem. Commun.* 480–482.

Henle, W. (1950). Interference Phenomena Between Animal Viruses: A Review. *J. Immunol.* *64*, 203–236.

Hess, D.T., Slater, T.M., Wilson, M.C., and Skene, J.H. (1992). The 25 kDa synaptosomal-associated protein SNAP-25 is the major methionine-rich polypeptide in rapid axonal transport and a major substrate for palmitoylation in adult CNS. *J. Neurosci. Off. J. Soc. Neurosci.* *12*, 4634–4641.

Hickford, D., Frankenberg, S., Shaw, G., and Renfree, M.B. (2012). Evolution of vertebrate interferon inducible transmembrane proteins. *BMC Genomics* *13*, 155.

Huang, I.-C., Bailey, C.C., Weyer, J.L., Radoshitzky, S.R., Becker, M.M., Chiang, J.J., Brass, A.L., Ahmed, A.A., Chi, X., Dong, L., et al. (2011). Distinct Patterns of IFITM-Mediated Restriction of Filoviruses, SARS Coronavirus, and Influenza A Virus. *PLoS Pathog* *7*, e1001258.

Huber, T., and Sakmar, T.P. (2014). Chemical Biology Methods for Investigating G Protein-Coupled Receptor Signaling. *Chem. Biol.* *21*, 1224–1237.

Huber, T., Naganathan, S., Tian, H., Ye, S., and Sakmar, T.P. (2013). Unnatural amino acid mutagenesis of GPCRs using amber codon suppression and bioorthogonal labeling. *Methods Enzymol.* *520*, 281–305.

Isaacs, A., and Lindenmann, J. (1957). Virus Interference. I. The Interferon. *Proc. R. Soc. Lond. B Biol. Sci.* *147*, 258–267.

Isaacs, A., Lindenmann, J., and Valentine, R.C. (1957). Virus Interference. II. Some Properties of Interferon. *Proc. R. Soc. Lond. B Biol. Sci.* *147*, 268–273.

Ivaldi, C., Martin, B.R., Kieffer-Jaquinod, S., Chapel, A., Levade, T., Garin, J., and Journet, A. (2012). Proteomic Analysis of S-Acylated Proteins in Human B Cells Reveals Palmitoylation of the Immune Regulators CD20 and CD23. *PLoS ONE* *7*, e37187.

Ji, Y., Leymarie, N., Haeussler, D.J., Bachschmid, M.M., Costello, C.E., and Lin, C. (2013). Direct Detection of S-Palmitoylation by Mass Spectrometry. *Anal. Chem.* *85*, 11952–11959.

Jia, R., Pan, Q., Ding, S., Rong, L., Liu, S.-L., Geng, Y., Qiao, W., and Liang, C. (2012). The N-terminal region of IFITM3 modulates its antiviral activity through regulating IFITM3 cellular localization. *J. Virol.*

Jia, R., Xu, F., Qian, J., Yao, Y., Miao, C., Zheng, Y.-M., Liu, S.-L., Guo, F., Geng, Y., Qiao, W., et al. (2014). Identification of an endocytic signal essential for the antiviral action of IFITM3. *Cell. Microbiol.* n/a – n/a.

Jiang, H., Khan, S., Wang, Y., Charron, G., He, B., Sebastian, C., Du, J., Kim, R., Ge, E., Mostoslavsky, R., et al. (2013). SIRT6 regulates TNF- α secretion through hydrolysis of long-chain fatty acyl lysine. *Nature* 496, 110–113.

John, S.P., Chin, C.R., Perreira, J., Feeley, E.M., Aker, A., Savidis, G., Smith, S.E., Elia, A.E.H., Everitt, A.R., Vora, M., et al. (2013). The CD225 Domain of IFITM3 is Required for both IFITM Protein Association and Inhibition of Influenza A Virus and Dengue Virus Replication. *J. Virol.*

Jones, M.L., Collins, M.O., Goulding, D., Choudhary, J.S., and Rayner, J.C. (2012). Analysis of Protein Palmitoylation Reveals a Pervasive Role in Plasmodium Development and Pathogenesis. *Cell Host Microbe* 12, 246–258.

Kang, R., Wan, J., Arstikaitis, P., Takahashi, H., Huang, K., Bailey, A.O., Thompson, J.X., Roth, A.F., Drisdell, R.C., Mastro, R., et al. (2008). Neural palmitoyl-proteomics reveals dynamic synaptic palmitoylation. *Nature* 456, 904–909.

Kim, J.-H., Peng, D., Schleich, J.P., Hadziselimovic, A., and Sanders, C.R. (2014). Modest Effects of Lipid Modifications on the Structure of Caveolin-3. *Biochemistry (Mosc.)*.

Kostiuk, M.A., Corvi, M.M., Keller, B.O., Plummer, G., Prescher, J.A., Hangauer, M.J., Bertozzi, C.R., Rajaiyah, G., Falck, J.R., and Berthiaume, L.G. (2008). Identification of palmitoylated mitochondrial proteins using a bio-orthogonal azido-palmitate analogue. *FASEB J. Off. Publ. Fed. Am. Soc. Exp. Biol.* 22, 721–732.

Krall, N., da Cruz, F.P., Boutureira, O., and Bernardes, G.J.L. (2015). Site-selective protein-modification chemistry for basic biology and drug development. *Nat. Chem. advance online publication.*

Kumari, B., Kumar, R., and Kumar, M. (2014). PalmPred: an SVM based palmitoylation prediction method using sequence profile information. *PloS One* 9, e89246.

Lakkaraju, A.K., Abrami, L., Lemmin, T., Blaskovic, S., Kunz, B., Kihara, A., Dal Peraro, M., and van der Goot, F.G. (2012). Palmitoylated calnexin is a key component of the ribosome-translocon complex: Palmitoylated calnexin is a key component of the RTC. *EMBO J.* 31, 1823–1835.

Lang, K., and Chin, J.W. (2014). Bioorthogonal Reactions for Labeling Proteins. *ACS Chem. Biol.* 9, 16–20.

- Lang, K., Davis, L., Torres-Kolbus, J., Chou, C., Deiters, A., and Chin, J.W. (2012). Genetically encoded norbornene directs site-specific cellular protein labelling via a rapid bioorthogonal reaction. *Nat. Chem.* *4*, 298–304.
- Lengyel, P. (1982). Biochemistry of Interferons and Their Actions. *Annu. Rev. Biochem.* *51*, 251–282.
- Li, K., Markosyan, R.M., Zheng, Y.-M., Golfetto, O., Bungart, B., Li, M., Ding, S., He, Y., Liang, C., Lee, J.C., et al. (2013). IFITM Proteins Restrict Viral Membrane Hemifusion. *PLoS Pathog* *9*, e1003124.
- Li, Y., Martin, B.R., Cravatt, B.F., and Hofmann, S.L. (2012). DHHC5 Protein Palmitoylates Flotillin-2 and Is Rapidly Degraded on Induction of Neuronal Differentiation in Cultured Cells. *J. Biol. Chem.* *287*, 523–530.
- Liang, X., Nazarian, A., Erdjument-Bromage, H., Bornmann, W., Tempst, P., and Resh, M.D. (2001). Heterogeneous Fatty Acylation of Src Family Kinases with Polyunsaturated Fatty Acids Regulates Raft Localization and Signal Transduction. *J. Biol. Chem.* *276*, 30987–30994.
- Linder, M.E., and Deschenes, R.J. (2007). Palmitoylation: policing protein stability and traffic. *Nat Rev Mol Cell Biol* *8*, 74–84.
- Linder, M.E., Middleton, P., Hepler, J.R., Taussig, R., Gilman, A.G., and Mumby, S.M. (1993). Lipid modifications of G proteins: alpha subunits are palmitoylated. *Proc. Natl. Acad. Sci. U. S. A.* *90*, 3675–3679.
- Liu, C.C., and Schultz, P.G. (2010). Adding New Chemistries to the Genetic Code. *Annu. Rev. Biochem.* *79*, 413–444.
- Lukinavičius, G., Umezawa, K., Olivier, N., Honigsmann, A., Yang, G., Plass, T., Mueller, V., Reymond, L., Corrêa Jr, I.R., Luo, Z.-G., et al. (2013). A near-infrared fluorophore for live-cell super-resolution microscopy of cellular proteins. *Nat. Chem.* *5*, 132–139.
- MacMicking, J.D. (2012). Interferon-inducible effector mechanisms in cell-autonomous immunity. *Nat. Rev. Immunol.* *12*, 367–382.
- Maeda, K., Poletto, M., Chiapparino, A., and Gavin, A.-C. (2014). A generic protocol for the purification and characterization of water-soluble complexes of affinity-tagged proteins and lipids. *Nat. Protoc.* *9*, 2256–2266.
- Magee, A.I., Gutierrez, L., McKay, I.A., Marshall, C.J., and Hall, A. (1987). Dynamic fatty acylation of p21N-ras. *EMBO J.* *6*, 3353–3357.
- Marin, E.P., Derakhshan, B., Lam, T.T., Davalos, A., and Sessa, W.C. (2012). Endothelial Cell Palmitoylproteomic Identifies Novel Lipid-Modified Targets and Potential Substrates for Protein Acyl Transferases. *Circ. Res.* *110*, 1336–1344.

- Martin, B.R., and Cravatt, B.F. (2009). Large-scale profiling of protein palmitoylation in mammalian cells. *Nat. Methods* 6, 135–138.
- Martin, B.R., Wang, C., Adibekian, A., Tully, S.E., and Cravatt, B.F. (2012). Global profiling of dynamic protein palmitoylation. *Nat. Methods* 9, 84–89.
- Martin, D.D.O., Vilas, G.L., Prescher, J.A., Rajaiah, G., Falck, J.R., Bertozzi, C.R., and Berthiaume, L.G. (2008). Rapid detection, discovery, and identification of post-translationally myristoylated proteins during apoptosis using a bio-orthogonal azidomyristate analog. *FASEB J.* 22, 797–806.
- Martin, D.D.O., Beauchamp, E., and Berthiaume, L.G. (2011). Post-translational myristoylation: Fat matters in cellular life and death. *Biochimie* 93, 18–31.
- Maurer-Stroh, S., and Eisenhaber, F. (2004). Myristoylation of viral and bacterial proteins. *Trends Microbiol.* 12, 178–185.
- Maurer-Stroh, S., and Eisenhaber, F. (2005). Refinement and prediction of protein prenylation motifs. *Genome Biol.* 6, R55.
- Merrick, B.A., Dhungana, S., Williams, J.G., Aloor, J.J., Peddada, S., Tomer, K.B., and Fessler, M.B. (2011). Proteomic Profiling of S-acylated Macrophage Proteins Identifies a Role for Palmitoylation in Mitochondrial Targeting of Phospholipid Scramblase 3. *Mol. Cell. Proteomics* 10, M110.006007.
- Meyer, H., Bug, M., and Bremer, S. (2012). Emerging functions of the VCP/p97 AAA-ATPase in the ubiquitin system. *Nat. Cell Biol.* 14, 117–123.
- Mitchell, D.A., Vasudevan, A., Linder, M.E., and Deschenes, R.J. (2006). Thematic review series: Lipid Posttranslational Modifications. Protein palmitoylation by a family of DHHC protein S-acyltransferases. *J. Lipid Res.* 47, 1118–1127.
- Mukai, T., Kobayashi, T., Hino, N., Yanagisawa, T., Sakamoto, K., and Yokoyama, S. (2008). Adding l-lysine derivatives to the genetic code of mammalian cells with engineered pyrrolysyl-tRNA synthetases. *Biochem. Biophys. Res. Commun.* 371, 818–822.
- Nagar, B., Hantschel, O., Young, M.A., Scheffzek, K., Veach, D., Bornmann, W., Clarkson, B., Superti-Furga, G., and Kuriyan, J. (2003). Structural Basis for the Autoinhibition of c-Abl Tyrosine Kinase. *Cell* 112, 859–871.
- Nimchuk, Z., Marois, E., Kjemtrup, S., Leister, R.T., Katagiri, F., and Dangl, J.L. (2000). Eukaryotic Fatty Acylation Drives Plasma Membrane Targeting and Enhances Function of Several Type III Effector Proteins from *Pseudomonas syringae*. *Cell* 101, 353–363.
- O'Brien, P.J., and Zatz, M. (1984). Acylation of bovine rhodopsin by [³H]palmitic acid. *J. Biol. Chem.* 259, 5054–5057.

- Olson, B.J.S.C., and Markwell, J. (2001). Assays for Determination of Protein Concentration. In *Current Protocols in Protein Science*, (John Wiley & Sons, Inc.),.
- Paige, L.A., Nadler, M.J., Harrison, M.L., Cassady, J.M., and Geahlen, R.L. (1993). Reversible palmitoylation of the protein-tyrosine kinase p56lck. *J. Biol. Chem.* *268*, 8669–8674.
- Patwardhan, P., and Resh, M.D. (2010). Myristoylation and Membrane Binding Regulate c-Src Stability and Kinase Activity. *Mol. Cell. Biol.* *30*, 4094–4107.
- Peng, T., and Hang, H.C. (2015). Bifunctional Fatty Acid Chemical Reporter for Analyzing S-palmitoylated Membrane Protein-Protein Interactions in Mammalian Cells. *J. Am. Chem. Soc.* *137*, 556–559.
- Peng, T., Thimon, E., and Hang, H.C. (2016). Proteomic analysis of fatty-acylated proteins. *Curr. Opin. Chem. Biol.* *30*, 77–86.
- Percherancier, Y., Planchenault, T., Valenzuela-Fernandez, A., Virelizier, J.-L., Arenzana-Seisdedos, F., and Bachelier, F. (2001). Palmitoylation-dependent Control of Degradation, Life Span, and Membrane Expression of the CCR5 Receptor. *J. Biol. Chem.* *276*, 31936–31944.
- Perreira, J.M., Chin, C.R., Feeley, E.M., and Brass, A.L. (2013). IFITMs Restrict the Replication of Multiple Pathogenic Viruses. *J. Mol. Biol.*
- Peseckis, S.M., Deichaite, I., and Resh, M.D. (1993). Iodinated fatty acids as probes for myristate processing and function. Incorporation into pp60v-src. *J. Biol. Chem.* *268*, 5107–5114.
- Pestka, S. (2007). The Interferons: 50 Years after Their Discovery, There Is Much More to Learn. *J. Biol. Chem.* *282*, 20047–20051.
- Pirooz, S.D., He, S., Zhang, T., Zhang, X., Zhao, Z., Oh, S., O’Connell, D., Khalilzadeh, P., Amini-Bavil-Olyaei, S., Farzan, M., et al. (2014). UVRAG is required for virus entry through combinatorial interaction with the class C-Vps complex and SNAREs. *Proc. Natl. Acad. Sci.* *111*, 2716–2721.
- Podell, S., and Gribskov, M. (2004). Predicting N-terminal myristoylation sites in plant proteins. *BMC Genomics* *5*, 37.
- Prescher, J.A., and Bertozzi, C.R. (2005). Chemistry in living systems. *Nat. Chem. Biol.* *1*, 13–21.
- Ranjbar, S., Haridas, V., Jasenosky, L.D., Falvo, J.V., and Goldfeld, A.E. (2015). A Role for IFITM Proteins in Restriction of Mycobacterium tuberculosis Infection. *Cell Rep.* *13*, 874–883.

- Ren, J., Wen, L., Gao, X., Jin, C., Xue, Y., and Yao, X. (2008). CSS-Palm 2.0: an updated software for palmitoylation sites prediction. *Protein Eng. Des. Sel.* *21*, 639–644.
- Ren, W., Jhala, U.S., and Du, K. (2013). Proteomic analysis of protein palmitoylation in adipocytes. *Adipocyte* *2*, 17–28.
- Resh, M.D. (2006). Trafficking and signaling by fatty-acylated and prenylated proteins. *Nat. Chem. Biol.* *2*, 584–590.
- Rocks, O., Peyker, A., Kahms, M., Verveer, P.J., Koerner, C., Lumbierres, M., Kuhlmann, J., Waldmann, H., Wittinghofer, A., and Bastiaens, P.I.H. (2005). An Acylation Cycle Regulates Localization and Activity of Palmitoylated Ras Isoforms. *Science* *307*, 1746–1752.
- Rocks, O., Gerauer, M., Vartak, N., Koch, S., Huang, Z.-P., Pechlivanis, M., Kuhlmann, J., Brunsveld, L., Chandra, A., Ellinger, B., et al. (2010). The Palmitoylation Machinery Is a Spatially Organizing System for Peripheral Membrane Proteins. *Cell* *141*, 458–471.
- Roth, A.F., Wan, J., Bailey, A.O., Sun, B., Kuchar, J.A., Green, W.N., Phinney, B.S., Yates, J.R., and Davis, N.G. (2006). Global analysis of protein palmitoylation in yeast. *Cell* *125*, 1003–1013.
- Sadler, A.J., and Williams, B.R.G. (2008). Interferon-inducible antiviral effectors. *Nat. Rev. Immunol.* *8*, 559–568.
- Sakurai, N., and Utsumi, T. (2006). Posttranslational N-Myristoylation Is Required for the Anti-apoptotic Activity of Human tGelsolin, the C-terminal Caspase Cleavage Product of Human Gelsolin. *J. Biol. Chem.* *281*, 14288–14295.
- Schlesinger, M.J., Magee, A.I., and Schmidt, M.F. (1980). Fatty acid acylation of proteins in cultured cells. *J. Biol. Chem.* *255*, 10021–10024.
- Schmidt, M.F.G., and Schlesinger, M.J. (1979). Fatty acid binding to vesicular stomatitis virus glycoprotein: a new type of post-translational modification of the viral glycoprotein. *Cell* *17*, 813–819.
- Schoggins, J.W., Wilson, S.J., Panis, M., Murphy, M.Y., Jones, C.T., Bieniasz, P., and Rice, C.M. (2011). A diverse range of gene products are effectors of the type I interferon antiviral response. *Nature* *472*, 481–485.
- Serwa, R.A., Abaitua, F., Krause, E., Tate, E.W., and O’Hare, P. (2015). Systems Analysis of Protein Fatty Acylation in Herpes Simplex Virus-Infected Cells Using Chemical Proteomics. *Chem. Biol.* *22*, 1008–1017.
- Shi, S.-P., Sun, X.-Y., Qiu, J.-D., Suo, S.-B., Chen, X., Huang, S.-Y., and Liang, R.-P. (2013). The prediction of palmitoylation site locations using a multiple feature extraction method. *J. Mol. Graph. Model.* *40*, 125–130.

- Siniooglou, S., and Pelham, H.R.B. (2001). An effector of Ypt6p binds the SNARE Tlg1p and mediates selective fusion of vesicles with late Golgi membranes. *EMBO J.* *20*, 5991–5998.
- Sinz, A. (2006). Chemical cross-linking and mass spectrometry to map three-dimensional protein structures and protein-protein interactions. *Mass Spectrom. Rev.* *25*, 663–682.
- Sletten, E.M., and Bertozzi, C.R. (2009). Bioorthogonal Chemistry: Fishing for Selectivity in a Sea of Functionality. *Angew. Chem. Int. Ed.* *48*, 6974–6998.
- Stevenson, F.T., Bursten, S.L., Locksley, R.M., and Lovett, D.H. (1992). Myristyl acylation of the tumor necrosis factor alpha precursor on specific lysine residues. *J. Exp. Med.* *176*, 1053–1062.
- Stevenson, F.T., Bursten, S.L., Fanton, C., Locksley, R.M., and Lovett, D.H. (1993). The 31-kDa precursor of interleukin 1 alpha is myristoylated on specific lysines within the 16-kDa N-terminal propeptide. *Proc. Natl. Acad. Sci.* *90*, 7245–7249.
- Stienstra, R., Tack, C.J., Kanneganti, T.-D., Joosten, L.A.B., and Netea, M.G. (2012). The Inflammasome Puts Obesity in the Danger Zone. *Cell Metab.* *15*, 10–18.
- Takada, R., Satomi, Y., Kurata, T., Ueno, N., Norioka, S., Kondoh, H., Takao, T., and Takada, S. (2006). Monounsaturated fatty acid modification of Wnt protein: its role in Wnt secretion. *Dev Cell* *11*, 791–801.
- Teng, Y.-B., Jing, H., Aramsangtienchai, P., He, B., Khan, S., Hu, J., Lin, H., and Hao, Q. (2015). Efficient Demyristoylase Activity of SIRT2 Revealed by Kinetic and Structural Studies. *Sci. Rep.* *5*, 8529.
- Thinon, E., and Hang, H.C. (2015). Chemical reporters for exploring protein acylation. *Biochem. Soc. Trans.* *43*, 253–261.
- Thinon, E., Serwa, R.A., Broncel, M., Brannigan, J.A., Brassat, U., Wright, M.H., Heal, W.P., Wilkinson, A.J., Mann, D.J., and Tate, E.W. (2014). Global profiling of co- and post-translationally N-myristoylated proteomes in human cells. *Nat. Commun.* *5*, 4919.
- Tian, H., Sakmar, T.P., and Huber, T. (2013). Site-specific labeling of genetically encoded azido groups for multicolor, single-molecule fluorescence imaging of GPCRs. *Methods Cell Biol.* *117*, 267–303.
- Triola, G., Waldmann, H., and Hedberg, C. (2012). Chemical Biology of Lipidated Proteins. *ACS Chem. Biol.* *7*, 87–99.
- Uttamapinant, C., Howe, J.D., Lang, K., Beránek, V., Davis, L., Mahesh, M., Barry, N.P., and Chin, J.W. (2015). Genetic Code Expansion Enables Live-Cell and Super-Resolution Imaging of Site-Specifically Labeled Cellular Proteins. *J. Am. Chem. Soc.* *137*, 4602–4605.

Valdez-Taubas, J., and Pelham, H. (2005). Swf1-dependent palmitoylation of the SNARE Tlg1 prevents its ubiquitination and degradation. *EMBO J.* *24*, 2524–2532.

Valentin-Hansen, L., Park, M., Huber, T., Grunbeck, A., Naganathan, S., Schwartz, T.W., and Sakmar, T.P. (2014). Mapping Substance P Binding Sites on the neurokinin-1 receptor Using Genetic Incorporation of a Photoreactive Amino Acid. *J. Biol. Chem.* jbc.M113.527085.

Valkevich, E.M., Guenette, R.G., Sanchez, N.A., Chen, Y., Ge, Y., and Strieter, E.R. (2012). Forging isopeptide bonds using thiol-ene chemistry: site-specific coupling of ubiquitin molecules for studying the activity of isopeptidases. *J. Am. Chem. Soc.* *134*, 6916–6919.

Vilas, G.L., Corvi, M.M., Plummer, G.J., Seime, A.M., Lambkin, G.R., and Berthiaume, L.G. (2006). Posttranslational myristoylation of caspase-activated p21-activated protein kinase 2 (PAK2) potentiates late apoptotic events. *Proc. Natl. Acad. Sci.* *103*, 6542–6547.

Walsh, C.T., Garneau-Tsodikova, S., and Gatto, G.J. (2005). Protein Posttranslational Modifications: The Chemistry of Proteome Diversifications. *Angew. Chem. Int. Ed.* *44*, 7342–7372.

Wan, J., Savas, J.N., Roth, A.F., Sanders, S.S., Singaraja, R.R., Hayden, M.R., Yates III, J.R., and Davis, N.G. (2013). Tracking Brain Palmitoylation Change: Predominance of Glial Change in a Mouse Model of Huntington's Disease. *Chem. Biol.* *20*, 1421–1434.

Wang, L., Brock, A., Herberich, B., and Schultz, P.G. (2001). Expanding the Genetic Code of Escherichia coli. *Science* *292*, 498–500.

Wang, X.-B., Wu, L.-Y., Wang, Y.-C., and Deng, N.-Y. (2009). Prediction of palmitoylation sites using the composition of k-spaced amino acid pairs. *Protein Eng. Des. Sel. PEDS* *22*, 707–712.

Wang, Z., Zhang, A., Wan, Y., Liu, X., Qiu, C., Xi, X., Ren, Y., Wang, J., Dong, Y., Bao, M., et al. (2013). Early hypercytokinemia is associated with interferon-induced transmembrane protein-3 dysfunction and predictive of fatal H7N9 infection. *Proc. Natl. Acad. Sci.* 201321748.

Weidner, J.M., Jiang, D., Pan, X.-B., Chang, J., Block, T.M., and Guo, J.-T. (2010). Interferon-induced cell membrane proteins, IFITM3 and tetherin, inhibit vesicular stomatitis virus infection via distinct mechanisms. *J. Virol.* *84*, 12646–12657.

Weston, S., Czieso, S., White, I.J., Smith, S.E., Kellam, P., and Marsh, M. (2014). A Membrane Topology Model for Human Interferon Inducible Transmembrane Protein 1. *PLoS ONE* *9*, e104341.

Wilson, J.P., Raghavan, A.S., Yang, Y.-Y., Charron, G., and Hang, H.C. (2011). Proteomic analysis of fatty-acylated proteins in mammalian cells with chemical reporters reveals S-acylation of histone H3 variants. *Mol. Cell. Proteomics MCP* *10*, M110.001198.

Wright, M.H., Clough, B., Rackham, M.D., Rangachari, K., Brannigan, J.A., Grainger, M., Moss, D.K., Bottrill, A.R., Heal, W.P., Broncel, M., et al. (2014). Validation of N-myristoyltransferase as an antimalarial drug target using an integrated chemical biology approach. *Nat. Chem.* **6**, 112–121.

Wright, M.H., Paape, D., Storck, E.M., Serwa, R.A., Smith, D.F., and Tate, E.W. (2015). Global analysis of protein N-myristoylation and exploration of N-myristoyltransferase as a drug target in the neglected human pathogen *Leishmania donovani*. *Chem. Biol.* **22**, 342–354.

Xue, Y., Chen, H., Jin, C., Sun, Z., and Yao, X. (2006). NBA-Palm: prediction of palmitoylation site implemented in Naïve Bayes algorithm. *BMC Bioinformatics* **7**, 458.

Yang, J., Brown, M.S., Liang, G., Grishin, N.V., and Goldstein, J.L. (2008). Identification of the Acyltransferase that Octanoylates Ghrelin, an Appetite-Stimulating Peptide Hormone. *Cell* **132**, 387–396.

Yang, W., Vizio, D.D., Kirchner, M., Steen, H., and Freeman, M.R. (2010a). Proteome Scale Characterization of Human S-Acylated Proteins in Lipid Raft-enriched and Non-raft Membranes. *Mol. Cell. Proteomics* **9**, 54–70.

Yang, Y.-Y., Ascano, J.M., and Hang, H.C. (2010b). Bioorthogonal chemical reporters for monitoring protein acetylation. *J. Am. Chem. Soc.* **132**, 3640–3641.

Yount, J.S., Moltedo, B., Yang, Y.-Y., Charron, G., Moran, T.M., López, C.B., and Hang, H.C. (2010). Palmitoylome profiling reveals S-palmitoylation-dependent antiviral activity of IFITM3. *Nat. Chem. Biol.* **6**, 610–614.

Yount, J.S., Charron, G., and Hang, H.C. (2011a). Bioorthogonal proteomics of 15-hexadecyloxyacetic acid chemical reporter reveals preferential targeting of fatty acid modified proteins and biosynthetic enzymes. *Bioorg. Med. Chem.*

Yount, J.S., Zhang, M.M., and Hang, H.C. (2011b). Visualization and Identification of Fatty Acylated Proteins Using Chemical Reporters. In *Current Protocols in Chemical Biology*, A.P. Arkin, L. Mahal, F. Romesberg, K. Shah, C. Shamu, and C. Thomas, eds. (Hoboken, NJ, USA: John Wiley & Sons, Inc.),.

Yount, J.S., Karssemeijer, R.A., and Hang, H.C. (2012). S-Palmitoylation and Ubiquitination Differentially Regulate Interferon-Induced Transmembrane Protein 3 (IFITM3)-Mediated Resistance to Influenza Virus. *J. Biol. Chem.* **287**, 19631–19641.

Zha, J., Weiler, S., Oh, K.J., Wei, M.C., and Korsmeyer, S.J. (2000). Posttranslational N-myristoylation of BID as a molecular switch for targeting mitochondria and apoptosis. *Science* **290**, 1761–1765.

Zhang, M., Lin, S., Song, X., Liu, J., Fu, Y., Ge, X., Fu, X., Chang, Z., and Chen, P.R. (2011). A genetically incorporated crosslinker reveals chaperone cooperation in acid resistance. *Nat Chem Biol* **7**, 671–677.

- Zhang, M.M., Tsou, L.K., Charron, G., Raghavan, A.S., and Hang, H.C. (2010). Tandem fluorescence imaging of dynamic S-acylation and protein turnover. *Proc. Natl. Acad. Sci. U. S. A.* *107*, 8627–8632.
- Zhang, M.M., Wu, P.-Y.J., Kelly, F.D., Nurse, P., and Hang, H.C. (2013a). Quantitative Control of Protein S -Palmitoylation Regulates Meiotic Entry in Fission Yeast. *PLOS Biol* *11*, e1001597.
- Zhang, Y.-H., Zhao, Y., Li, N., Peng, Y.-C., Giannoulatou, E., Jin, R.-H., Yan, H.-P., Wu, H., Liu, J.-H., Liu, N., et al. (2013b). Interferon-induced transmembrane protein-3 genetic variant rs12252-C is associated with severe influenza in Chinese individuals. *Nat. Commun.* *4*, 1418.
- Zhang, Z., Liu, J., Li, M., Yang, H., and Zhang, C. (2012). Evolutionary Dynamics of the Interferon-Induced Transmembrane Gene Family in Vertebrates. *PLoS ONE* *7*, e49265.
- Zhou, B., An, M., Freeman, M.R., and Yang, W. (2014). Technologies and Challenges in Proteomic Analysis of Protein S-acylation. *J. Proteomics Bioinform.* *7*, 256–263.
- Zhu, X., He, Z., Yuan, J., Wen, W., Huang, X., Hu, Y., Lin, C., Pan, J., Li, R., Deng, H., et al. (2014). IFITM3-containing exosome as a novel mediator for anti-viral response in dengue virus infection. *Cell. Microbiol.* n/a – n/a.
- Zou, C., Ellis, B.M., Smith, R.M., Chen, B.B., Zhao, Y., and Mallampalli, R.K. (2011). Acyl-CoA:Lysophosphatidylcholine Acyltransferase I (Lpcat1) Catalyzes Histone Protein O-Palmitoylation to Regulate mRNA Synthesis. *J. Biol. Chem.* *286*, 28019–28025.
- Zuckerman, D.M., Hicks, S.W., Charron, G., Hang, H.C., and Machamer, C.E. (2011). Differential regulation of two palmitoylation sites in the cytoplasmic tail of the beta1-adrenergic receptor. *J. Biol. Chem.* *286*, 19014–19023.